Novel drug development for KRAS-mutated non-small cell lung cancer

Md. Salman Shakil

A thesis submitted for the degree of

Master of Science

at the University of Otago

Dunedin, New Zealand

October 2020

Abstract

Lung cancer is the leading cause of cancer-related death among both men and women and non-small cell lung cancer (NSCLC) accounts for 85 to 88% of all lung cancer cases. In NSCLC, kirsten rat sarcoma (KRAS) viral oncogene homologue mutations are the third most frequent mutation. KRAS-mutant patients show a shorter overall survival as a clinically approved therapeutic agent against KRAS has yet to be developed. Therefore, novel drugs are urgently needed for these patients. The current project examined the cytotoxic effects, selectivity, and anticancer mechanism of novel synthetic compounds towards KRAS-mutated NSCLC *in vitro*. In this study, A549 (KRAS-mutated NSCLC cells), H522 (p53-mutated NSCLC cells), NIH-3T3 (pre-neoplastic) and PNT1A (normal prostate epithelial cells) cell lines were used to screen out potent drug candidate for KRAS-mutated NSCLC. A549 cells were treated with 11 different metal-based and non-metal-based novel compounds of four different drug class (HDAC inhibitors: JAZZ-90, JAZZ-166, and JAZZ-167; Hydroxythiopyridone derivatives: M1S, M2S, M1S-Ru, and M2S-Ru; Metal-based PCA ligands and complexes: AASH-122 and JAZZ-121; Kinetically inert metal(arene) complexes of PCA: ZR-012 and ZR-014) at 0.015 to 200 µM for 72 h and cell viability was determined using the sulforhodamine B assay. Hydroxythiopyridone derivatives M1S and M2S were the smallest but most potent compounds in A549 cells with EC_{50} values of 0.36 and 0.32 µM, respectively. Additionally, M1S and M2S were 1.3 and 1.4 times more potent against H522 cells. Furthermore, M1S and M2S exhibited more selectivity towards these NSCLC cells and pre-neoplastic NIH3T3 cells as compared to PNT1A cells. Time-course cytotoxicity studies showed that both the drug candidates had cytostatic and cytotoxic effects at $2\times EC_{50}$ concentration in A549 and H522 cells, respectively. Western blotting results indicated that the drug candidates were unable to increase the acetylation of histone 3. In A549 cells the drug candidates did not change cyclin D1 levels, after 24 h. However, $2\times EC_{50}$ concentration of M1S and M2S significantly decreased cyclin D1 expression in H522 cells by 68.1 and 84.9% of control, respectively at 24 h. In both the cell lines, the drug candidates did not produce a significant effect in reducing cyclin B1 expression. Cell cycle analysis showed that the $2\times EC_{50}$ concentration of M1S and M2S arrested 3.3 and 7.1% of A549 cells at the G2/M phase compared to control at 12 h. While 9.9 and 8.9% of H522 cells were arrested at the G1 phase after M1S and M2S treatment at $2\times EC_{50}$ concentration. The same treatment also increased the number of sub-G1 apoptotic H522 cells. Thus, our findings provide evidence that M1S and M2S have potent anticancer activity in KRAS-mutated A549 cells and p53 mutated H522 cells, both the compounds warrant further *in vitro* experimentation to elucidate their specific mechanism of action(s).

Acknowledgments

Foremost, I would like to praise the Almighty for his consent to accomplish the journey. Then, my heartiest gratitude and deepest respect go to my mentor, Prof. Rhonda J. Rosengren, for her continuous support, expert guidance, motivation, enthusiasm, and sharing of immense knowledge to finish my MSc thesis. Your professionalism always teaches me how to handle difficult situations so easily.

My special thanks to Dr. Muhammad Hanif for providing novel compounds that are key to explore novel drugs for the KRAS-mutant NSCLC line. I am also grateful to A/Prof. John Aston, Dr. Greg Giles, and Prof. Helen Nicholson for donating experimental cell lines.

My appreciation also extends to my friendly lab colleagues (Zohaib, Mhairi, Abby, Ravneel, Nensi, Jessie, Risha, Lucy, Nayla, Matt, Yi Zhen) and postgrads (Steph, Jamie, Geetanjali, Amreen, Ben, Hayley, Helen, Ellie, Caitlin, Maddie, Fergus, Monica, and Louise) for their insightful comments, motivation, and guidance. Especially, I would like to thank Zohaib for teaching me core research skills, knowledge sharing, continuous motivation, and inspiration. I would also like to recall helpful guidance from Rumpa, Arpita, and Mhairi for Western blotting trouble shootings. I am thankful to Katie, Abby, and Mhairi for teaching data analysis for flow cytometry. I also acknowledge the valuable comments from Dr. Laura Burga and Dr. Belinda Cridge during lab meetings.

I am highly indebted to Fred Fastier Summer Student Scholarship and the University of Otago, Masters Scholarship; these fundings facilitated my cancer research. I appreciate the continuous support from the Dept. of Pharmacology and Toxicology, its administrative staff, and especially the HOD (Prof. Michelle Glass).

I want to express my gratitude to Adib who has been supportive to me through my ups and downs since the beginning. I am also grateful to OUSA members (especially Brony and Hahna) and BDSA members (especially Sabbir, Saif, Lutfur, Saadlee, Tajul, Supti) for their guidance and motivation during my hard times. I am thankful to my nice flatmates (Ifti, Rabbi, Maruf, and Riad) for taking care of me and offering delicious cuisine. Lastly, I recall all of my previous mentors, seniors, juniors, and peers especially Dr. Ashraf, Dr. Sattya, Papri, Sakib, Shihab, Dr. Shiplu, Forhad, Morshed, Yasir, Rayhan, Leon, Muhit and Achal who always inspire me.

Above all, I am extremely grateful highly indebted to my family for their unconditional love and support throughout my life. I also acknowledge my beloved wife Niloy for her motivation that synthesised energy for my hard work.

Table of contents

List of figures

List of tables

List of abbreviations

10a	1-Phenyltriazolylethyl-3-hydroxypyridine-2-thione
10d	1-Phenyltriazolylpentyl-3-hydroxypyridine-2-thione
1-HPT	1-Hydroxypyridine-2-thiones
3-HP	3-Hydroxypyridin-2-one
3-HPT	3-Hydroxypyridin-2-thione
7k	4-((3-((4,6-Dioxo-2-thioxotetrahydropyrimidine-5(2H)-ylidene)methyl)-2-methyl-1H-indol-1-yl)methyl)benzoate)
8i	5-Methoxy-2-(6-oxo-1-*o*-tolyl-1,6-dihydropyridine-3-carbonyl)phenyl propyl carbonate
AASH-122	[Chlorido(η^6-p-cymene)(N-(4-fluorophenyl)-2-pyridinecarbothioamide) ruthenium(II)]chloride
ADC	Adenocarcinoma
ADM	Adenomas
AIB1	Amplified in breast cancer 1
AKT	Protein kinase B
AMP	Adenosine monophosphate
AMPK	AMP activated protein kinase
ANOVA	Analysis of variance
AR	Androgen receptor
ATP	Adenosine triphosphate
ATPis	ATP-competitive inhibitors
BCA	4, 4′-Dicarboxy-2, 2′-biquinoline acid
BIM	Bcl-2-like protein 11
bip	Biphenyl
BRCA2	Breast cancer 2 gene
bz	Benzene
C/EBPβ	CCAAT-enhancer-binding proteins β
C1	2-(4-Hexyloxyphenyl)-5-(4-hydroxyphenyl)pyrimidine
CBP	CREB-binding protein
CDKs	Cyclin depended kinases
CGMARN	Cancer Genome Atlas Research Network

cGMP	Cyclic guanosine monophosphate
CKIs	Cyclin-dependent kinase inhibitors
clogP	Calculated logP
c-Met	A receptor tyrosine kinase belonging to the MET
Cp	Pentamethylcyclopentadienato
cyp	Cyclopentadienyl
Cur	Curcumin
DHA	Dihydroanthracene
DMP1	Dentin matrix acidic phosphoprotein 1
DMSO	Dimethyl sulfoxide
DNA	Deoxyribonucleic acid
DOX	Doxorubicin
EC_{50}	The concentration of a drug that gives half-maximal response
EDTA	Ethylenediaminetetraacetic acid
EGFR	Epidermal growth factor receptor
EGTA	Ethylene glycol tetraacetic acid
ERKs	Extracellular signal-regulated kinases
ERα	Oestrogen receptor-α
FAK	Focal adhesion kinase
FBS	Foetal bovine serum
FDA	Food and Drug Administration
FOXM1	Forkhead box transcription factor M1
FOXO1	Forkhead box protein O1
FOXO3a	Forkhead box protein O3a
FSC	Forward scattered
GDC	Genome Data Commons
GDP	Guanosine diphosphate
GRB2	Growth factor receptor-bound protein 2
GRIP1	Glutamate receptor-interacting protein 1
GTP	Guanosine triphosphate
HATs	Histone acetyltransferases
HC11	[(η6-Tetrahydroanthracene)Ru(ethylenediamine)Cl]PF6

HDACis	Histone deacetylase inhibitors
HDACs	Histone deacetylases
HIF-1α	Hypoxia-induced factor-1α
HSP90	Heat-shock protein 90
IC_{50}	The concentration of an inhibitor where the response is reduced by half
IKK	IkB kinase
Ir	Iridium
JAHA	Jay amin hydroxamic acid
JAZZ-121	[Chlorido(η^5-pentamethylcyclopentadienyl)(*N*-(4- fluorophenyl) pyridine-2-carbothioamide)rhodium(III)]chloride
JAZZ-166	[Chlorido(η^5-pentamethylcyclopentadienyl)(N^1-hydroxy-N^8-(4-(pyridine-2-carbothioamido-κ^2N,S)phenyl)octanediamide)iridium(III)] chloride
JAZZ-167	[Chlorido(η^5-pentamethylcyclopentadienyl)(N^1-hydroxy-N^8-(4-(pyridine-2-carbothioamido- κ^2N,S)phenyl)octanediamide) rhodium(III)]chloride
JAZZ-90	N^1-hydroxy-N^8-(4-(pyridine-2-carbothioamido)phenyl)octanediamide
KRAS	Kirsten rat sarcoma
L1	1,2-bis(diphenylphosphino)-benzene
M1S	1-Benzyl-2-methyl-3-hydroxypyridin-4-(1H)-thione
M1S-Ru	Chlorido[3-oxo-1-benzyl-2-methylpyridin-4(1H)-thionato-κ^2O,S](p-cymene)ruthenium(II)]
M2S	1-Ethylbenzyl-2-methyl-3-hydroxypyridin-4-thione
M2S-Ru	Chlorido[3-oxo-1,ethylbenzyl-2-methylpyridin-4(1H)-thionato-κ^2O,S] (cymene) ruthenium(II)
MAPK	Mitogen-activated protein kinase
MEK	Mitogen-activated protein kinase kinase
MI	Mdm2 inhibitor
M-OTf	Metal triflates
mTOR	Mammalian target of rapamycin
MTS	[5-(3-Carboxymethoxyphenyl)-2-(4,5,-dimethylthiazolyl)-3-(4-sulfophenyl)tetrazolium, inner salt]
MTT	3-(4,5-Dimethylthiazol-2yl)-2,5-diphenyltetrazolium bromide
MW	Molecular weight

MYOD1	Myoblast determination protein 1
NAD	Nicotinamide adenine dinucleotide
$NADP^+$	Nicotinamide adenine dinucleotide phosphate
NCI	National Cancer Institute
NEUROD1	Neurogenic differentiation factor 1
NFKB	Nuclear factor of the κ-chain in B-cells
NRU	Neutral red uptake
NSCLC	Non-small cell lung cancer
Os	Osmium
OTf	Trifluromethylsulfonate
P/CAF3	CBP-associated factor 3
PCA	Pyridine-2-carbothioamide
p-cym	p-cymene
PDEδ	Phosphodiesterase 6 delta
PI	Propidium iodide
PI3K	Phosphoinositide-3-kinase
PLD1	Phospholipase D1
Plecstatin-1	[Chlorido(η^6-p-cymene)(N-(4-fluorophenyl)-2-pyridinecarbothioamide) ruthenium(II)]chloride
PMSF	Phenylmethylsulfonyl fluoride
PP1	Protein phosphatase 1
PPARγ	Peroxisome proliferator-activated receptor-γ
PPh_3	Tri-phenyl phosphine
PTEN	Phosphatase and tensin
PTMs	Post-translational modifications
PVDF	Polyvinylidene difluoride
QTc	Corrected QT interval
RAC	A subfamily of the Rho family of GTPases
RAF	Rapidly accelerated fibrosarcoma
RAL	Ras-like
RALGDS	Ral guanine nucleotide dissociation stimulator
RAS	Rat sarcoma

RES	Resazurin reduction
Rh	Rhodium
RHOA	Ras homologue family member A
RNA	Ribonucleic acid
ROS	Reactive oxygen species
RTK	Receptor tyrosine kinase
Ru	Ruthenium
SAHA	Suberoylanilide hydroxamic acid
SAR	Structure-activity relationship
SCLC	Small-cell lung carcinoma
SDS	Sodium dodecyl sulfate
SDS-PAGE	Sodium dodecyl sulfate-polyacrylamide gel electrophoresis
SEM	Standard error of the mean
SH	Thiol
SI	Selectivity index
SIRT	Sirtuin
SOS	Son of sevenless
SRB	Sulforhodamine B
SRC1	Steroid receptor coactivator 1
SS	Disulfide
SSC	Side scattered
STAT3	Signal transducer and activator of transcription 3
TAF1	TATA binding protein-associated factor 1
TBP2	Thioredoxin binding protein 2
TCA	Trichloroacetic acid
TEMED	Tetramethylene diamine
THA	Tetrahydroanthracene
TIAM1	T-cell lymphoma invasion and metastasis inducing factor 1
TKIs	Tyrosine kinase inhibitors
TME	Tumour microenvironment
Tris HCl	Trizma hydrochloride
Trx	Thioredoxin

VEGF	Vascular endothelial growth factor
VEGFR2	Vascular endothelial growth factor receptor 2
WEE1	A tyrosine kinase
WST-1	4-[3-(4-Iodophenyl)-2-(4-nitrophenyl)-2H-5-tetrazolio]-1,3-benzene disulfonate
XTT	2,3-Bis(2-methoxy-4-nitro-5-sulfophenyl)-5-[(phenylamino)carbonyl]-2H-tetrazolium hydroxide
ZBG	Zinc-binding group
ZR-012	[(Triphenylphosphine)(η^6-p-cymene)(N-(4-chlorophenyl)pyridine-2-carbothioamide)]ruthenium(II)triflate
ZR-014	[(Triphenylphosphine)(η^6-biphenyl)(N-(4-chlorophenyl)pyridine-2-carbothioamide)]osmium(II)triflate

CHAPTER 1

Introduction

1. Introduction

1.1 Lung cancer

1.1.1 Epidemiology and risk factors of lung cancer

Lung cancer has the highest mortality and morbidity globally, with 1.38 million new cases and over one million deaths in the world annually [1]. According to GLOBOCAN 2018, lung cancer is the most frequently diagnosed cancer (11.6% of the total cases) in both males and females, and causes 18.4% of the total cancer deaths globally [2]. Lung cancer is more common in Polynesians and is rare among Western Africans (Figure 1.1). Didkowska and colleagues predicted that 3 million people will die globally due to lung cancer in the year 2035 [3].

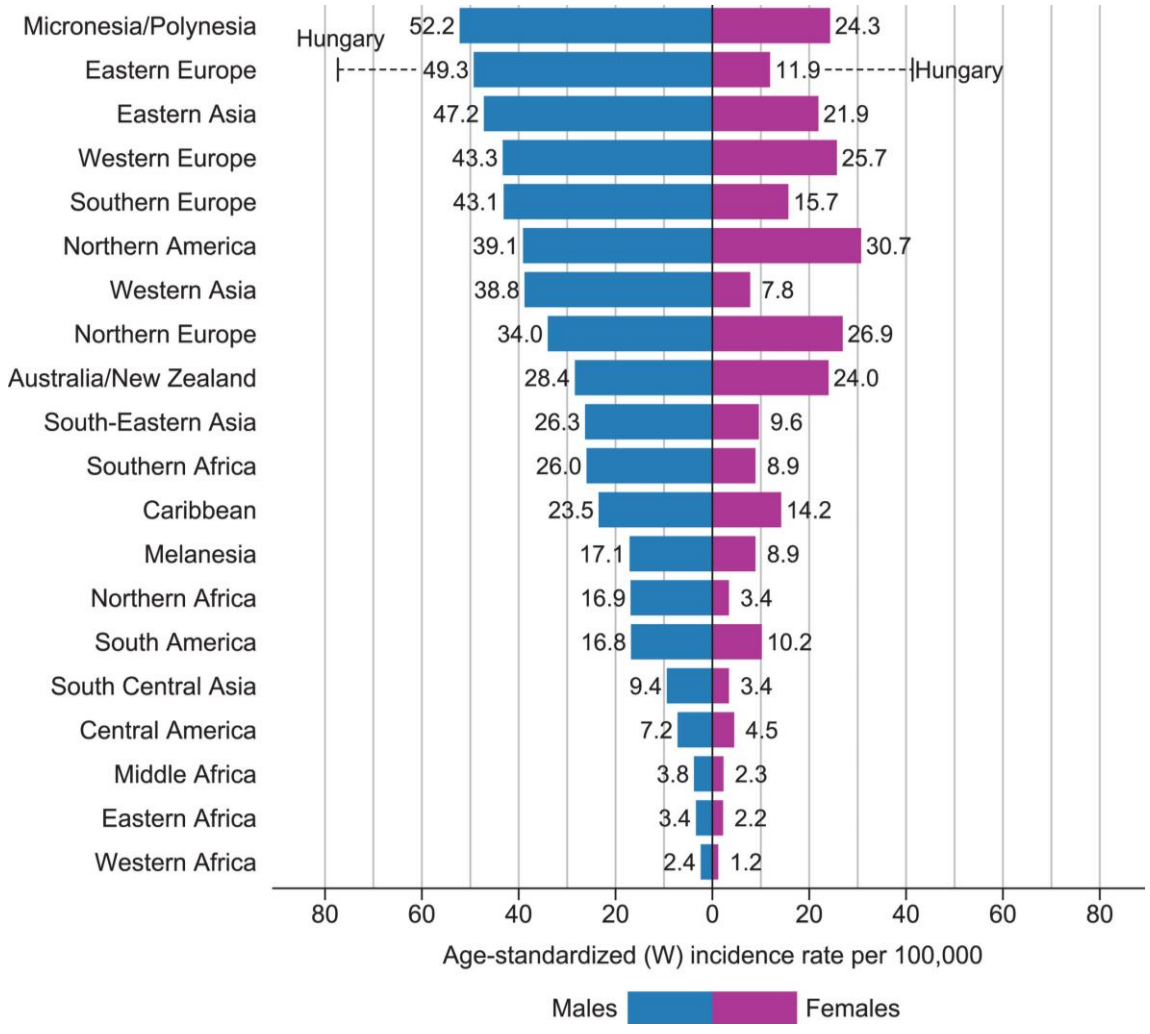

Figure 1.1: Region-specific incidence rates by sex for lung cancer in 2018. Rates are displayed in descending order of the world (W) age-standardised rate among men, and the highest national rates among men and women are superimposed. Source: GLOBOCAN 2018. Adapted from Bray et al. [2].

Cigarette smoking is the greatest risk factor for the progression of lung cancer, other risk factors include age, race, gender, radon exposure, occupational exposures, environmental pollution, and pre-existing lung disease. However, people without any known risk factors can also develop

lung cancer [4]. It has been confirmed that genetic changes make some people susceptible to lung cancer [5]. Additionally, smokers respond differently towards lung carcinogens (only 15% of smokers develop lung cancer) and acquired genetic changes, for instance, current or ex-smokers more frequently gain transversion mutations (substitution of a pyrimidine to a purine nucleotide or vice versa) while never smokers commonly have transition mutations (pyrimidine to pyrimidine or purine to purine nucleotide exchange) in the KRAS kirsten rat sarcoma (KRAS) viral oncogene homologue [5-7].

1.1.2 Histological classification of lung cancer

Lung cancer is a heterogeneous disease [8] and histologically is divided into two major classes: small-cell lung carcinoma (SCLC) and non-small cell lung carcinoma (NSCLC) [9]. SCLC is more aggressive and metastatic than NSCLC, which comprises around 12–15% of total lung cancers [9-11]. NSCLC accounts for at least 85-88% of all lung cancer cases and is divided into three subtypes: large cell carcinoma (10%), squamous cell carcinoma (30%) and adenocarcinoma (50%) [9].

1.1.3 KRAS mutation and NSCLC

KRAS mutations are placed third among the ten most frequent mutations in NSCLC patients according to the cBioPortal (https://www.cbioportal.org/) database [12, 13] that compute the published data on NSCLC (Figure 1.2) [14-20]. KRAS-mutant NSCLC patients show a shorter median survival compared to KRAS wild-type NSCLC patients [21-23]. Additionally, the KRAS-mutant patients are genetically heterogeneous with a high frequency of co-occurring mutations in lung cancer-linked pathways [24]. In NSCLC, KRAS mutations predominate in lung adenocarcinomas and rarely occur in squamous-cell cancers [25].

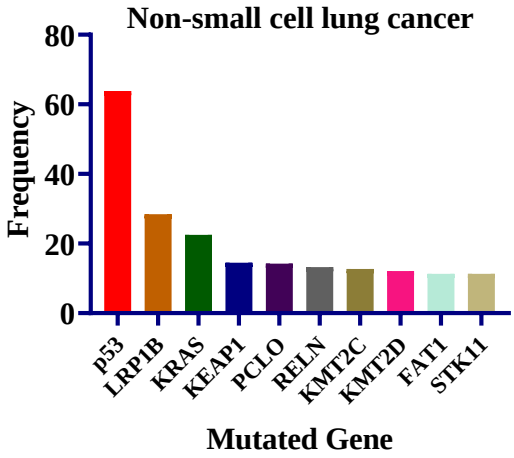

Figure 1.2: Ten most common mutated genes in NSCLC. This frequency distribution was calculated based on cBioPortal data on NSCLC patients (n=1872) [26].

As the response of KRAS-mutant NSCLC to chemotherapy is not satisfactory, numerous novel therapeutic strategies including direct targeting of KRAS, targeting KRAS membrane associations, the use of KRAS synthetic lethality, targeting downstream signalling pathways, and immunotherapy have been tried as an alternative to chemotherapy [25]. However, clinically approved therapies for KRAS-mutant NSCLC have yet to be developed.

1.2 Therapeutic targets of KRAS-mutated NSCLC

1.2.1 Targeting RAS and associated pathways

KRAS mutations are diagnosed in around 20-40% of NSCLC patients and occur frequently, but not exclusively, in adenocarcinoma and life-long smokers [27, 28]. In NSCLC KRAS is linked to poor prognosis and drug resistance [29]. The high frequency of KRAS mutations in NSCLC identifies it as a potential therapeutic target, however, KRAS remains an undruggable target as it is difficult to downregulate mutated KRAS-induced intracellular activity [30-34]. The development of drugs that target KRAS remains a key challenge in cancer research for the following reasons. Firstly, the activation and inactivation of KRAS is depended on its GTP or GDP binding status in preference to a substrate catalytic reaction [28, 35]. Secondly, KRAS has an affinity towards GTP at the picomolar level and cancer cells have micromolar levels of GTP [28]. Finally, KRAS lacks a suitable binding pocket for small molecule inhibitors, aside from the challenging nucleoside binding pockets [28]. Considering the key challenges, Figure 1.3 illustrates the possible therapeutic targets for KRAS-mutant NSCLC.

RAS proteins must associate with the cell membrane to link with guanine nucleotide exchange factors and other upstream regulators to transfer the extracellular signal to the downstream molecules. RAS proteins are produced as soluble precursors, these soluble precursors then undergo post-translational modifications (PTMs) before they interact with cell membranes. PTMs are mediated by enzymes that are an interesting target for therapy [25]. KRA-533, a novel KRAS agonist, suppressed KRAS-mutant lung cancer cells both *in vitro* and *in vivo* [28]. KRA-533 specifically interacts with the GTP/GDP binding pocket of KRAS to inhibit GTP cleavage, thereby increasing active GTP-bound KRAS which induced apoptotic and autophagic cell signalling pathways in cancer cells. cGMP phosphodiesterase 6 delta (PDEδ) subunit protein has a hydrophobic pocket that interacts with a farnesylatedhydrphobic cysteine residue located at the C terminus of RAS proteins. Deltarasin, a small molecule inhibitor, interfered with the interaction of PDEδ with RAS proteins, thereby inhibiting activation of RAS. *In vitro* and *in vivo* investigations confirmed that deltarasin induced apoptosis and autophagy in KRAS-mutant lung cancer cells. After binding with PDEδ, deltarasin induced apoptosis through RAS downstream signalling pathways, while it induced autophagy via the AMPK (AMP activated

protein kinase)-mTOR (mammalian target of rapamycin) signalling pathway. Interestingly, 3-methyl adenine (an autophagy inhibitor) enhanced deltarasin-mediated apoptosis through elevation of reactive oxygen species (ROS). On the other hand, the ROS scavenger N-acetylcysteine remarkably suppressed deltarasin-mediated cell death [36].

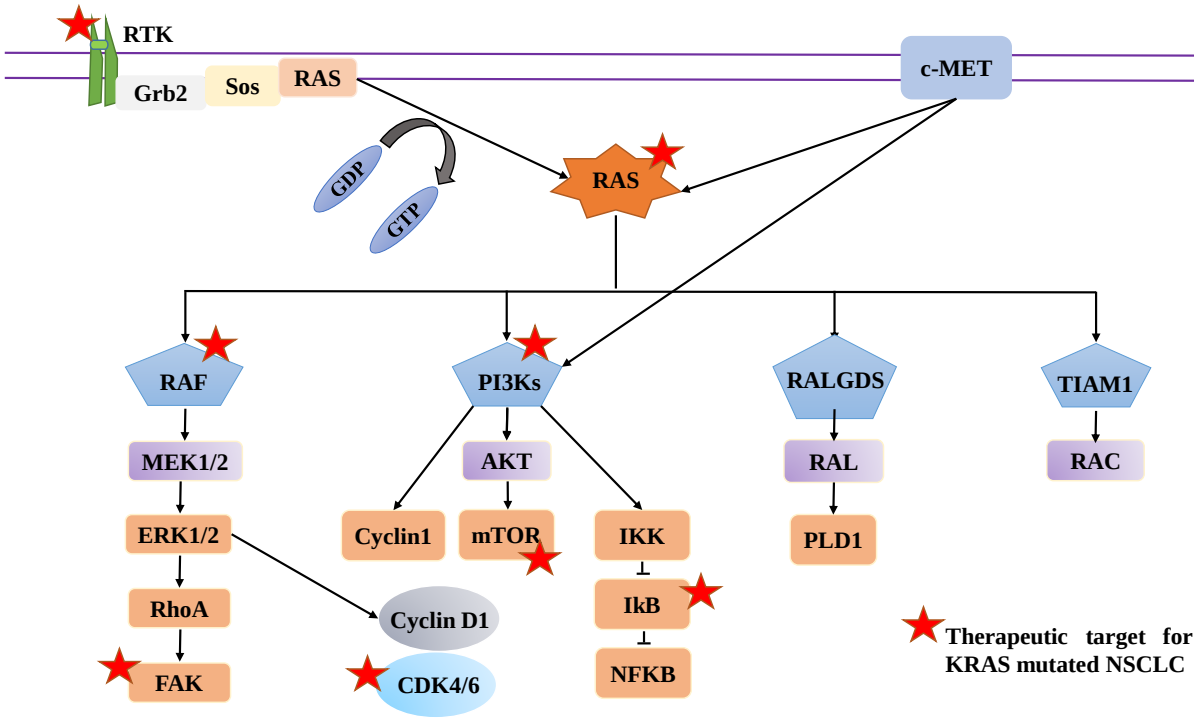

Figure 1.3: Potential therapeutic targets for KRAS-mutated NSCLC. Direct targeting of RAS protein or its downstream effector molecules linked with cell proliferation are potential therapeutic targets for KRAS-mutant NSCLC. RTK: receptor tyrosine kinase; GRB2: growth factor receptor-bound protein 2; SOS: son of sevenless; RAS: rat sarcoma; c-Met: a receptor tyrosine kinase belonging to the MET; RAF: rapidly accelerating fibrosarcoma; MEK: mitogen-activated protein kinase kinase; ERK: extracellular signal-regulated kinases; RHOA: ras homologue family member A; FAK: focal adhesion kinase; phosphatidylinositol-3-kinase (PI3K); AKT: Protein kinase B; mTOR: mammalian target of rapamycin; IKK: IkB kinase; NFKB: nuclear factor of the κ-chain in B-cells; RALGDS: Ral guanine nucleotide dissociation stimulator; RAL: Ras-like; PLD1: phospholipase D1; TIAM1: T-cell lymphoma invasion and metastasis inducing factor 1; RAC: a subfamily of the Rho family of GTPases. Information for the figure was taken from Roman et al. [21].

Epidermal growth factor receptor (EGFR) tyrosine kinase inhibitors (TKIs, *e.g.* gefitinib and erlotinib) suppress the RAS-RAF (rapidly accelerating fibrosarcoma)-MEK (mitogen-activated protein kinase kinase)-ERK (extracellular signal-regulated kinases) signalling pathway by inhibiting the catalytic activity of EGFR. However, the TKIs fail to inhibit the signalling cascades in the presence of KRAS mutation as RAS remains downstream to EGFR [37]. Antibody-based small molecule ligands interact with mutant KRAS (at sub-μM affinity), thereby inhibit RAS-effector protein-protein interactions and endogenous RAS-linked signalling in cancer cells of human origin including lung cancer cells [38]. RAS mutations

(particularly KRAS) leads to hyperactivation of RAF-MEK-ERK signalling [39]. For example, KYA1797K is an antiproliferative agent that effectively suppressed KRAS-mediated tumourigenesis by inhibiting the RAS-ERK pathway in a $KRAS^{LA2}$ mouse model [37]. Another therapeutic strategy is to target MEK as a downstream effector of RAS [39]. Kelly et al. reported that the combination of trametinib (a MEK inhibitor) and pemetrexed (an antimetabolite used in NSCLC treatment) produced a therapeutic benefit in 50% of KRAS-mutant NSCLC patients (n=20) with a disease control rate 65% of in a phase I/Ib study. These patients experienced fatigue, nausea, and peripheral oedema due to the side effects of the combination [40]. Additionally, selumetinib, a MEK inhibitor, suppressed the growth of NSCLC cells in a dose-depended manner while the growth inhibitory activity was accelerated by co-treatment with LY2228820 (a p38 inhibitor) [41]. Genetically modified mouse models of $KRAS^{G12C}$ lung tumours displayed significantly higher sensitivity to selumetinib in comparison to $KRAS^{G12D}$ tumours. MEK inhibition also enhanced chemotherapeutic activity and significantly promoted progression-free survival in $KRAS^{G12C}$ mice. However, the co-mutation of p53 rendered $KRAS^{G12C}$ lung tumours less responsive to combination treatment with selumetinib and chemotherapy [42]. Furthermore, small interfering RNAs towards MAPK14 that encodes p38α MAPK, accelerated the growth inhibitory potential of MEK inhibitors [41]. On the other hand, preclinical studies showed that phosphatidylinositol-3-kinase (PI3K) inhibitors are inefficient in KRAS mutations since the RAS-ERK signalling cascade hijacks tumour proliferation via a compensatory mechanism [21]. Combination therapy with mTOR inhibitor AZD2014 and WEE1 tyrosine kinase inhibitor AZD1775 exhibited synergistic and selective antiproliferative activity against KRAS-mutant NSCLC cell lines, which delayed the growth of human NSCLC xenografts and regressed murine adenocarcinoma. Furthermore, mTOR inhibition potentiated WEE1 inhibition through inactivation of DNA repair, accelerating DNA damage in KRAS-mutant NSCLC, and reduced cyclin D1 [43]. In addition, forkhead box transcription factor M1 (FOXM1) is a crucial transcription factor for KRAS-ERK signalling pathway in respiratory epithelial cells. FOXM1 is also involved in oncogenic KRAS-ERK signalling in neoplastic lung epithelial cells. FOXM1 deletion suppressed the $KRAS^{G12D}$ activated lung tumourigenesis. Therefore, it is postulated that pharmacological inhibition of FOXM1 could be beneficial for KRAS-mutant lung cancer patients [44]. KRAS mutation inactivates tumour suppressor genes INK4a/ARF/p16 leading to hyperactivation of the GTPase RHOA (ras homologue family member A) by MEK1/2 and ERK1/2 and RHOA-FAK (focal adhesion kinase) signalling cascade is involved in cell migration. Currently, defactinib, a FAK inhibitor is under clinical trial in KRAS-mutant NSCLC [21].

1.2.2 Cell cycle as a therapeutic target for KRAS-mutant NSCLC

Cell cycle occurs through different phases including G0/G1 (Gap phase), S (DNA synthesis phase), and G2/M (cell division) [45]. In the G1 phase, cells examine the internal and external environment to ensure conditions are favourable and complete the preparation before proceeding to the S and M phases [46]. Each stage of the cell cycle is controlled by the activity of a unique combination of cyclins and cyclin depended kinases (CDKs). The level of cyclins fluctuate throughout the cell cycle, which is primarily controlled by transcriptional activation and proteolytic degradation [47]. The net effect controls the "on" or "off" switches of CDK proteins and thereby regulates the stages of the cell cycle [48]. Additionally, the cyclin-CDK complexes often bind to cyclin-dependent kinase inhibitors (CKIs) such as p15, p18, p21, and p27, which inhibits the activity of CDKs, and control cell cycle progression [49]. The efficiency of an antiproliferative drug depends on the ability to stop the division of cancer cells by cell cycle arrest in the aforementioned phases [45].

The G1 cyclins consist of D-type cyclins such as cyclins D1, D2, and D3. G1 cyclins act in the early G1 phase of the cell cycle along with CDK4 and CDK6 [50]. G1 cyclins are relatively unstable when not bound with their catalytic partner (CDK). Cellular level of G1 cyclins remain low in the G0 phase and increase gradually upon the activity of mitogens [51]. Cyclin D1, D2, and D3 are almost indistinguishable biochemically and only cyclin D1 overexpression is prominent in cancer [52]. Compared to cyclin D2 and cyclin D3, cyclin D1 has greater functional characterisation and plays a widespread role in human cancers including lung cancer [53, 54]. Mitogens activate cyclin D1 through a complex mechanism that occurs at transcriptional and posttranscriptional levels. At the transcriptional level, growth factor-induced activation of cyclin D1 is dependent on the RAS-RAF-MEK-ERK signalling pathways [51]. Furthermore, disruption of the G1-S checkpoints leads to uncontrolled cell division and cancer progression [55]. Cyclin D1 together with CDK4/6 and cyclin E/CDK2 inactive the retinoblastoma protein through phosphorylation, thereby committing the cell to progress into DNA replication and mitosis [55, 56]. Cyclin D1 overexpression is linked to the early onset of cancer and enhance the risk of cancer progression and metastasis [56]. Cyclins A, D, and E control the transition from Gl phase to S phase, while cyclins A and B regulate the passage from the G2 phase to M phase [57]. G1 to S phase progression is not only dependent on the cyclins and CDK activity but also dependent on the down-regulation of CDK inhibitors, such as p27 and p21 [58]. In mammalian cells, cyclin B1 and Cdk1 expression occurs in late S and G2 phases and are active at the late G2 phase. Cyclin B1 is synthesised in the cytoplasm during S phase and imported to the nucleus at the late G2 phase, and degraded during anaphase through

a ubiquitin-related pathway [59].

KRAS-mutant lung cancer cells are susceptible to impairment of cell cycle control, as they have a particular requirement for kinases that control key components of cell cycle transition [60]. Among the driver's of cyclin/CDK complexes, cyclin D1/CDK4/6 and cyclin B1/Cdc2 have drawn considerable attention as cell cycle regulator as the former controls G1-S-phase transition while the latter regulates the G2-M-phase checkpoint [61]. Puyol et al. reported that there is a synthetic lethal interaction between CDK4 and KRAS oncogene in a mouse tumour model which mimics human NSCLC. Briefly, inhibition of CDK4 activity either by genetic knockdown or CDK4 selective inhibitor (*e.g.* PD0332991) in the mice carrying $KRAS^{G12V}$ lung tumours halted tumour progression and confirmed the role of CDK4 in KRAS-mutant lung cancer. Therefore, targeting CDK4 could be a potent therapeutic target for KRAS-mutant NSCLC [62]. There is a positive correlation between KRAS mutation and CKD4/cyclin D levels in lung cancer patients. Therefore, ATP-competitive inhibitors (ATPis) of CDK4 could be used in the treatment of cancer patients, unfortunately, these inhibitors have limited specificity and efficacy. Targeting the interaction of CDK4 and cyclin D is an alternative to the ATPis. Abemaciclib (a competitive inhibitor of ATP) in combination with staple peptide. Staple peptide rapidly and efficiently enters into the cultured cells and inhibits CDK4 catalytic activity by colocalising with CDK4 and cyclin D1, thereby suppressed KRAS-mutant orthotopic NSCLC tumours [63].

Cyclin D1 is not only involved in cell cycle progression at the G1 checkpoint but also in the regulation of apoptosis and growth suppression by binding with several transcription factor families (Figure 1.4) [53, 64]. Multifunctional activities of cyclin D1 could influence the therapeutic response of NSCLC patients (cyclin D1 positive) [64]. KRAS-mutant NSCLC patients having low cyclin D1 expression showed a better prognosis compared to patients having high cyclin D1 expression (median overall survival 41.7 vs 3.5 months, p=0.037) [65].

Like cyclin D1, cyclin B1 is also overexpressed in KRAS mutations [66]. Cyclin B1 not only controls G2/M phase progression but is also involved in differentiation, cell growth, metastasis, and apoptosis in many cancers including lung cancer [67, 68]. The knockdown of cyclin B1 suppressed the proliferation of cancer cells in both *in vitro* and *in vivo* models [69]. Additionally, purvalanol A, a highly selective inhibitor of CDK1 (cyclin B1 partner), accelerated taxol-induced apoptosis, inhibited colony formation, and cell proliferation in NCI-H1299 NSCLC cells [70]. Additionally, NSCLC patients with cyclin B1 positive tumours showed shorter survival time compared to cyclin B1 negative tumours [57]. Therefore, cyclin

B1 has become a novel prognostic marker and potential therapeutic target for NSCLC [61].

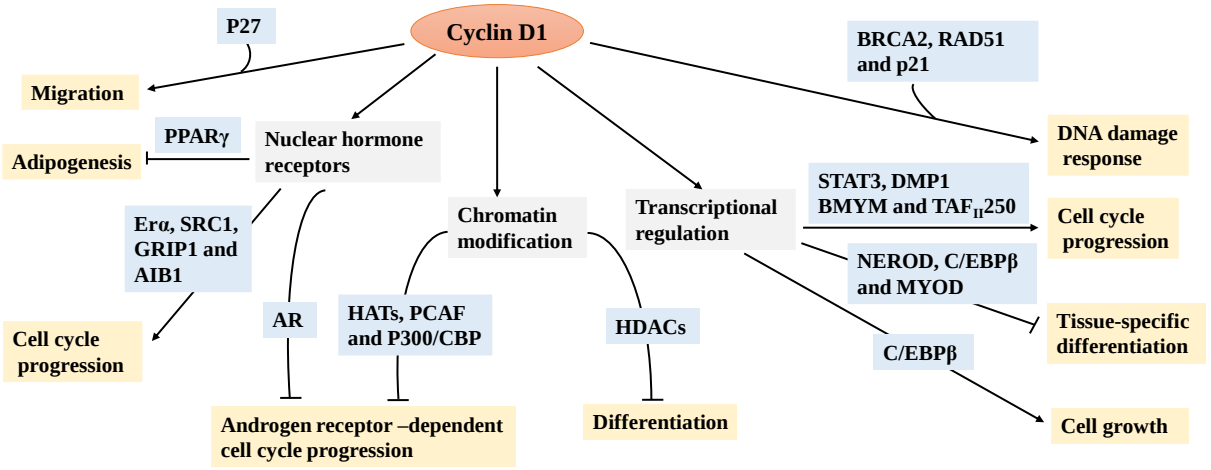

Figure 1.4: Non-catalytic functions of cyclin D1. Although p21 and p27 are constituents of CDK4 or CDK6 complexes, cyclin D1 binding to p21 or p27 leads to effects on migration and response to DNA damage, respectively. The DNA damage responses can be achieved via interactions with RAD51 and breast cancer 2 gene (BRCA2). Additionally, cyclin D1 regulates cell proliferation, cell growth, and differentiation by binding with nuclear hormone receptor family members (oestrogen receptor-α (ERα), androgen receptor (AR) and peroxisome proliferator-activated receptor-γ (PPARγ) and their co-activators (SRC1, GRIP1, and AIB1), BMYB and the MYB-related transcription factor DMP1, as well as the helix–loop–helix transcription factors NEUROD1, MYOD, and C/EBPβ. Furthermore, cyclin D1 binds with histone acetyltransferases (HATs) such as P/CAF3, p300/CBP, and histone deacetylases (HDACs). Generalised effects of cyclin D1 on transcription results from its binding to TAFII250 (also known as TAF1), a subunit of the basal transcriptional machinery. SRC1: steriod receptor coactivator 1; AIB1: amplified in breast cancer 1; GRIP1: glutamate receptor-interacting protein 1; NEUROD1: neurogenic differentiation factor 1; MYOD: myoblast determination protein 1; C/EBPβ: CCAAT-enhancer-binding proteins β; P/CAF3: CBP-associated factor 3; STAT3: signal transducer and activator of transcription 3. Information for the figure was taken from Musgrove et al. [53].

1.3 Novel metal-based drugs

Transition metal complexes are found in a diverse range of novel diagnostic and therapeutic agents, including anticancer drugs [71]. Metal-based drugs became a focus of potential cancer therapeutic agents after the discovery of platinum drugs (such as cisplatin, oxaliplatin, and carboplatin) [72, 73]. The growing interest of metal-incorporated complexes in cancer therapy is due to unique properties of metals such as charge variation, geometry, variable coordination modes, lewis acid property, redox activity and reactivity towards organic substrates [74, 75]. Interestingly, metals form positively charged ions in aqueous solution which can interact with the negatively charged biomolecules. The charge can be manipulated based on coordination molecules, leading to the generation of cationic, anionic, or neutral species [73]. Furthermore, the lewis acid properties of metal ions characterised by high electron affinity can remarkably polarise groups that are linked with them, thus promoting hydrolysis reactions [73, 74]. It has

been reported that single charged cations are generally more toxic, and alkyl group linked metals displayed higher toxicity compared to the aryl group [76]. Another feature of metals is their redox potential that makes them a suitable candidate to target cancer cells with disturbed redox homeostasis [77]. Additionally, organometallic complexes are "pro-drugs" that can be activated by the cellular environment (by redox reactions or ligand exchange), and the ligands may act as the active drug [75, 78]. The special features of metals become an attractive probe in metal-based drug design via ligand modification and substitution of the available chemical structures or novel structures that selectively interact with the cellular target with an improved cytotoxic and pharmacokinetic profile [74].

Platinum-based metallodrugs, cisplatin, and its analogue have been prescribed for lung cancer treatment. However, noticeable side effects and tumour resistance have limited their clinical application [79]. Many platinum-based drugs have been investigated as an alternative to cisplatin, however, due to the lack of a superior advantage platinum drugs including spiroplatin, miboplatin, sebriplatin, cycloplatam, SPI-077, BBR3464, SPI-077, aroplatin, TRK-710, iproplatin, enloplatin, zeniplatin, ormaplatin, NSC 170898 and JM 11 have been discontinued from clinical trials [74]. Therefore, rhodium (Rh), iridium (Ir), ruthenium (Ru), and osmium (Os) based compounds have been considered as an alternative to platinum-based compounds [80, 81].

Rh is one of the noble, rare, and precious transition metals of the platinum metals group [82]. Rh complexes have drawn much attention due to their synthetic versatility and a range of potential biomedical applications including antimicrobial and anticancer agents [83, 84]. Organorhodium complexes are present in various oxidation states and are reported to inhibit cell division by disrupting DNA synthesis and act as cytostatic agents before inducing cell death [83]. Many Rh compounds exhibited antiproliferative activity against Lewis lung carcinoma, lung metastatic tumours, B16 melanoma, Ehrlich ascitic tumours, oral carcinoma, P388 lymphocytic leukaemia, L1210 leukaemia, and MCa mammary carcinoma among others [85, 86]. Rh (III) complexes are the most explored organorhodium [83]. Rh (III) metalloinsertors exhibited anticancer activity at low micromolar concentration against HCT116O and HCT116N isogenic colon cancer cell lines. The potential mechanism was their binding with DNA mismatches and thereby disruption of DNA synthesis [87]. Specifically, pentamethylcyclopentadienato (Cp) arene ring containing half sandwich Rh curcumin (cur) complex [Rh(*Cp)Cl(cur)] displayed antiproliferative activity against human epithelial A549 lung cancer cell lines with an IC_{50} value of 31 μM [88]. Due to promising anticancer potential, many Rh complexes have entered the phase I clinical trials [86].

Ir is found in four oxygenation states (II, III, IV, and VI) and has excellent electrical and thermal properties [89]. In recent times, Ir based compounds have been explored extensively for medical and biological applications including anticancer therapy [90]. Ma et al. tested four half sandwich Ir (III) complexes against A549 cells, two of them (IC_{50} values of <4.3 μM) showed promising antiproliferative activity compared to cisplatin which exhibited an IC_{50} value of 21.3 μM [91]. Liu and colleagues examined the growth inhibitory activity of eight half-sandwich cyclopentadienyl Ir (III) pyridine complexes and all the compounds displayed promising antiproliferative activity against A549, A2780 ovarian, and MCF7 breast cancer cells. Among these, the 4-dimethylaminopyridine based complex exhibited the highest anticancer activity in the submicromolar range and was more potent than cisplatin [92].

Ru based complexes showed quite promising pharmacological behaviour along with an acceptable toxicological profile [93]. Ru containing new chemotherapeutic agents in cancer treatment have drawn considerable attention due to their iron mimicking properties (*i.e.*, bind to plasma proteins including transferrin, albumin), strong interaction with biomolecules such as proteins, RNA and DNA, the presence of two oxidation states (II and III), ligand exchange kinetics, low toxicity and non-cross resistance with conventional platinum-based drugs [79, 94-96]. Three ruthenium-based drugs namely NAMI-A, KP1019, and NKP-1333 (a sodium salt of KP1019) have reached clinical trials [79, 97]. NAMI-A was the first Ru compound used in clinical practice. It was proven to be effective against metastatic lung cancer. Recently, NAMI-A was used in combination with gemcitabine (a deoxycytidine analogue) as a second-line chemotherapy in managing advanced NSCLC [89, 98].

Os is the densest metal and is slightly denser than Ir [99]. The three-dimensional configuration of the Os compounds (generally octahedral with 6 ligands) offers a versatile platform for the selective identification and interaction with therapeutic targets (*e.g.* protein, DNA). Os compounds have different oxidation states such as Os (II), Os (III), Os (IV), and even higher, diverse oxidation states allows Os to regulate biological redox in cancer cells [100]. Additionally, Os displayed antiproliferative activity in a variety of oxidative states and it possessed oxidative stress via a multi-targeted mechanism that mitigated the chance of drug resistance [101]. It has been reported that the Os complex FY26 exhibited submicromolar anticancer activity towards A549, MCF7, A2780, and HCT116 (colon cancer) cell lines [80]. Furthermore, *trans*-$[Os^{III}Cl_2(pyrazole)_4]Cl$ displayed antiproliferative activity in the micromolar range against A549, CH1 (ovarian cancer), and SW480 (colon cancer) cell lines while the corresponding Ru analogue was less potent against these three cell lines [102]. Buchel and colleagues reported that KP1019 (a Ru based antiproliferative drug in phase I clinical trials)

was inactive towards A549 cells while its Os (IV) analogue exhibited anticancer activity [103].

1.4 Organometallic arene complexes

Organometallic transition metal-arene complexes have drawn considerable attention as anticancer drug candidates. The metal-carbon bond and π-bound arene bond in metal-arene complexes offers high reactivity and kinetic stability [104]. The arene substituent shares a lipophilic surface which facilitates cellular diffusion at the lipophilic cell membrane [105]. The hydrophobicity and hydrophilicity of the metal-arene complexes can be tuned via a metal-arene system, resulting in selective uptake into cancer cells [104]. Additionally, coordination of the organic compound to a metal center offers stability and facilitates the unique chemical space that cannot be attained by the organic molecule itself. Furthermore, metal coordination facilitates the outreach of the organic compound in the intracellular region [106]. Recently, metal-arene complexes were reported to have promising anticancer activity [90, 95, 107, 108]. For instance, novel organometallic tetranuclear Ru (II) arene complexes, $[Ru_4(\eta^6\text{-p-cymene})_4(benzil)(Cl)_6]$ and $[Ru_4(\eta^6\text{-p-cymene})_4(oxalaldehyde)(Cl)_6]$ possessed both anticancer and antimetastatic activity against cisplatin resistant A549 lung cancer cells [95]. In another study, the anticancer potential of six half-sandwich luminescent Ir and Ru complexes containing P^P-chelating ligands 1,2-bis(diphenylphosphino)-benzene (L1) and 1,8-bis-(diphenylphosphino)-naphthalene were examined in A549 and HeLa (human cervical cancer) cells. All the compounds showed a more potent effect compared with cisplatin in both cell lines. The most potent drug $[(\eta^5\text{-}Cp^{xbiph})Ir(L1)Cl]PF_6$ (where, Cp^{xbiph}=1-(4-biphenylyl)-2,3,4,5-tetramethyl-1,3-cyclopentadiene) was 73 times more efficient than cisplatin towards A549 cells [90]. Furthermore, some half-sandwich piano-stool Os (II) complexes displayed considerable anticancer activity *in vitro* without cisplatin cross-resistance [109-111]. Additionally, Peacock and coworkers tested the anticancer potential of piano stool Os (II) arene complexes with the general formula [(η6-arene)Os(N,O)Cl] against A549 and A2790 (ovarian cancer) cell lines. Three of these compounds, $[(\eta^6\text{-p-cymene})Os(picolinate)Cl]$, $[(\eta^6\text{-biphenyl})Os(picolinate)Cl]$ and $[(\eta^6\text{-p-cymene})Os(8\text{-hydroxyquinolinate})Cl]$ showed anticancer activity comparable to the platinum-based drug carboplatin [112]. Gatti et al. synthesised two structurally similar novel half-sandwich Os (II) and two Ru (II) thiocarbazone complexes that showed antiproliferative activity against A549, A2780, A2780i cisplatin-resistant ovarian, PC3 prostate and HCT116 cancer cells [107]. Three Os (II) arene complexes bearing phenylazopyridine ligands with dimethylaminyl or hydroxyl substitution on the phenyl ring and chloride iodide leaving groups displayed concentration- (submicromolar to micromolar range) and time-dependent toxicity against A549 cancer cells. These compounds

were also reported to have nanomolar anticancer activity towards human breast, colon, ovarian, prostate, and bladder cancer cell lines [108].

Diverse structure and ligand orientation in half-sandwich complexes are an attractive choice in novel drug development [113]. Metal-based half sandwich piano-stool type arene complexes offer a wide range of chemical modifications to the arene (such as η^5-C_5H_5, η^6-C_6H_6) and its substituents (R), the monodentate leaving group (X), the ligands Y and Z (can be chelating or monodentate ligands), and net charge of the metal complex (n+) (Figure 1.5). Fine-tuning of structural architecture, kinetics, and thermodynamics of the system is a sensible drug design alternative to platinum-based drugs [114-117]. The fine-tuning offers desired chemical reactivity and pharmacological properties such as cellular uptake, biomolecular interactions, distribution, cytotoxic effects, and detoxification mechanisms [117, 118].

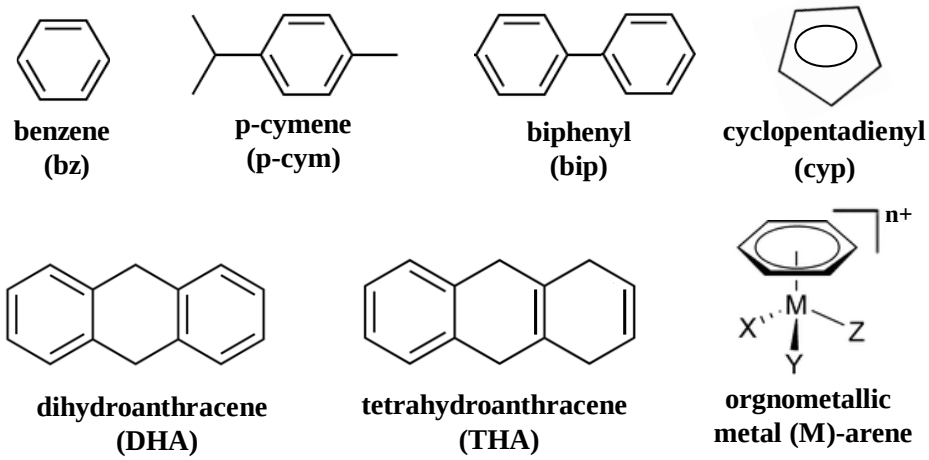

Figure 1.5: Various arene and organometallic metal arene structures. In the organometallic M-arene complex bz is used as a representative of arene (p-cym, bip, cyp, DHA, THA). In this piano-stool type M-arene complex X is the leaving group, Y and Z are chelating or monodentate ligand.

1.5 Different drug classes investigated in the current study

1.5.1 HDAC inhibitors

Epigenetics studies heritable changes in gene expression that are not exerted by the alteration of genomic code [119, 120]. Three interconnected epigenetic processes control gene expression at the chromatin level including DNA methylation, nucleosomal remodeling, and covalent modifications of histone [120]. PTMs of the N-terminal end of the histone proteins occurs through acetylation, methylation, phosphorylation, deamination, ubiquitination, sumoylation, proline isomerisation, and ADP ribosylation [121]. Histone modifications via acetylation plays a major role in epigenetic regulation of gene expression which is controlled through the balance between histone acetyltransferases (HAT) and histone deacetylases (HDAC) [122]. In many

cancer cells including NSCLC, the balance between HAT and HDAC is disrupted (Figure 1.6) [120, 123].

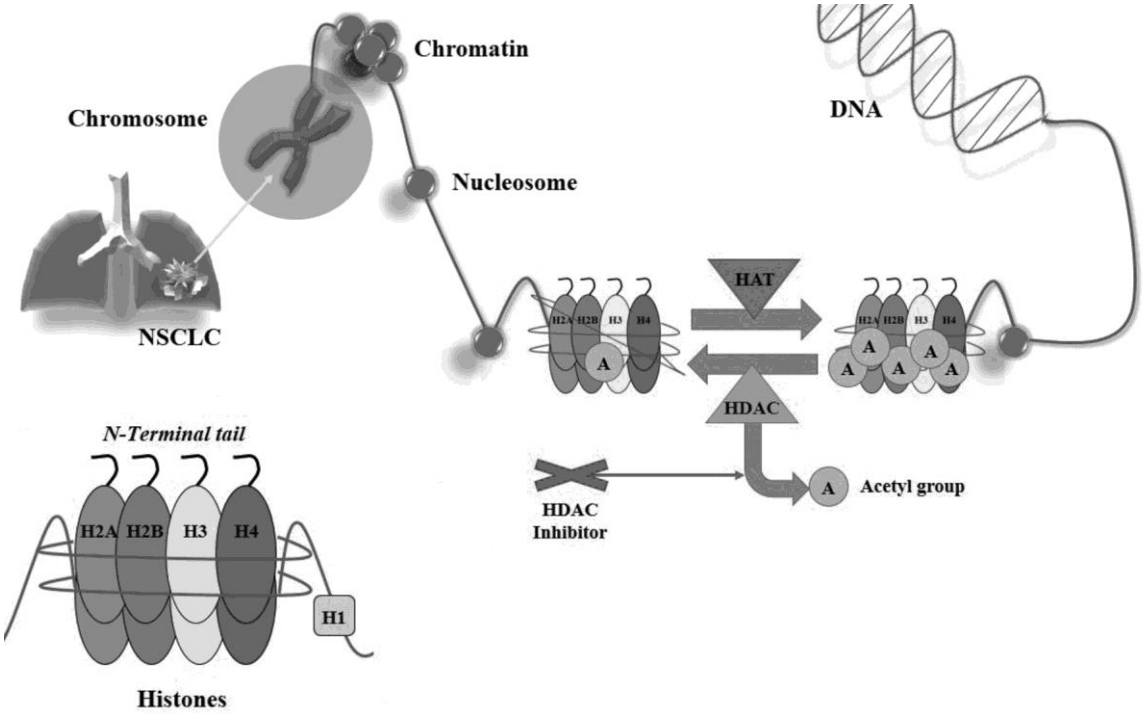

Figure 1.6. Histone deacetylase (HDAC) mechanism of action. NSCLC: non-small cell lung cancer; HAT: histone acetyltransferase [124].

Eighteen human HDAC enzymes are divided into four classes based on their homology with yeast HDACs [125]. Class I, II, and IV are Zn^{2+} -dependent on metalloproteins, while class III is a nicotinamide adenine dinucleotide (NAD^{+})-dependent enzyme (Table 1.1) [126]. Class I comprises HDACs 1, 2, 3 and 8 that are located in the nucleus; class II includes HDACs 4, 5, 7, 9, and 10, which are located both the cytoplasm and nucleus; class IV comprises HDAC 11. Unlike conventional HDACs, class III is composed of seven mammalian sirtuins (SIRT1-7) [125]. The acetylation of histones in the nucleosomes alters chromatin conformation and thereby regulates gene expression. It has been reported that the aberrantly overexpressed HDACs in different tumours leads to carcinogenesis, cancer progression, and poor therapeutic outcome. Therefore, HDAC can be a therapeutic target to reverse the genetic changes that are linked with cancer progression and drug resistance [127].

Histone deacetylase inhibitors (HDACis) based dual molecular targeted therapy could be a promising therapeutic approach for KRAS-mutant NSCLCs [128, 129]. An HDACi (belinostat) in combination with a MEK inhibitor (trametinib) exhibited synergistic activity towards RAS mutated lung cancer cells via an increase of forkhead box protein O1 (FOXO1), forkhead box

protein O3a (FOXO3a), bcl-2-like protein 11 (BIM), cell cycle inhibitors ($p21^{Cip1}$ and $p27^{Kip1}$) and acetyl H3 level [128]. Suberoylanilide hydroxamic acid (SAHA) showed antiproliferative activity against the KRAS-mutant A549 cells, it also enhanced the efficacy of carboplatin and paclitaxel in the same cell line [130].

Table 1.1: Classification of HDACs

Group	Class	Homology to yeast	Name	Subcellular location	Location in body
Classical (Zn dependent)	Class I	Rpd3	HDAC 1	Nucleus	Ubiquitous
			HDAC 2		
			HDAC 3		
			HDAC 8		
	Class IIa	Had1	HDAC 4	Nucleus/ cytoplasm	Tissue specific
			HDAC 5		
			HDAC 7		
			HDAC 9		
	Class II b	Had1	HDAC 6	Cytoplasm	Tissue specific
			HDAC 10		
	Class IV	Rpd3/Had1	HDAC 11	Nucleus/ cytoplasm	Tissue specific
NAD Dependent	Class III	Sir2	SIRT (1-7)	Nucleus/ cytoplasm/ mitochondria	Tissue specific

HDAC: histone deacetylase; NAD: nicotinamide adenine dinucleotide; SIRT=sirtuin [120, 126, 131-133].

HDACis are relatively novel antiproliferative agents that target zinc domain to induce apoptosis, cell death, and cell cycle arrest in cancer cells through epigenetic and non-epigenetic regulation (Figure 1.7) [125, 134]. Class I, II, and IV HDACis contain a metal-binding moiety in the protein active site, an alkyl linker which is encompassed by a hydrophobic tunnel, and a capping group that is exposed to the surroundings. The metal-binding moiety is structurally similar in HDAC class I, II, and IV and is crucial for HDACi activity [135]. HDACis are categorised based on the chemical structure into hydroxamates (*e.g.* SAHA), benzamides (*e.g.* entinostat), aliphatic acids (*e.g.* phenylbutyrate) and cyclic peptides (*e.g.* romidepsin). These HDACis are active at a wide range of concentrations, millimolar to micro and nanomolar values for butyrates, entinostat/SAHA, and trichostatin A/tetrapeptides, respectively [134].

Hydroxamic acid is a potent moiety in the field of cancer therapy. Compared to other hydroxamic acid derivatives, SAHA has drawn considerable attention as a potent anticancer agent [136]. SAHA has a broad range of HDAC inhibitory activity, specifically, it inhibits class I and class II. The transcriptional effects of SAHA could be exerted either by direct binding

with HDAC or indirectly acting on the transcriptional factors such as E2F-1, Smad 7, YY-1, p53, GATA-1, and Bcl-2. The non-transcriptional effects of SAHA include inhibition of angiogenesis, cell cycle arrest, apoptosis, and downregulation of immunosuppressive interleukins [138]. Following FDA approved doses the most common side effects include fatigue and gastrointestinal symptoms (*e.g.* diarrhoea, anorexia, and nausea) [138-140]. Thrombocytopaenia, severe anaemia, pulmonary oembolism, dehydration, and squamous cell carcinoma are the life treating side effects that require specialised care and hospitalisation [138, 140]. Additionally, corrected QT interval (QTc) prolongation has also been reported for some patients after SAHA treatment. SAHA (category D drug in pregnancy) could have a potential risk when used by pregnant women, as SAHA crosses the placenta and could harm the developing foetus [138]. SAHA is more effective against haematological malignancy than solid tumours. To overcome this therapeutic barrier SAHA is used in combination with other anticancer agents in clinical trials. However, due to the unpredictable drug-drug interaction and pharmacokinetic profile, the desired therapeutic effect could not be achieved by combination treatment [141].

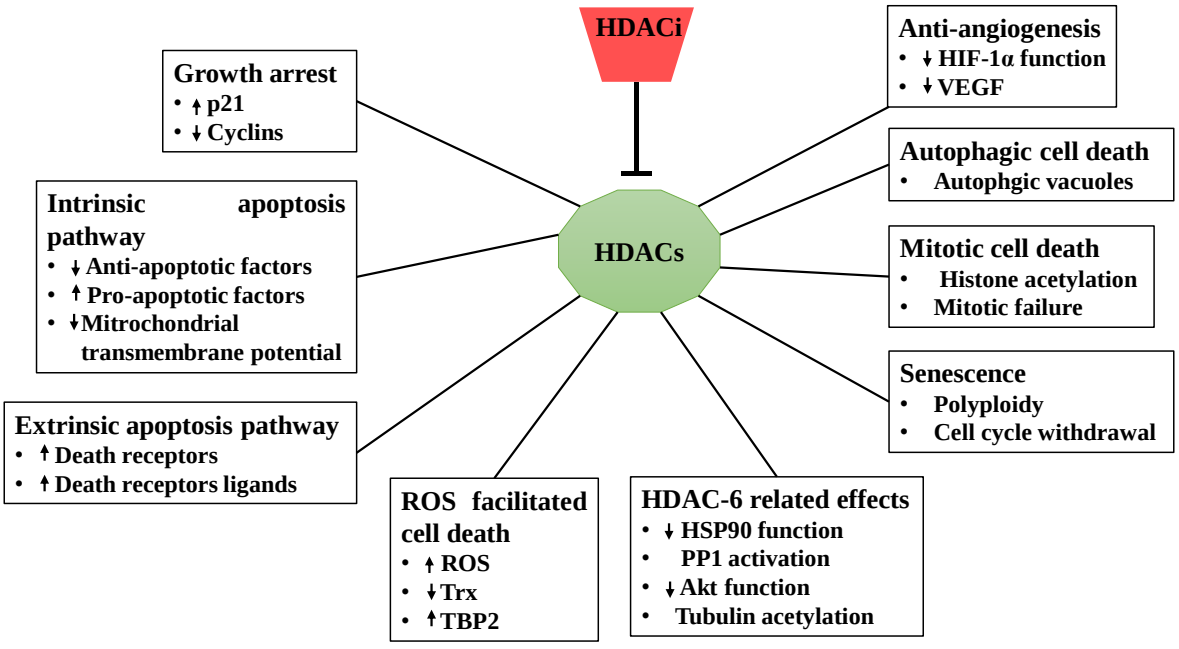

Figure 1.7: Multiple HDACi-activated antitumour pathways. HDAC6: histone deacetylase 6; HIF-1α: hypoxia-induced factor-1α; HSP90: heat-shock protein 90; PP1: protein phosphatase 1; ROS: reactive oxygen species; TBP2: thioredoxin binding protein 2; Trx: thioredoxin; VEGF: vascular endothelial growth factor. Information for the figure was taken from Xu et al. [137].

Toxicity and efficacy of HDACis are a major concern, both of them are at least partially due to the failure of the target-specific delivery of HDACis [135]. As only a few isoform-selective

HDACis have been reported and the clinical toxicity of HDACis is poorly characterised. Furthermore, the sequence similarity at the active site of the isoform is another concern in the design of selective HDACis [142]. Structure-activity relationship (SAR) studies, especially on SAHA's linker area remains relatively unexplored, even though the linker region could influence efficacy [142]. C2, C3, C6-SAHA libraries summarised that the steric effect on the SAHA carbon linker reduced inhibitory activity and influenced selectivity [142-144]. Crebinostat, a hydroxamic acid-based HDACi, differs from SAHA in the length of aliphatic linker (n) and cap moiety. Variation in the linker length (n=4-6), crebinostat (n=5) analogues showed different selectivity and inhibitory activity towards HDAC 1, 2, or 3. Specifically, as the carbon number in the linker region increased the HDAC 1, 2, or 3 inhibitory potential of the crebinostat analogue [145]. Zong et al. modified SAHA through the addition of an azido linker with the hydroxamic acid group either an ester (SAHA-eAzide, ester-linker-modified SAHA) or amide bond (SAHA-aAzide, amide-linker-modified SAHA). SAHA alone and ester-linker-modified SAHA (*i.e.* SAHA-eAzide) increased apoptosis and induced hyperacetylation of histone protein in comparison to control. Interestingly, SAHA-eAzide failed to improve the apoptotic actions of SAHA. On the other hand, the amide modified SAHA (*i.e.* SAHA-aAzide) did not promote histone hyperacetylation or apoptosis, indicating that such chemical modification inactivates SAHA [135]. From docking studies, it has been reported that the linker group connects the ZBG and cap group. The ZBG chelates the Zn^{2+} at the active site while the cap interacts with the active site. Modification of the cap group could be an effective strategy to regulate the HDAC inhibitory activity by controlling the affinity of the compounds towards the surface group of the HDAC enzymes [141]. Spencer and colleagues reported that the three-dimensional tuning of the aryl "cap" of SAHA is a promising strategy that broadens the potential in HDACi design [146]. Modification of the cap group of the SAHA analogue showed improved HDAC inhibitory activity and selectivity [141]. Jay amin hydroxamic acid (JAHA) and homo-JAHA are metal-based analogues of SAHA that incorporate the ferrocene unit in the structure (at the cap site of SAHA). Like SAHA, the metal-based analogues exhibited broad inhibitory activity toward class I HDACs, including HDAC 8. Compared to SAHA, homo-JAHA was more effective against HDAC 8 and less potent towards HDAC 6 [146]. Since the application of JAHA, several metal-based analogues, including Rh and Ir complexes, have appeared [147, 148].

Amide-based molecules have drawn the attention in drug research due to their biocompatibility and potential biological activities including anticancer, antibacterial, insecticidal, fungicidal, and herbicidal actions. An amide linkage (-CO-NH-), is a core structural unit that connects the amino acids in the protein and is pervasive in nature [149]. Pyridine-2-carbothioamide (PCA)

contains an amide bond in its structure. PCA could act as a bidentate chelating agent through the pyridine nitrogen and either the nitrogen or the sulfur of the carbothioamide group [150]. PCA derivatives have shown promise as antimicrobial and antiproliferative agents [151, 152]. N-(8-quinolyl)pyridine-2-carboxamide, a PCA based compound that displayed significant antiproliferative activities towards the HL60 (human leukaemia), P388 (murine leukaemia), BEL7402 (human hepatocellular carcinoma) and A549 cell lines [151].

Multitargeted antiproliferative agents developed through a combination of more than one bioactive moiety may show synergistic activity [153]. Based on this idea, PCA and hydroxamic acid (a moiety of SAHA) were combined by our collaborators to synthesise N^1-hydroxy-N^8-(4-(pyridine-2-carbothioamido)phenyl)octanediamide (JAZZ-90), a novel hydroxamate that differs from SAHA in the length of the aliphatic linker and the cap, modified with the addition of PCA with the phenyl group of SAHA [153]. [Chlorido(η^5-pentamethylcyclopentadienyl)(N^1-hydroxy-N^8- (4- (pyridine-2-carbothioamido-κ^2N,S) phenyl) octanediamide) iridium (III)] chloride (JAZZ-166) and [chlorido(η^5-pentamethylcyclopentadienyl)(N^1-hydroxy-N^8-(4-(pyridine-2-carbothioamido-κ^2N,S)phenyl)octanediamide)rhodium(III)]chloride (JAZZ-167) are the Ir and Rh complexes of JAZZ-90, respectively (Figure 1.8). JAZZ-166 and JAZZ-167 contain a cyclopentadienyl ligand (Cp, also called 1,2,3,4,5-pentamethylcyclopentadiene) linked with the metal group. Cyclopentadienyl ligands increases the hydrophobicity, which may accelerate the antitumour efficacy of the metal complexes [104].

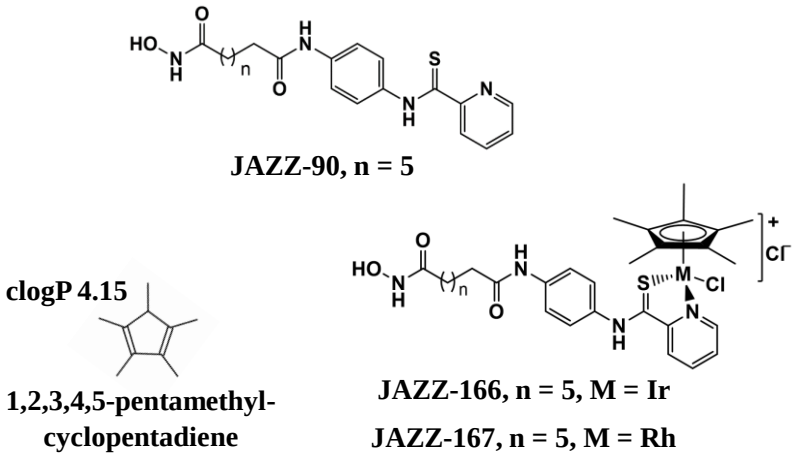

Figure 1.8: Novel HDAC inhibitors examined in this study. clog P denotes calculated log P, clogP the value determined using Molinspiration online software tool [154].

JAZZ-90, JAZZ-166, and JAZZ-167 displayed anticancer activity towards human cancer cells including HCT116, H460 (KRAS-mutated NSCLC), SiHa (cervical cancer), and SW480. The antiproliferative activity of JAZZ-90 was comparable to SAHA [153]. Additionally, JAZZ-167

exhibited low toxicity in haemolysis studies and in zebrafish and this might be due to the metal centre. Furthermore, JAZZ-167 downregulates vascular endothelial growth factor receptor 2 (VEGFR2) expression, while SAHA upregulated VEGFR2 [153].

1.5.2 Hydroxythiopyridone derivatives

The pyridine ring is considered one of the simplest heteroaromatic structures incorporated in many natural (*e.g.* niacin, pyridoxine, the ubiquitous redox system $NADP^+$/NADPH, etc.) and synthetic compounds [155]. Pyridine moieties are often used in synthetic drugs due to several special features such as water solubility, basicity, molecular size, hydrogen bond-forming ability, and stability [155, 156]. Pyridine moieties play an important role in drug discovery due to their activity as the bioisosteres of amides, amine, benzene rings, and heterocyclic rings [156]. Functionalisation with the pyridine moieties sometimes exerts biological activities of the parent compounds such as anticancer, antiviral, antimicrobial, antidepressant, antidiabetic, cardiotonic, anticonvulsant, and insecticidal [157]. Furthermore, pyridine compounds coupled with metals display high cytotoxicity and anticancer activity [158]. Pyridine ring containing water-soluble Ru (II) thiosemicarbazone complex ($C_{22}H_{39}Cl_3N_{10}P_2RuS \cdot C_2H_5OH \cdot H_2O$) showed anticancer activity against 41M ovarian cancer, SK-BR-3 breast cancer, HT29 colon cancer, and A549 cells with IC_{50} values of 0.87, 39, 186, and 47 µM, respectively [159].

Many synthetic biomolecules that have thiol-reactive moieties in the structure displayed enhanced cellular association and internalisation (Figure 1.9) [160]. For instance, modification of doxorubicin (DOX), an anticancer drug, with the thiol (SH) group improved the biological function of DOX. Briefly, DOX-SH and DOX-SS-pyridine (SS=disulfide) showed significantly higher or comparable cytotoxicity against HT-1080 fibrosarcoma, HEK293 human embryonic kidney, and CCRF-CEM human leukaemia cells compared to DOX alone, which might be due to high cellular uptake and activity in these cells [161].

Selective inhibitors against HDAC remains a challenge for researchers [162]. To explore alternatives to hydroxamic acid as the zinc-binding group (ZBG), Patil et al. tested 3-hydroxypyridin-2-one (3-HP) and 3-hydroxypyridin-2-thione (3-HPT) as a novel ZBG and their potential HDACi activity [163]. Preliminary *in silico* molecular docking analysis using AutoDock 4.2 revealed that 3-HP and 3-HTP groups were potentially able to bind at the active site of HDAC 1, 6, and 8, suggesting the heterocyclic compounds could provide the critical ZBG in the HDACi pharmacophoric model. *In vitro* experiments showed that HDAC 6 and HDAC 8 were inhibited by 3-HPT with IC_{50} values of 681 nM and 3.7 µM, respectively, however, it was inactive towards HDAC 1 [163]. On the other hand, 3-HP was inactive in these three HDAC isoforms. The variation in HDAC inhibitory activity of 3-HP and 3-HPT might be

due to the thiophilicity of zinc that favours 3-HPT [163]. 1-Hydroxypyridine-2-thiones (1-HPT) is another key pharmacophore for zinc-binding that form zinc-specific five-membered complex though its oxygen and sulfur atoms. The 1-HPT analogue, 1-HPT-6-carboxylic acid, exhibited selective HDAC 6 inhibitory activity (IC_{50} value of 150 nM). The other two analogues of 1-HPT with simple amino acids exhibited 600-fold selectivity towards eleven zinc-depended HDACs. These 1-HPT analogues also displayed growth inhibitory activity against HDAC 8 overexpressing chronic myelogenous leukaemia cells at low micromolar concentrations [162].

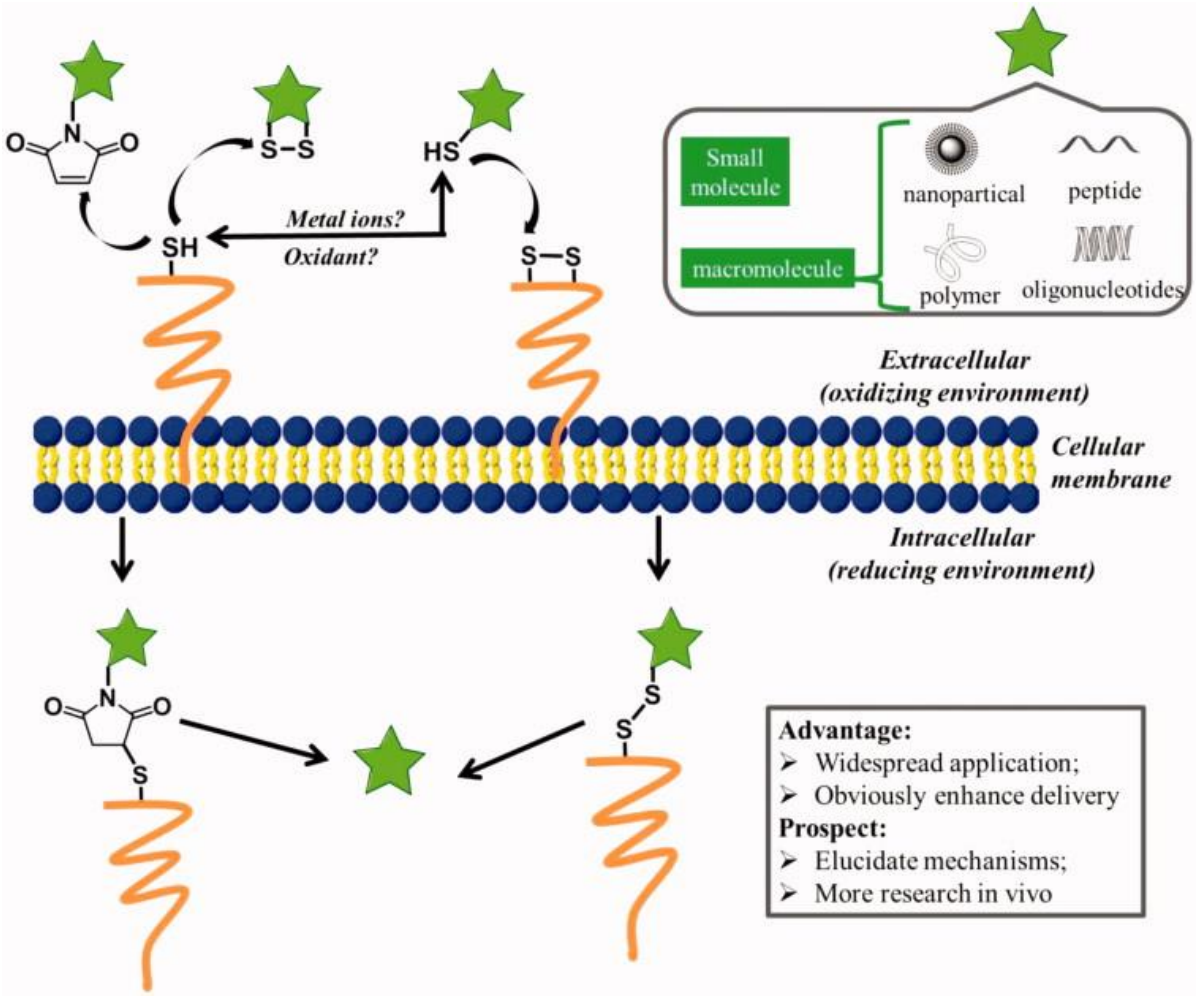

Figure 1.9: Cellular uptake mechanism of thiol-reactive groups. Mechanism of cellular entry of thiol-reactive groups (such as free thiols, disulfide bonds, and maleimide moiety), modified biomolecules (pentacle) upon interaction with exofacial thiols. When these biomolecules reach to the cell membrane, they internalised to free cargoes through cleavage [160].

Thiopyridones are a relatively new class of S, O chelating agents and the potential applications of these compounds are under investigation. The chemical and biological properties of thiopyridones can be fine-tuned through chemical modification of the heterocyclic backbone [164]. Interestingly S, O chelating thiomaltolato ligand containing compounds displayed promising anticancer activity with low µM range IC_{50} values while the corresponding maltolato

compounds were inactive [164]. 1-Adamantylthiopyridine derivative 2-(1-adamantylthio)-5-hydroxypyridine exhibited anticancer activity against HepG2 (human liver cancer), MOLT-3 (lymphoblastic leukaemia), HuCCA-1 (human cholangiocarcinoma), and A549 cells with IC_{50} values of 35, 17.90, 44, and 45 µg/mL, respectively [165]. Novel 1-hydroxy-2-thiopyridine derivatives displayed cytotoxicity against HepG2 cells (IC_{50} value range from 1.73 to 3.84 µg/mL) and A549 cells (IC_{50} value range from 4.96 to 8.24 µg/mL) [166]. Additionally, low toxicity and high affinity of thipyridones towards metal ions in different oxidation states are one of the influential factors for their growing demand [164]. Ru based anticancer drugs generally have low toxicity and high selectivity towards cancer cells [167]. Ru(II)-η^6-p-cymene complexes containing (O, S) hydroxythiopyridone ligands exhibited anticancer activity towards human A549, SW480, and CH1 cancer cells [168]. The arene Ru unit has amphiphilic properties as the lipophilic arene ligand is counterbalanced by the hydrophilic Ru metal center. The amphiphilic properties and the diversity of the arene ligand makes Ru arene complexes an excellent scaffold for the coupling of organic moieties for targeted chemotherapy [167]. Figure 1.10 shows the hydroxythiopyridone based novel Ru arene complexes chlorido[3-oxo-1-benzyl-2-methylpyridin-4(1H)-thionato-κ^2O,S](p-cymene)ruthenium(II)] (M1S-Ru) and chloride[3-oxo-1,ethylbenzyl-2-methylpyridin-4(1H)-thionato- κ^2O,S](cymene)ruthenium(II) (M2S-Ru) complexes, and their respective ligands *i.e.* 1-benzyl-2-methyl-3-hydroxypyridin-4-(1H)-thione (M1S) and 1-ethylbenzyl-2-methyl-3-hydroxypyridin-4-thione (M2S) synthesised by our collaborators.

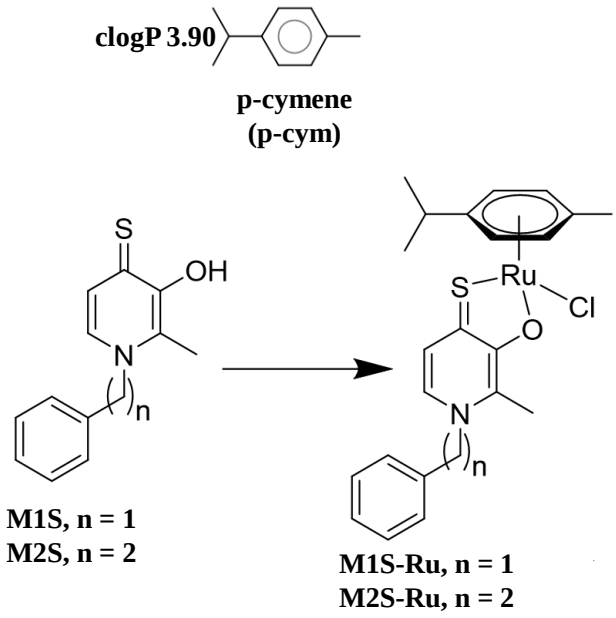

Figure 1.10: Hydroxythiopyridone derivatives used in this study. clogP value determined using Molinspiration online software tool [154].

1.5.3 Metal-based PCA ligands and complexes

Half-sandwich Ru (II) arene or Rh (III) arene complexes can exhibit promising anticancer activity which in many cases is superior or comparable to approved anticancer drugs [153, 169]. Carbon-linked π-bound arenes or cyclopentadienyl ligands can influence cellular uptake and targeting by controlling the lipophilicity and hydrophilicity of the faces of the metal arene complexes [78]. One of the key challenges in organometallic drug development is to identify the active pharmacophore, including the activity of both the ligands and the metal ion. The structural and electronic features of the pharmacophore are essential for the identification of specific cellular targets and thereby, controlling the cellular response. The electronic and steric effects regulate both the kinetics and thermodynamics of ligand exchange and redox balance of metal ions. Hence, understanding the SAR for metal-arene and metal-cyclopentadienyl containing anticancer drug candidates is crucial for drug development [170].

Plectin is a structural protein and lung cancer stem cell biomarker. Plectin is associated with invasiveness of lung adenocarcinoma and poor survival in these patients [171, 172]. Raymond and colleagues confirmed that plectin overexpressed on the surface of KRAS-mutated H358 NSCLC cells and its knockdown reduced mobility, migration, and colony formation of these cells [172]. Previously, it has been reported that PCA based Ru arene (p-cym) complexes namely plecstatin displayed target selectivity for plectin. Plectin targeting potentially suppresses tumour invasiveness in the *in vitro* tumour spheroid model while oral administration (30 mg/kg) of [chlorido(η^6-p-cymene)(N-(4-fluorophenyl)-2-pyridinecarbothioamide) ruthenium(II)]chloride (plecstatin-1 or AASH-122) reduced tumour growth more efficiently in the B16 melanoma model than in the CT26 colon tumour model in mice [173]. A strong interaction of plecstatins with the target depends on the hydrogen bond acceptor (-F) of plecstatins. In sodium chloride media (104 nM NaCl) AASH-122 (approximate half-life of 50 min) hydrolysed faster than its corresponding isosteric osmium analogue (no significant hydrolysis within 14 h). Both the compounds displayed identical distribution patterns and remain largely intact *in vivo* model after 2 h post-administration [174]. AASH-122 and its Os analogue accumulated in the liver, kidney, lung, muscle, and tumours of murine CT-26 tumour-bearing mice after a single i.p. dose (15 mg/kg). Interestingly, AASH-122 penetrated deeper into the organs and tumours while its Os analogue deposited more at the edge or periphery of organs and tumours [175]. AASH-122 is structurally similar with its Rh analogue [chloride(η^5-pentamethylcyclopentadienyl)(*N*-(4-fluorophenyl)pyridine-2-carbothioamide)rhodium(III)] chloride (JAZZ-121), except the p-cym is replaced with 1,2,3,4-tetramethyl-cyclopenta-1,3-diene (Figure 1.11). These two compounds were synthesised by our collaborators.

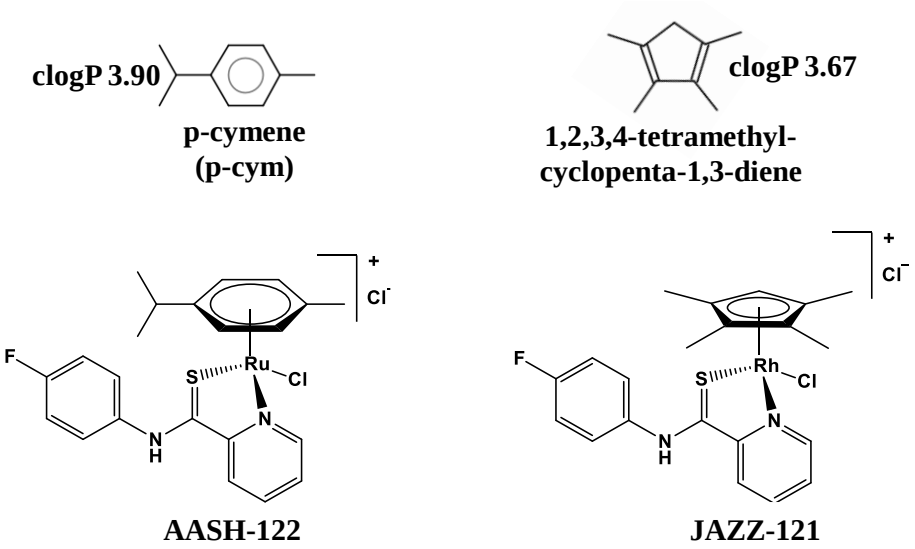

Figure 1.11: Structure of metal-based PCA ligands and complexes. AASH-122 and JAZZ-121 were examined in this study. clogP value determined using Molinspiration online software tool [154].

1.5.4 Kinetically inert metal(arene) complexes of PCA

Kinetically inert metal complexes are potential tools for targeting biomolecules (other than DNA), especially protein. Recent literature reported that the kinetically inter half-sandwich Ru complexes selectively inhibited protein kinases [106]. Kinases catalyse cellular reactions that transfer the phosphate group from ATP to substrates and these reactions are linked with cell division and proliferation [106, 176, 177]. Thus, kinases are one of the crucial targets for anticancer drugs [178, 179].

Antiproliferative activity of the functional compounds is dependent on the metal centers, electronic configuration, oxidative state, and hard-soft nature [180]. Os is slightly softer than Ru, thereby it has different coordination preferences to biomolecules. Another interesting property of Os compounds is the increased inertness of ligand substitution compared to Ru. Therefore, Os compounds are less prone to the hydrolysis of metal-halide bonds. Furthermore, upon hydrolysis, Os-aqua species tend to be more acidic than the corresponding analogue of the Ru-aqua species [181]. An increase in intracellular acidity could not only induce apoptosis due to acidic stress but also decrease invasion and migration [182]. The cytotoxicity, cellular uptake, and mechanism of antiproliferative activity may also be relying on the coordinated halide in the metal arene complexes [183]. The trans-effect of chloride ligands stabilises the reactive ligands at the metal center electronically. The chloride ligands, therefore, are vital as the strength of the metal-carbon bond accelerates the final rate of the metathesis reaction [170].

The majority of Ru (II) and Os (II) based arene complexes have the half-sandwich piano-stool motif, where the η^6-coordinating arene such as p-cymene (p-cym) and biphenyl (bip) stabilise

the low oxidation state [184]. Interestingly, isostructural piano-stool complexes (RM175, Ru II bip complex, and AFAP51, Os II bip complex) that only differed in the metal center displayed significant differences in the antiproliferative activity both *in vitro* and *in vivo* [180]. AFAP51 showed higher cytotoxic potential towards malignant breast MDA-MB-231, MCF-7, and normal breast HBL-100 cells (with IC_{50} values of 48, 15, and 16 µM, respectively) compared to its isostructural congener Ru II compounds with IC_{50} values of 62, 93 and 54 µM, respectively. On the other hand, RM175 displayed anti-lung metastasis activity in the *in vivo* mammary cancer MCa model while AFAP51 did not [185]. In another study, N-substituted PCAs containing Ru (II) and Os (II) arene (p-cym) complexes showed antiproliferative activity against SW480, CH1, and A549 cancer cells. The smaller and lipophilic congeners were most effective in the low micromolar range [184]. It has been reported that the presence of the tri-phenyl phosphine (PPh_3) moiety in the η^6-arene (p-cym) Ru II complexes enhanced the antiproliferative activity towards the leukaemia HL-60 cell line [118]. Additionally, viscosity measurement and ethidium bromide displacement experiments confirmed that the presence of PPh_3 ligand in the arene-Ru II complexes promoted DNA base pairs intercalation through intra-molecular π-π interactions while with PPh_3 moiety bound DNA in a covalent manner. However, the reduced protein binding capability of PPh_3 ligand bearing complexes could be due to steric hindrance. These effects could have an influential consequences in the cellular uptake and drug detoxification mechanisms of these complexes [118]. Trifluromethylsulfonate (trifilate, OTf, $CF_3SO_3^-$) is an outstanding leaving group and widely used in organic chemistry [186]. Trifilate is well known classical non-coordinating anion, some transition metal triflates (M-OTf) act as a cationic coordinately unsaturated species that allows easy coordination of other auxiliary ligands (L) (*e.g.* pyridine, water, and phosphine), resulting in removal of the triflate anion out of the coordination sphere: $M\text{-}OTf + L \rightarrow M(L) + (OTf)^-$ [187]. Figure 1.12 shows the pharmacophore modified PCAs containing Ru (II) and Os (II) arene complexes [(triphenylphosphine) (η^6-p-cymene) (N-(4-chlorophenyl) pyridine-2-carbothioamide)] ruthenium(II)triflate (ZR-012) and [(triphenylphosphine) (η^6-biphenyl) (N-(4-chlorophenyl) pyridine-2-carbothioamide)]osmium(II)triflate (ZR-014) synthesised by our collaborators.

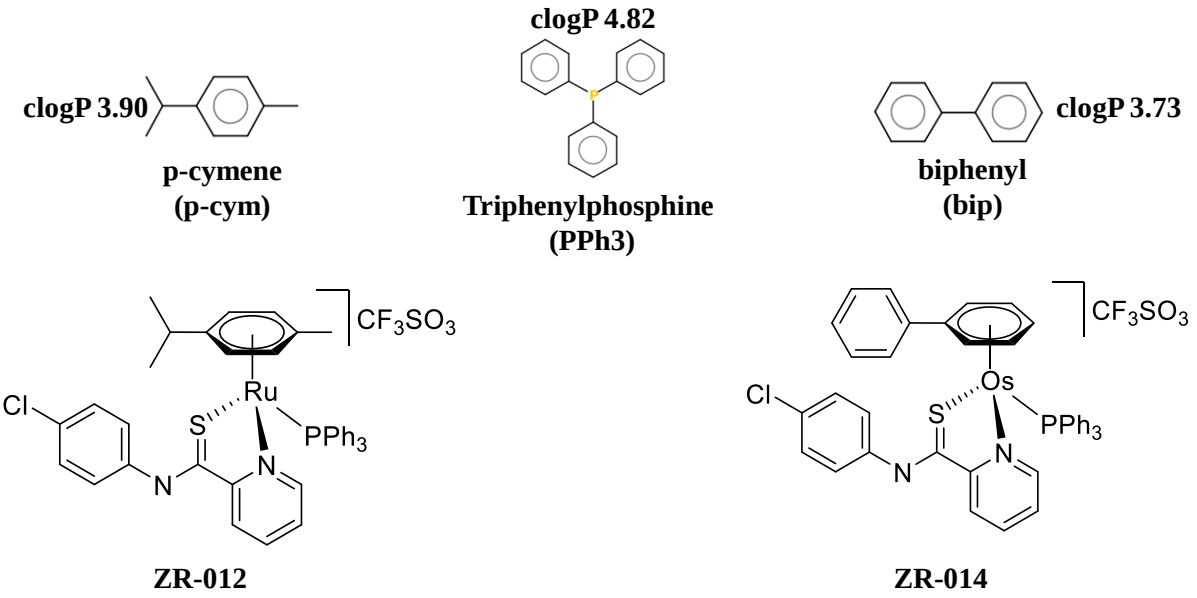

Figure 1.12: Kinetically inert metal(arene) complexes of PCA examined in this study. clogP value determined using Molinspiration online software tool [154].

1.6 Aims of the current study

HDACis offer therapeutic benefits to patients with KRAS-mutant NSCLC. Development of multitargeting HDACis (JAZZ-90, JAZZ-166, and JAZZ-167) through pharmacophore modification could offer additional benefits in the treatment of KRAS-mutant NSCLC patients by minimising the side effects and improving therapeutic targeting. Additionally, hydroxythiopyridone derivatives showed promising anticancer activities and the presence of a thiol group enhanced the cellular uptake of these compounds. M1S, M2S, M1S-Ru, and M2S-Ru are predicted to have HDACi activities due to their pharmacophore, and their potential cytotoxic activity and underlying mechanism have yet to be investigated. It has been reported that Ru based PCA ligands and complexes target plectin, a protein overexpressed in KRAS-mutant NSCLC. Previously, PCA based Ru and Os complexes exhibited anticancer activities against A549 cells. AASH-122 displayed antiproliferative activities against a CT-26 tumor model *in vivo* and have lung tissue penetration potential. Therefore, AASH-122 and its Rh analogue JAZZ-121 could also have potential antiproliferative activities in KRAS-mutant cell lines. Another PCA based drug class (*i.e*. kinetically inert metal(arene) complexes of PCA) composed of pharmacophore modified novel compounds (ZR-012 and ZR-014) could have antiproliferative activity against KRAS-mutant cells. As KRAS remains an undruggable target, the current study aimed to investigate the efficacy of novel compounds in different classes towards KRAS- mutated NSCLC cells.

1.7 Hypothesis and objectives of the project

Previous studies showed that all the drug candidates displayed antiproliferative activity towards HCT116, H460, SiHa, and SW480 cell lines in the nanomolar to micromolar range (M. Hanif, personal communication). Based on the preliminary findings it was hypothesised that these novel compounds will exhibit cytotoxic EC_{50} values in the nanomolar to micromolar range against A549 cells. The most potent drugs will have cytotoxic activities in other NSCLC cells and have more selectivity towards cancer cells. Additionally, the potent compounds will significantly change the expression of proteins linked with cell growth and proliferation, thereby altering cell cycle progression.

The following objectives will address these hypotheses:

1) To screen the potential anticancer activity of several metal-based and non-metal-based novel compounds in the KRAS-mutated A549 NSCLC cell line.
2) To examine the antiproliferative activity of potent drug candidates in p53 mutated H522 NSCLC cells.
3) To investigate the effect of the two most potent drugs in pre-neoplastic NIH3T3 cells and normal prostate epithelial PNT1A cells.
4) To examine the potential antiproliferative mechanism mediated by the two most potent drugs, M1S and M2S, by examining their effect on cell signalling proteins (acetyl H3, cyclin D1, and B1), and cell cycle progression.

CHAPTER II

Materials and Methods

2 Materials and Methods

2.1 Materials

2.1.1 Cell lines

A549 and H522 cells were kindly donated by A/Prof. John Aston, Department of Pharmacology and Toxicology, University of Otago. NIH3T3 cell line was kindly donated by Dr. Greg Giles, Department of Pharmacology and Toxicology, University of Otago, and the PNT1A cell line was kindly donated by Professor Helen Nicholson, Department of Anatomy, University of Otago. All the cell lines were originally purchased from American Type Culture Collection (USA).

2.1.2 Chemicals

Sulforhodamine B (SRB), ammonium persulfate, copper sulfate ($CuSO_4.5H_20$), potassium chloride (KCl), sodium pyrophosphate ($Na_4P_2O_7$), sodium orthovanadate (Na_3VO_4), sodium fluoride (NaF), sodium hydroxide (NaOH), hydrochloric acid (HCl), trizma hydrochloride (Tris HCl), triton-X 100, methanol, ponceau red stain, tetramethylene diamine (TEMED), trizma base (Tris base), ethylenediaminetetraacetic acid (EDTA), NP-40, ethylene glycol tetraacetic acid (EGTA), dimethyl sulfoxide (DMSO), bromophenol blue, β-mercaptoethanol, complete protease inhibitor cocktail tablets, glycerol and glycine for electrophoresis were purchased from Sigma-Aldrich (USA). RPMI 1640 media and foetal bovine serum (FBS) were purchased from Sigma-Aldrich (UK) and Moregate Biotech (NZ), respectively. Trypsin, penicillin-streptomycin, phenylmethylsulfonyl fluoride (PMSF), 4, 4′-dicarboxy-2, 2′-biquinoline acid (BCA), SuperSignal West Pico Plus Chemiluminescent substrate were purchased from Thermo Fisher Scientific (USA). Potassium dihydrogen phosphate (KH_2PO_4) was purchased from Fisher Scientific (UK). Acetic acid (CH_3COOH), sodium chloride (NaCl), and trichloroacetic acid (TCA) were purchased from Merck (Germany). Sodium dodecyl sulfate (SDS), sodium hydrogen carbonate ($NaHCO_3$), disodium hydrogen phosphate (Na_2HPO_4), and ethanol (96%) was purchased from Scharlau (Spain). Molecular weight marker, acetylated histone-H3, cyclin D1, cyclin B1, β-tubulin, and β-actin primary antibodies were purchased from Cell Signalling Technology (USA). Acrylamide, bisacrylamide, polyvinylidene difluoride (PVDF) membrane, goat anti-rabbit, and goat anti-mouse secondary antibodies were purchased from Bio-Rad Laboratories (USA). FxCycle propidium iodide (PI)/RNase staining solution was purchased from Life Technologies Corporation (USA).

2.1.3 Experimental drugs

JAZZ-90, JAZZ-166, JAZZ-167, M1S, M2S, M1S-Ru, M2S-Ru, AASH-122, JAZZ-121, ZR-012, and ZR-014 were synthesised by Dr. Muhammad Hanif of the Faculty of Science, University of Auckland, NZ and he also kindly donated SAHA.

2.2 Methods

2.2.1 Cell maintenance

A549, H522 lung cancer, NIH3T3 mouse embryonic fibroblast, and PNT1A normal prostate epithelial cell lines were seeded in RPMI 1640 media supplemented with 2%, 10%, 10%, and 10% FBS, respectively, and 1% penicillin-streptomycin. Cells were cultured in 75 or 175 cm^2 flasks and incubated in 5% CO_2 at 37°C. Cells were passaged under sterile conditions when the cells were ~85% confluent. Cell culture media was aspirated off and cells were washed with 5 mL PBS. Cells were then incubated with 1 mL of trypsin for 2-3 min in 5% CO_2 at 37ºC to detach the cells from the flask. The deactivation of trypsin was conducted by the addition of 5 mL complete growth media. The entire cell suspension was transferred into a 14 mL centrifuge tube and centrifuged at 1200 rpm for 3 min at 4°C. The supernatant was discarded and the cell pellet was diluted with 10 mL of fresh growth media. The cell number was determined using a haemocytometer.

2.2.2 Drug preparation

Stock solutions of JAZZ-90, M1S, M2S, and SAHA were prepared by dissolving in 100% DMSO and stored at -20°C. Since the metal-based drugs could interact with DMSO in long term storage, all the metal-based drugs including JAZZ-166, JAZZ-167, M1S-Ru, M2S-Ru, AASH-122, JAZZ-121, ZR-012, and ZR-014 were freshly prepared by dissolving in 100% DMSO. The stocks of all the drugs were diluted into RMPI-1640 to a final concentration of 0.5% DMSO. DMSO (0.5 %) was used as the vehicle control.

2.2.3 Cell cytotoxicity study using the SRB assay

A549, H522, NIH3T3, and PNT1A cells were seeded in 96 well plates at 4000, 10000, 3500, and 10000 cells per well, respectively, and incubated for 24 h in 5% CO_2 at 37°C. Cells were then treated with metal and non-metal-based anticancer drugs at a range of different concentrations (0.015-200 µM) while vehicle control cells were treated with DMSO (0.5%). At the end of the incubation period (72 h), the viable cell number in each well was determined by the SRB assay. Briefly, the media of each well was aspirated off and cells were fixed with 100 µL of 10% TCA. Plates were then kept at 4°C for 30 min, followed by a gentle wash with distilled water. The plates were then dried for 45 min. 100 µL of SRB (0.4% SRB in 1% acetic

acid) was then added to each well to stain the viable cells and plates were incubated for 30 min at room temperature. Subsequently, the unbound stain was aspirated off and cells were washed 4 times with 1% acetic acid and dried for 45 min. Finally, the SRB dye in each well was solubilised in 100 µL of 10 mM Tris base (pH 10.5) and the absorbance was read at 510 nm using a Bio-Rad Benchmark Plus microplate reader. The experiments were conducted in triplicate with three technical replicates.

2.2.4 Western blotting

2.2.4.1 Preparation of protein extracts

A549 (1.0×10^6 cells per dish) and H522 (2.5×10^6 cells per dish) cells were seeded in 10 cm cell culture dishes in 10 mL of complete growth media and incubated for 24 h. The cells were then treated with M1S (0.36, 0.72 µM for A549 cells and 0.28, 0.56 µM for H522 cells), M2S (0.32, 0.64 µm for A549 cells and 0.23, 0.46 µM for H522 cells) and vehicle control (0.5% DMSO) for 12 h and 24 h. The media was aspirated off and cells were washed with 5 mL of ice-cold PBS (4°C) followed by the addition of 100 µL and 150 µL of lysing buffer (50 mM Tris base, 0.5% NP-40, 0.5% SDS, 150 mM NaCl, 1 mM EDTA, 1 mM EGTA, 1 mM sodium orthovanadate, 1 mM sodium pyrophosphate, 1 mM PMSF, 10 mM sodium fluoride and complete protease inhibitor cocktail tablets) for A549 and H522 cells, respectively. The dishes were incubated for 10 min and the cells were detached with a cell scraper. The cells were transferred to a 1.5 mL heat resistant Eppendorf tube and incubated for 12 h. Cell lysates were then sonicated for 3 × 7 sec and centrifuged at 14,000 rpm for 8 min at 4°C and the supernatant was collected.

Protein concentrations were determined using the BCA assay. 3 µL of protein lysate of each sample was added to a 96-well plate in triplicate followed by the addition of 17 µL of Mili Q water. BSA with a range of concentrations of 0-500 µg/µL was used to obtain the standard curve. 200 µL of BCA (BCA and 4% $CuSO4.5H_2O$ in a 50:1 ratio) was then added and the plate was then incubated for 45 min at 37°C. Absorbance was determined using a Bio-Rad Benchmark Plus microplate reader at 560 nm. A standard curve was used to determine the protein concentration of the samples. The normalisation of each sample was diluted with the required volumes of lysing buffer. Finally, a 4X sample buffer (62.5 mM tris HCl pH 6.8, 1% SDS, 10% glycerol, 0.005% bromophenol blue, 355 mM β-mercaptoethanol) was added to all samples at 1:3 (4X sample buffer: sample) ratio and the samples were heated at 95°C for 5 min and cooled on ice. Samples were then stored at −20°C until further analysis.

2.2.4.2 Gel electrophoresis

Each gel consisted of a resolving gel and stacking gel (0.43 mL acrylamide/bisacrylamide solution (29:1), 0.63 mL upper Tris buffer, 25 µL 10% APS, 1.45 µL TEMED). There were two types of resolving gel used, one was 10% gel (2.5 mL acrylamide/bisacrylamide solution (29:1), 1.88 mL lower Tris buffer, 250 µL 50% glycerol, 37.5 µL 10% APS, 2.83 mL dH2O, 5 µL TEMED) and the another was 15% gel (3.75 mL acrylamide/bisacrylamide solution (29:1), 1.88 mL lower Tris buffer, 300 µL 50% glycerol, 37.5 µL 10% APS, 1.55 mL dH2O, 5 µL TEMED). 15% gel was used for cyclin D1, acetyl H3, and β-tubulin, while 10% gel was used for cyclin B1 and β-actin. Sodium dodecyl sulfate-polyacrylamide gel electrophoresis (SDS-PAGE) was used to separate proteins based on molecular weight (MW). Samples containing 25 µg and 20 µg of protein extracted from A549 and H522 cell lysis, respectively, were loaded on each well of the upper gel along with an MW marker to identify the location of the protein of interest. Gels were initially run in SDS buffer (25mM Tris-base, pH 8.3, 0.192 M glycine, 0.1% (w/v) SDS) at a voltage of 70V and after the passing of upper gel, the voltage was maintained at 100V until the dye front had reached to the bottom of the resolving gel.

2.2.4.3 Transferring to PVDF membrane

At the end of electrophoresis the upper gel was removed and resolving gel was transferred into transfer buffer to remove excess SDS. A sandwich of equilibrated fibre pad, blotting paper, resolving gel and an activated PVDF membrane was made in the cassettes. To transfer the protein from gel to the activated PVDF membrane transfer buffer (25mM tris-base, pH 8.3, 0.192 M glycine, and 10% methanol) was used. To avoid the overheating of the apparatus, ice packs stored at −80°C were placed inside the apparatus. The proteins were transferred to PVDF membrane at 100 V for 1.5 h using a Bio-Rad wet transfer system.

2.2.4.4 Blocking and antibody incubation

The membrane was blocked using 2% non-fat milk powder for 30 min to prevent the non-specific binding of antibodies. The membrane was then washed 2 times (5 min each) with TBS (0.025 mM Tris-base, 0.1 M NaCl, pH 7.4) to remove the blocking solution and then incubated overnight with the primary antibody at 4°C. At the end of the incubation period, the membrane was washed 6 times with TBST (0.05% Tween 20, 0.025 mM Tris-base, 0.1 M NaCl, pH 7.4) for 5 min each and then treated with a secondary antibody containing horseradish peroxidase enzyme for 1 h. After that the membrane was further washed 6 times with TBST, the membrane was then taken to the darkroom.

2.2.4.5 X-ray film development

Chemilunescent solutions were added and X-ray film was exposed to the membrane, following this step the films were developed. Films were analysed using the Bio-Rad GS710 scanner and protein density was determined as a ratio of β-actin or β-tubulin. The experiments were conducted in triplicate, technical replicates were not included.

As the same blot was used to screen the expression of different proteins, after the successful development of the X-ray film the blot was washed 6 times with TBST before additional primary antibody treatment.

2.2.5 Cell cycle analysis by flow cytometry

2.2.5.1 Cell fixing

A549 (1.0×10^6 cells per dish) and H522 (3.0×10^5 cells per well) cells were seeded in 10 cm cell culture dishes and 6-well plates with 10 mL and 2 mL of complete media and incubated for 24 h, respectively. The cells were then treated with M1S (0.36, and 0.72 µM for A549 cells; 0.28, and 0.56 µM for H522 cells), M2S (0.32, and 0.64 µM for A549 cells; 0.23, and 0.46 µM for H522 cells) using 0.5 % DMSO as the vehicle control for 6 h and 12 h. After treatment, the A549 and H522 cells were washed twice with 2 mL and 400 µL of cold isotonic PBS (137 mM NaCl, 2.7 mM KCL, 4.3 mM Na_2HPO_4, 1.47 mM KH_2PO_4; pH 7.4 maintained at 4ºC), respectively. Then 1 mL (A549 cells) and 500 µL (H522 cells) of pre-warmed trypsin were added to each well followed by incubation at 37ºC for less than 5 min. Plates were immediately placed on ice and the cell suspension was transferred into a fresh 15 mL tube. The tubes were centrifuged at 2000 rpm for 5 min at 4ºC. The supernatant was removed from each tube and the cell pellet was resuspended in 300 µL isotonic PBS (4ºC). The above centrifugation step and supernatant removing steps were repeated once. The pellet was then fixed by adding 600 µL cold 70% ethanol and vortexing gently. The tubes were stored at 4ºC until analysis.

2.2.5.2 Propidium iodide staining

The tubes containing the cell suspensions were centrifuged at 2000 rpm for 5 min at 4ºC. After that the supernatant was removed, the cells were washed two times with 500 µL cold PBS. The cell pellet was then resuspended in 250 and 200 µL of cold FxCycle PI/RNase (0.1% sodium citrate, 0.1% triton-X, 1 mg/mL PI) staining solution for A549 and H522 cells, respectively and transferred to a FAC tube followed by incubation in the dark for 30 min at room temperature. The samples were analysed via flow cytometry using a Beckman Coulter Gallios flow cytometer (USA) and data were analysed by Kaluza software. Technical replicates were not included in this experiment.

2.2.6 Experimental data calculation and statistical analysis

To calculate the EC_{50} (the concentration of drug required to decrease the cell number by 50% of vehicle control) concentration, the cell number was analysed by nonlinear regression using Prism-GraphPad 8 software (USA) [188, 189]. The following formula was used to determine the EC_{50} value [190].

$$EC_{50} = \text{Minimum cell viability (\%)} + \frac{(\text{Maximum cell viability (\%)} - \text{Minimum cell viability (\%)})}{1 + 10^{\wedge}((\text{Log } EC_{50} - \text{Drug Concentration}) \times \text{Hill Slope})}$$

In the published literature the terminology IC_{50} (the concentration of drug required for 50% inhibition) and EC_{50} are used interchangeably for representing cytotoxicity data [91, 185, 188, 189, 191]. Yadav and colleagues presented the cytotoxicity results using the term EC_{50} and inhibitory activity using the term IC_{50} [188]. It appeared more logical to present the cytotoxic effect of a drug using the terminology EC_{50}, as it measures the effect of a drug on cell number, not their inhibitory effects underlying this activity. Therefore, the cytotoxicity data of the current study is presented using EC_{50}. However, in the introduction and discussion sections, the terminology used in each publication is what has been stated.

The selectivity index (SI) of M1S and M2S was calculated according to the following formula [192].

$$SI = \frac{EC_{50} \text{ of drug in normal cell line}}{EC_{50} \text{ of drug in cancer cell line}}$$

Where PNTA1 was used as a normal cell line

Western blotting results were obtained by scanning the developed blots using a Bio-Rad GS-710 calibrated imaging densitometer (USA) and quantified using Quantity One software from Bio-Rad (USA). The scanner was set to scan blue x-ray film at 42.3 × 42.3 resolution. Using the volume rectangle tool in the Quantity One software, boxes of the same size were used to calculate the density of the protein as well as the corresponding background surrounding the protein band. The volume analysis report was set to determine the density of the bands. The average background density values were subtracted from the protein-band density. The value was then divided by the corresponding band of housekeeping protein *i.e.* either β-tubulin or β-actin as a loading control.

Statistical analysis was performed using Prism-GraphPad 8 software (USA) and the values presented as mean ± standard error of the mean (SEM). A one-way analysis of variance

(ANOVA) coupled with a Bonferroni post-hoc test was performed to determine the shift of a novel drug's potency in comparison to SAHA. While data from the time-course cytotoxicity assay, Western blotting, and cell cycle analysis were analysed using a two-way ANOVA (parameters of time and treatment) coupled with a Bonferroni post-hoc test. Statistical significance was set at $p<0.05$.

CHAPTER III

Results

3 Results

3.1 Cytotoxicity

3.1.1 Dose-response cytotoxicity of novel compounds in A549 cells

To select the most potent drug with cytotoxicity toward KRAS-mutant NSCLC, eight metal-based and three non-metal-based synthetic compounds of four different classes were screened in A549 lung cancer cells using the SRB assay. The EC_{50} values for all the drugs are shown in Table 3.1. The non-metal-based HDACi JAZZ-90 displayed potent cytotoxicity compared with the control drug SAHA with EC_{50} values of 0.76 and 1.01 µM, respectively. On the other hand, the metal-based HDACis JAZZ-166, and JAZZ-167 were 3.2 and 4.2 times less cytotoxic than SAHA (Figure 3.1). Interestingly, of the metal-based PCA ligands and complexes, AASH showed considerable potency with an EC_{50} value of 2.02 µM, while JAZZ -121 was unable to reach 50 percent viability over the range of concentrations tested (0.15 to 200 µM) (Figure 3.1). Additionally, as shown in Figure 3.2, non-metal-based hydroxythiopyridone derivatives, M1S, and M2S were 4.8 and 5.2-fold more potent, respectively, compared with their metal-based complexes M1S-Ru and M2S-Ru. Furthermore, kinetically inert metal(arene) complexes of PCA, ZR-012, and ZR-014 showed almost equal potency to that of M1S-Ru and M2S-Ru (Figure 3.2). Overall, all three non-metal-based synthetic compounds M2S, M1S, and JAZZ-90 and metal-based derivatives ZR-012, ZR-014, M1S-Ru, and M2S-Ru displayed cytotoxic potential comparable to SAHA, while AASH-122, JAZZ-166 and JAZZ-167 exhibited cytotoxic activity that was significantly weaker compared to SAHA (Table 3.1).

The three most potent drugs M2S, M1S, and JAZZ-90 were chosen for further study. Additionally, as the metal-based derivatives ZR-012, ZR-014, M1S-Ru, and M2S-Ru showed similar potency, M1S-Ru and M2S-Ru were selected for further examination because they contained the same moieties contained within M1S and M2S, which elicited submicromolar EC_{50} values.

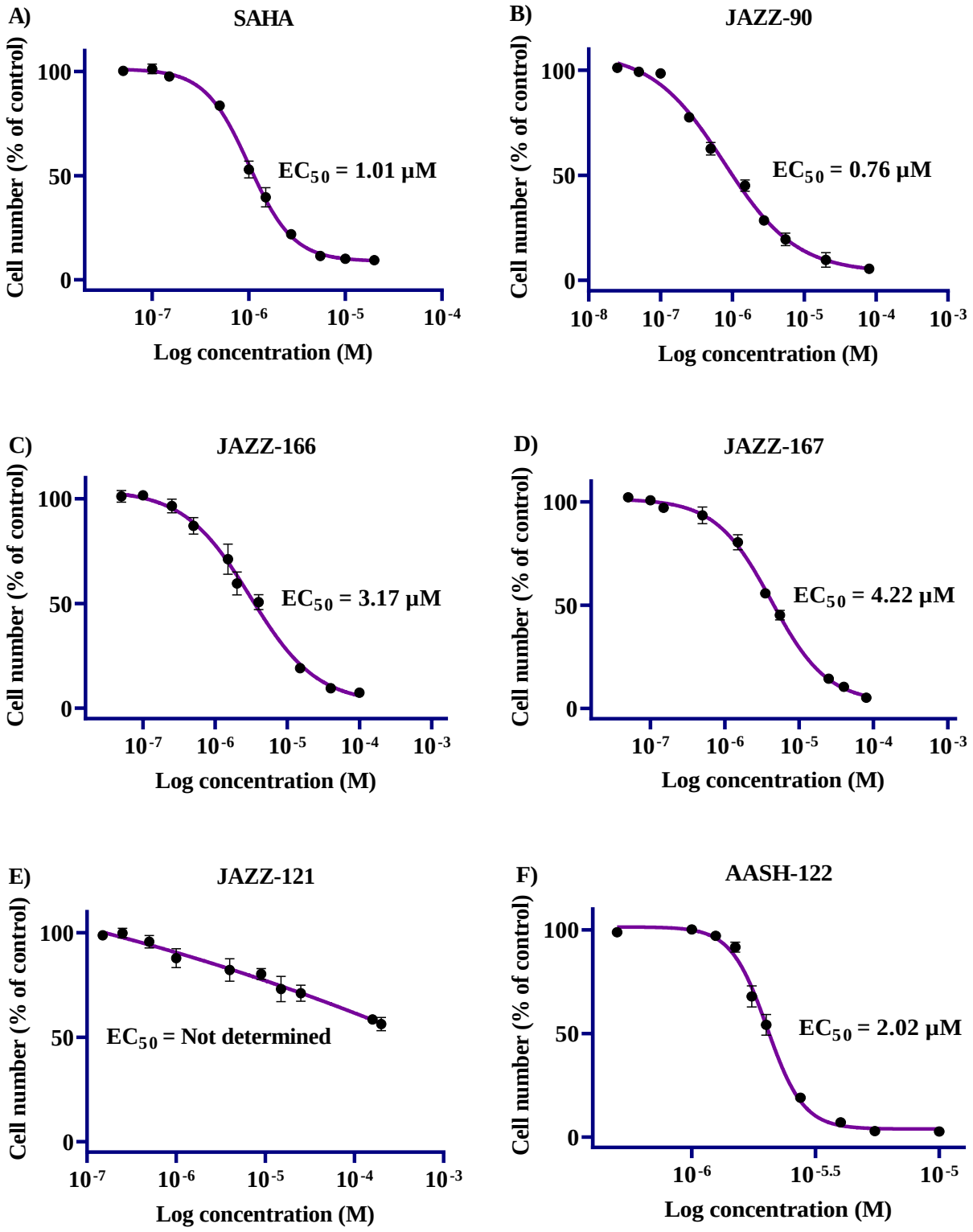

Figure 3.1: Cytotoxicity of SAHA, JAZZ-90, JAZZ-166, JAZZ-167, JAZZ-121, and ASH-122 in A549 cells. A549 cells were seeded in 96-well plates at 4×10^3 cells per well and incubated for 24 h at 37ºC. The cells were then treated with SAHA (A), JAZZ-90 (B), JAZZ-166 (C), JAZZ-167 (D), JAZZ-121 (E), and AASH-122 (F) (0.015 to 200 µM) for 72 h. Vehicle control cells were treated with DMSO (0.5%). At the end of the treatment period, the cell number was determined by the SRB assay. The points represent the mean ± SEM (n=3). EC_{50} values were obtained using non-linear regression using Prism software.

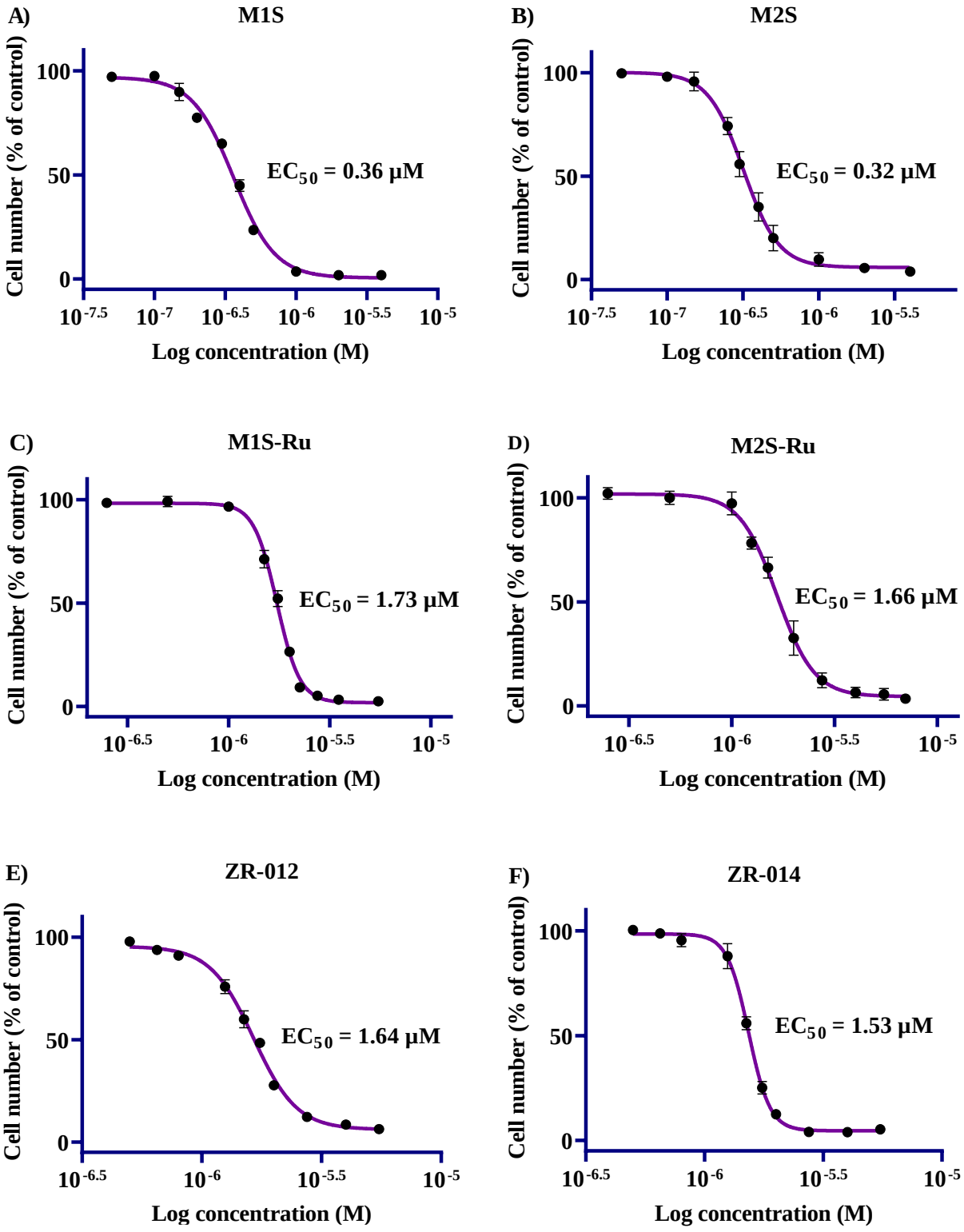

Figure 3.2: Cytotoxicity of M1S, M2S, M1S-Ru, M2S-Ru, ZR-012, and ZR-014 in A549 cells. A549 cells were seeded in 96-well plates at 4×10^3 cells per well and incubated for 24 h at 37ºC. The cells were then treated with M1S (A), M2S (B), M1S-Ru (C), M2S-Ru (D), ZR-012 (E), and ZR-014 (F) (0.025 to 80 µM) for 72 h. Vehicle control cells were treated with DMSO (0.5%). At the end of the treatment period, the cell number was determined by the SRB assay. The points represent the mean ± SEM (n=3). EC_{50} values were obtained using non-linear regression using Prism software.

Table 3.1: EC_{50} values of different classes of drug candidates in A549 cells

Class	Name	Molecular (Mol.) formula	Mol. weight (g/mol)	EC_{50} (µM)	95% confidence interval
I	SAHA	$C_{14}H_{20}N_2O_3$	234.32	1.01	0.92 to 1.10
	JAZZ-90	$C_{20}H_{24}N_4O_3S$	400.49	0.76	0.59 to 0.97
	JAZZ-166	$C_{30}H_{38}Cl_2IrN_4O_3S$	797.83	3.17*	2.29 to 4.30
	JAZZ-167	$C_{30}H_{38}Cl_2RhN_4O_3S$	708.52	4.22*	3.69 to 4.99
II	JAZZ-121	$C_{22}H_{24}Cl_2FN_2RhS$	541.31	Not determined**	Not determined
	AASH-122	$C_{22}H_{23}Cl_2FN_2RuS$	538.47	2.02*	1.95 to 2.09
III	M1S	$C_{13}H_{13}NOS$	231.31	0.36	0.34 to 0.38
	M2S	$C_{14}H_{15}NOS$	245.34	0.32	0.29 to 0.34
	M1S-Ru	$C_{23}H_{26}NOSClRu$	501.05	1.73	1.69 to 1.77
	M2S-Ru	$C_{24}H_{28}NOSClRu$	515.07	1.66	1.56 to 1.77
IV	ZR-012	$C_{41}H_{37}ClF_3N_2O_3RuPS_2$	894.37	1.64	1.58 to 1.70
	ZR-014	$C_{43}H_{33}ClF_3N_2O_3OsPS_2$	1003.52	1.53	1.50 to 1.57

I: HDACis; II: Metal-based PCA ligands and complexes; III: Hydroxythiopyridone derivatives; IV: Kinetically inert metal(arene) complexes of PCA.

*Significantly increased compared to SAHA, $p<0.01$. Data were analysed with one-way ANOVA coupled with a Bonferroni post-hoc test. **Cytotoxicity did not reach 50%.

3.1.2 Dose-response cytotoxicity of novel potent compounds in H522 cells

To examine the consistency of JAZZ-90, M1S, M2S, M1S-Ru, and M2S-Ru potency towards other NSCLC cells, their activity was examined in H522 cells. SAHA was nearly 4.5 times more potent in H522 cells compared with JAZZ-90 (Table 3.2) but the potency of JAZZ-90 in H522 cells was reduced by 2-fold when compared to A549 cells (Figure 3.1 and 3.3). On the other hand, M1S and M2S displayed more cytotoxicity in comparison with their metal-based counterparts M1S-Ru and M2S-Ru (Table 3.2). Notably, in comparison with A549 cells, the potency of M1S and M2S increased nearly 1.3 and 1.4 times against H522 cells, while the cytotoxic potential of MIS-Ru and M2S-Ru decreased by almost 3.8 and 4.5-fold, respectively (Figure 3.2 and 3.3).

In summary, M1S and M2S were the most potent compounds against H522 cells and cytotoxicity was comparable with the control drug SAHA, which was similarly seen in A549 cells. The antiproliferative activity of the other three potent drugs JAZZ-90, M1S-Ru, and M2S-Ru (in A549) shifted significantly in comparison to SAHA in H522 cells (Table 3.1, 3.2). Since M1S and M2S exhibited submicromolar EC_{50} values in multiple cell lines, they were selected for further examination.

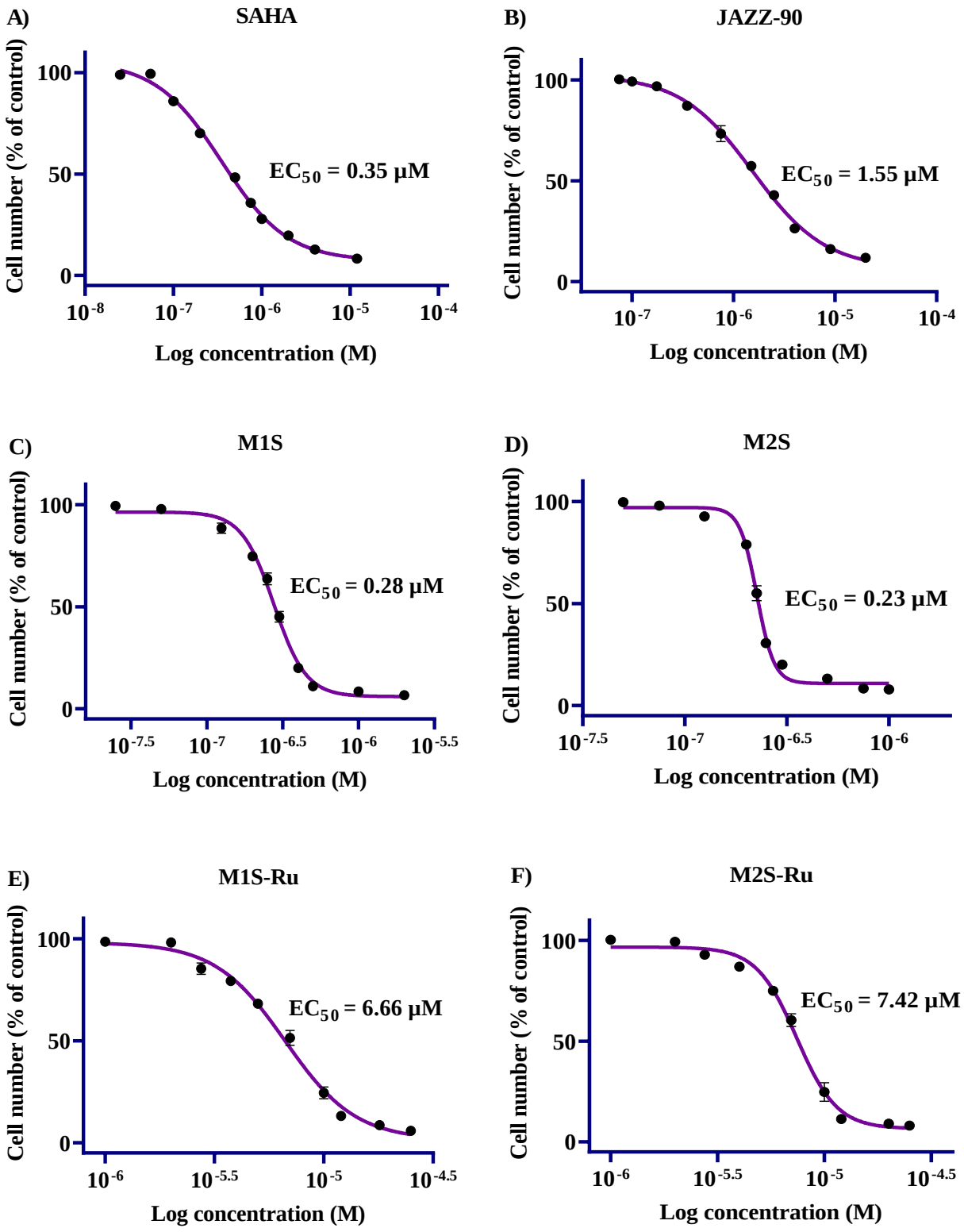

Figure 3.3: Cytotoxicity of SAHA, JAZZ-90, M1S, M2S, M1S-Ru, and M2S-Ru in H522 cells. H522 cells were seeded in 96-well plates at 10×10^3 cells per well and incubated for 24 h at 37ºC. The cells were then treated with SAHA (A), JAZZ-90 (B), M1S (C), M2S(D), M1S-Ru (E), and M2S-Ru (F) (0.025 to 20 µM) for 72 h. Vehicle control cells were treated with DMSO (0.5%). At the end of the treatment period, the cell number was determined by the SRB assay. The points represent the mean ± SEM (n=3). EC_{50} values were obtained using non-linear regression using Prism software.

Table 3.2: EC_{50} values of different classes of drug candidates in H522 cells

Class	Name	EC_{50} (µM)	95% confidence interval
HDACis	SAHA	0.35	0.31 to 0.39
	JAZZ-90	1.55*	1.37 to 1.77
Hydroxythiopyridone derivatives	M1S	0.28	0.26 to 0.29
	M2S	0.23	0.22 to 0.23
	M1S-Ru	6.66*	6.16 to 7.21
	M2S-Ru	7.42*	7.09 to 7.77

*Significantly increased compared to SAHA, $p<0.01$. Data were analysed with one-way ANOVA coupled with a Bonferroni post-hoc test.

3.1.3 Dose-response cytotoxicity of M1S and M2S on NIH3T3 cells

To investigate the potency of M1S and M2S towards cell lines with a different origin, both the compounds were examined in pre-neoplastic NIH3T3 cells (mouse embryonic fibroblast cell line) (Figure 3.4). Similar to the results from A549 and H522 cells, M1S (EC_{50} value of 0.44 µM, 95% confidence interval, 0.43 to 0.47 µM) and M2S (EC_{50} value of 0.34 µM, 95% confidence interval, 0.33 to 0.36 µM) showed consistent cytotoxic potential towards NIH3T3 cells. The potency of M2S in NIH3T3 cells is almost identical to A549 cells while in comparison with A549 cells the cytotoxicity of M1S decreased by 1.2-fold. On the other hand, the potency of M1S and M2S decreased by 1.6 and 1.5-fold in NIH3T3 cell compared with H522 cells.

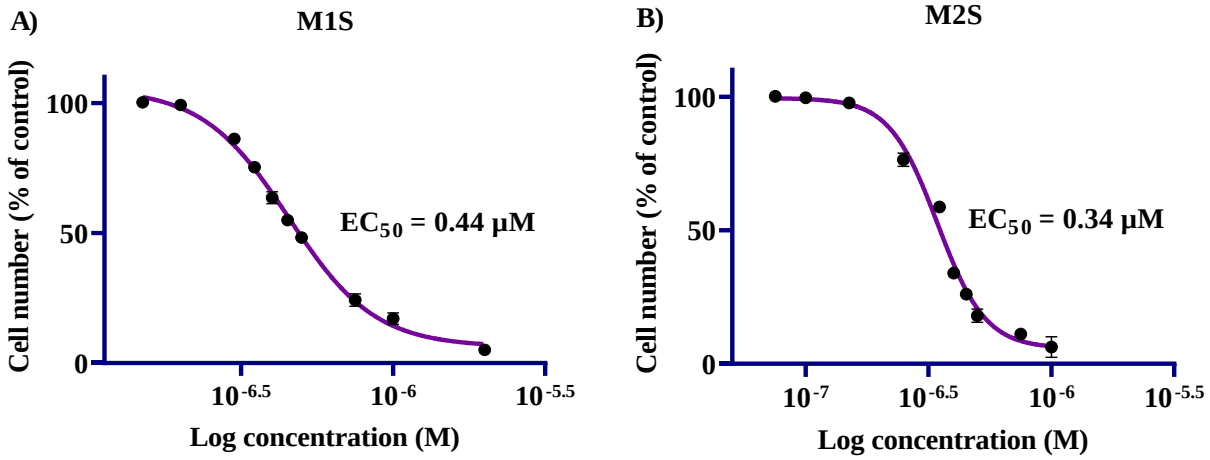

Figure 3.4: Cytotoxicity of M1S and M2S in NIH3T3 cells. NIH3T3 cells were seeded in 96-well plates at 3.5×10^3 cells per well and incubated for 24 h at 37ºC. The cells were then treated with M1S (A) and M2S (B) (0.075 to 2) µM for 72 h. Vehicle control cells were treated with DMSO (0.5%). At the end of the treatment period, the cell number was determined by the SRB assay. The points represent the mean ± SEM (n=3). EC_{50} values were obtained using non-linear regression using Prism software.

3.1.4 Dose-response cytotoxicity of M1S and M2S on PNT1A cells

To screen the selectivity of M1S and M2S against non-cancerous cells, the potency of the compounds was tested on PNT1A cells (normal prostate epithelial cells) (Figure 3.5). In comparison with the neoplastic (A549 and H522 cells) and pre-neoplastic cells (NIH3T3 cells), the potency of M1S (EC_{50} value of 1.29 µM, 95% confidence interval, 1.19 to 1.39 µM) and M2S (EC_{50} value of 1.12 µM, 95% confidence interval, 1.08 to 1.16 µM) decreased (Figure 3.2, 3.3, 3.4, and 3.5). The highest selectivity of M1S and M2S was observed in H522 cells, with a SI value of 4.47 and 4.87, respectively. While the SI value decreased to 3.55 and 3.5 in A549 cells. The drugs showed the lowest selectivity for NIH3T3 cells as the SI value further decreased to 2.91 and 3.29 for M1S and M2S, respectively (Table 3.3).

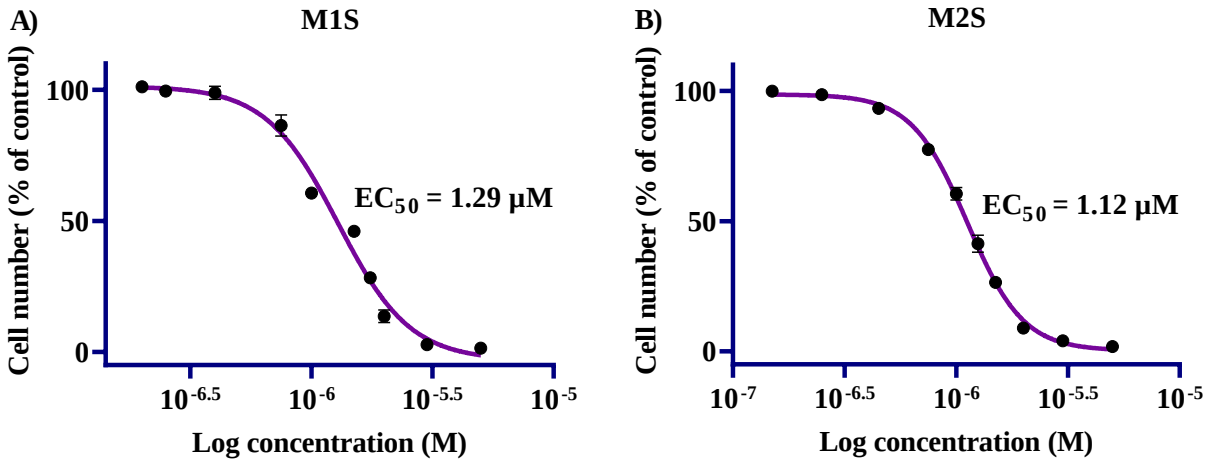

Figure 3.5: Cytotoxicity of M1S and M2S in PNT1A cells. PNT1A cells were seeded in 96-well plates at 10×10^3 cells per well and incubated for 24 h at 37ºC. The cells were then treated with M1S (A) and M2S (B) (0.15 to 5 µM) for 72 h. Vehicle control cells were treated with DMSO (0.5%). At the end of the treatment period, the cell number was determined by the SRB assay. The points represent the mean ± SEM (n=3). EC_{50} values were obtained using non-linear regression using Prism software.

Table 3.3: Selectivity index (SI) of M1S and M2S

Drug	EC_{50} values in normal cell line	EC_{50} values in neoplastic or pre-neoplastic cell lines	SI
M1S	PNT1A (1.29 µM)	A549 (0.36 µM)	3.55
		H522 (0.28 µM)	4.46
		NIH3T3 (0.44 µM)	2.91
M2S	PNT1A (1.12 µM)	A549 (0.32 µM)	3.5
		H522 (0.23 µM)	4.87
		NIH3T3 (0.34 µM)	3.29

The values of SI were determined using PNT1A as a normal cell line.

3.2 Time course cytotoxicity assessment in A549 and H522 cells

To determine the time-dependent cytotoxicity of M1S and M2S, A549 and H522 cells were treated at 2×EC_{50} concentrations for 12, 24, 36, 48, 60, and 72 h (Figure 3.6 A and B). M1S and M2S produced a similar cytostatic pattern in A549 cells (Figure 3.6 A). A statistically significant decrease in cell number was observed following 12 and 24 h of M2S and M1S treatment, respectively, and cell number was relatively stable throughout the remainder of the treatment period compared to control (Figure 3.6 A). Though the cytotoxic profile of both the

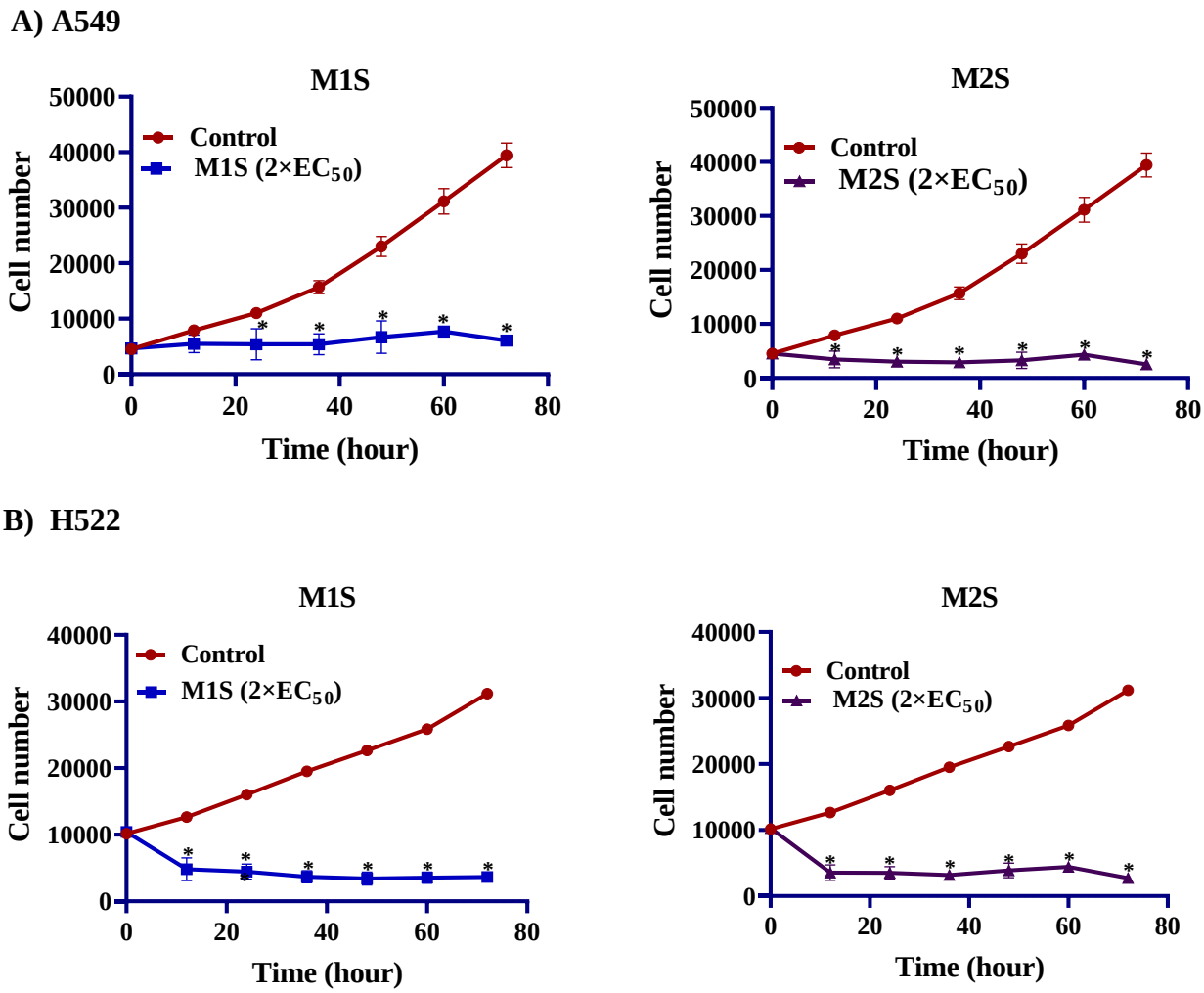

Figure 3.6: Time course cytotoxicity assessment of M1S and M2S in A549 and H522 cells. A549 cells and H522 were seeded in 96-well plates at 4 × 10^3 and 10 × 10^3 cells per well respectively and incubated for 24 h at 37ºC. A549 cells were then treated with 0.72 µM of M1S and 0.64 µM of M2S (A) while H522 cells were treated with 0.56 µM of M1S and 0.46 µM of M2S (B) for 12-72 h. Vehicle control cells were treated with DMSO 0.5%. At the end of the treatment period, the cell number was determined by the SRB assay. The points represent the mean ± SEM (n=3). Data were analysed using a two-way ANOVA coupled with a Bonferroni post-hoc test. *Significantly different from control, $p<0.01$. No significant differences were calculated between each treatment point from 12 to 72 h.

compounds towards H522 cells (Figure 3.6 B) was different in comparison to A549 cells (Figure 3.6 A), the two drugs showed almost identical initial cytotoxicity against H522 cells. Specifically, M1S and M2S showed a significant (nearly 2 and 2.9-fold, respectively) decrease in cell number at 12 h, and this effect was maintained for the rest of the treatment time.

The cytotoxicity of M1S and M2S was different in the two NSCLC cell lines. To investigate the potential mechanism that drives the time and cell line dependent variation in cytotoxicity, Western blotting was performed to determine the expression of acetyl H3, cyclin D1, and cyclin B1.

3.3 Drug-mediated changes in protein levels

3.3.1 Acetylated histone-H3 (Acetyl H3)

While the hydroxythiopyridone derivatives are not strong candidates for HDAC inhibition, this was confirmed by examining for changes in acetyl H3 following treatment with M1S and M2S in A549 and H522 cells. The expression of acetyl H3 was analysed using Western blotting. No significant difference in the expression of acetyl H3 was observed after the treatment of either M1S or M2S at the EC_{50} or $2\times EC_{50}$ concentrations (Figure 3.7).

A)

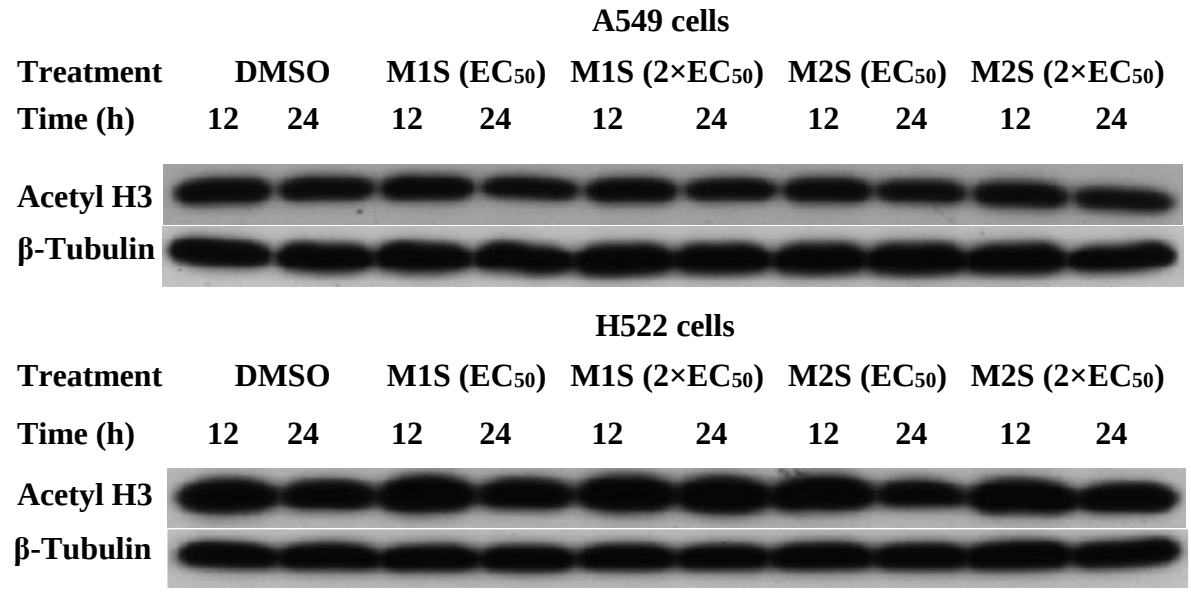

B)

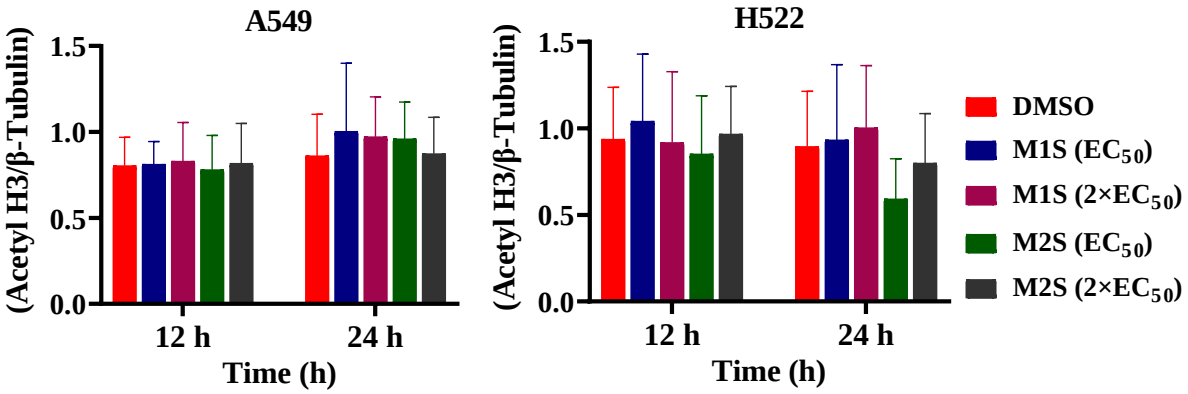

Figure 3.7: Effect of M1S and M2S on acetyl H3 expression in A549 and H522 cells. A549 (1×10^6 cells per dish) and H522 (2.5×10^6 cells per dish) cells were seeded in 10 cm cell culture dishes and left to attach for 24 h at 37ºC. A549 cells were then treated with 0.36, 0.72 µM of M1S and 0.32, 0.64 µM of M2S while H522 cells were treated with 0.28, 0.56 µM of M1S and 0.23 0.46 µM of M2S for 12-24 h. Vehicle control cells were treated with DMSO 0.5%. Cell lysates were subjected to Western blotting with a specific antibody against acetyl H3. A) Blots shown are representative of n=3. B) Scanning densitometry of the ratio of acetyl H3 to β-tubulin. Data were analysed with a two-way ANOVA coupled with a Bonferroni post-hoc test. None were significantly different.

3.3.2 Cyclin D1

To determine the potential mechanism by which M1S and M2S inhibit cell proliferation since the drugs were not HDACis, the expression of cyclin D1 protein (a G1 progression regulator) was examined in A549 and H522 cells (Figure 3.8). In A549 cells, M1S and M2S did not significantly change the cyclin D1 levels compared to control. Similarly in H522 cells treatment for 12 and 24 h with M1S or M2S at the EC_{50} concentration also failed to alter the cyclin D1/β-

tubulin ratio. However, doubling the M1S concentration to 2×EC_{50} reduced the cyclin D1 expression by 59.8% of control at 12 h while the same concentration significantly decreased the expression by 68.1% of control at 24 h. Furthermore, increasing the concentration of M2S to 2×EC_{50} significantly decreased the cyclin D1/β-tubulin ratio by 69.7 and 84.9% of control at 12 and 24 h, respectively.

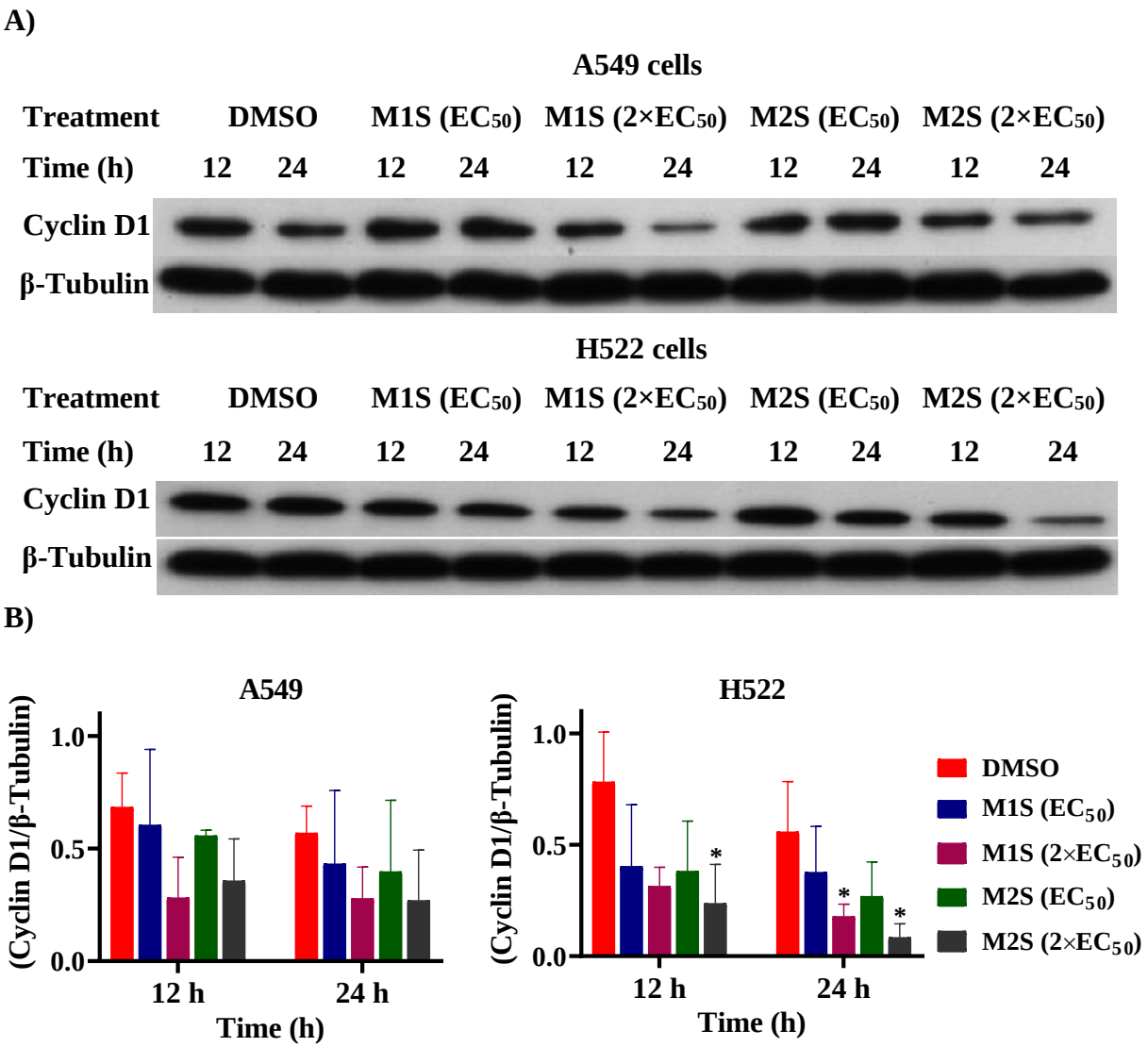

Figure 3.8: Effect of M1S and M2S on cyclin D1 expression in A549 and H522 cells. A549 (1×10^6 cells per dish) and H522 (2.5×10^6 cells per dish) cells were seeded in 10 cm cell culture dishes and left to attach for 24 h at 37ºC. A549 cells were then treated with 0.36, 0.72 µM of M1S and 0.32, 0.64 µM of M2S while H522 cells were treated with 0.28, 0.56 µM of M1S and 0.23 0.46 µM of M2S for 12-24 h. Vehicle control cells were treated with DMSO 0.5%. Cell lysates were subjected to Western blotting with a specific antibody against cyclin D1. A) Blots shown are representative of n=3. B) Scanning densitometry of the ratio of cyclin D1 to β-tubulin. Data were analysed with a two-way ANOVA coupled with a Bonferroni post-hoc test. *Significantly different from control, $p<0.01$.

3.3.3 Cyclin B1

To confirm the cell line and time-dependent effect on protein that regulate the cell cycle, the expression of cyclin B1, a G2/M progression regulator was also investigated. No significant changes in cyclin B1/β-actin ratio was seen when A549 and H522 cells were treated with either 1X or 2X the EC_{50} concentration of M1S or M2S for 12 or 24 h when compared to vehicle control (Figure 3.9).

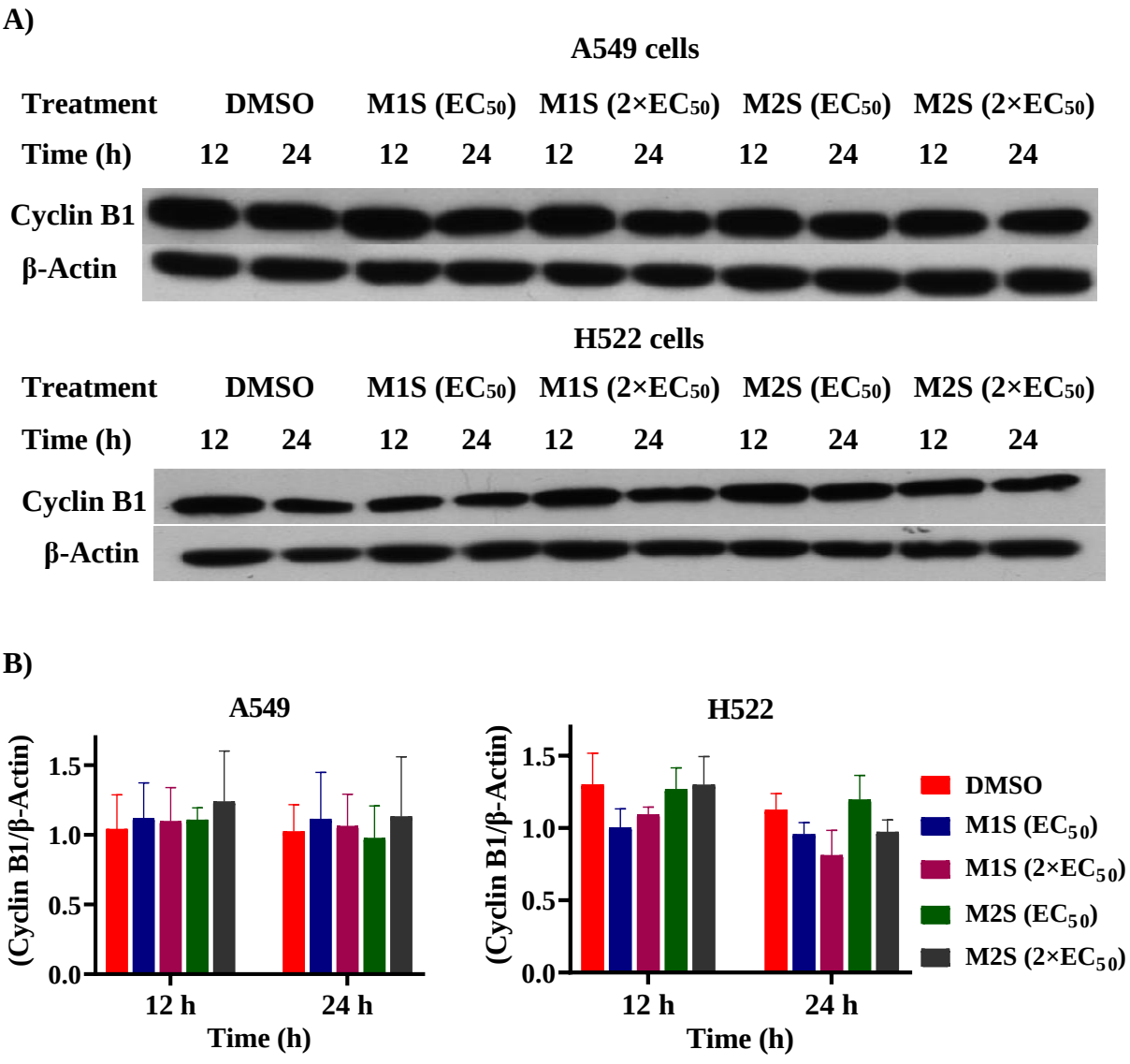

Figure 3.9: Effect of M1S and M2S on cyclin B1 expression in A549 and H522 cells. A549 (1×10^6 cells per dish) and H522 (2.5×10^6 cells per dish) cells were seeded in 10 cm cell culture dishes and left to attach for 24 h at 37ºC. A549 cells were then treated with 0.36, 0.72 µM of M1S and 0.32, 0.64 µM of M2S while H522 cells were treated with 0.28, 0.56 µM of M1S and 0.23 0.46 µM of M2S for 12-24 h. Vehicle control cells were treated with DMSO 0.5%. Cell lysates were subjected to Western blotting with a specific antibody against cyclin B1. A) Blots shown are representative of n=3. B) Scanning densitometry of the ratio of cyclin B1 to β-actin. Data were analysed with a two-way ANOVA coupled with a Bonferroni post-hoc test. None were significantly different.

In the time course assay, M1S and M2S showed a cytostatic and cytotoxic pattern in A549 and H522 cells, respectively. Additionally, a significant difference in cell number was seen in A549 cells after 12 h of M2S treatment at $2\times EC_{50}$ concentration, while the same concentration of M1S and M2S significantly decreased cell number in H522 cells (Figure 3.6). However, M1S and M2S failed to produce any significant changes in acetyl H3, cyclin D1, and cyclin B1 expression in A549 cells as shown by Western blotting after 12 h (Figure 3.7, 3.8 and 3.9). Similar to A549 cells, after 12 h the compounds were unable to significantly change acetyl H3 and cyclin B1 levels at $2\times EC_{50}$ concentration in H522 cells (Figure 3.7 and 3.9). Interestingly, both the compounds showed a concentration-dependent (EC_{50} and $2\times EC_{50}$) trend in the reduction of the cell cycle protein cyclin D1 in both A549 and H522 cells after 12 h. However, within this period only M2S significantly decreased cyclin D1 level at $2\times EC_{50}$ in H522 cells (Figure 3.8). Therefore, cell cycle analysis at 12 h and one earlier time point, 6 h were conducted to examine how these compounds drive the cell cycle changes and generate their cytostatic or cytotoxic effects evident at 12 h.

3.4 Cell cycle analysis

To investigate the effects of M1S and M2S on cell cycle progression of A549 and H522 cells, cell cycle analysis was performed using flow cytometry. M1S and M2S did not produce any significant effect in the cell cycle progression of A549 cells compared to control (Figure 3.10). In H522 cells significance of M1S and M2S treatments could not be determined from two biological repeats. It appeared as though the compounds exhibited a concentration-dependent trend of arresting H522 cells in the G1 phase at 12 h (Figure 3.11). However, triplicate experiments in H522 cells will be required to confirm this effect. In the sub-G1 phase, a small peak far left of the G1 peak was observed in H522 cells (Figure 3.11 A), which is an indicator of apoptotic cells. The significance of the apoptotic cells in M1S and M2S groups could not be confirmed from duplicate experiments. However, it appeared as though a higher proportion of apoptotic cells might be present in the treatment groups compared to control at 6 and 12 h (Figure 3.12). Triplicate experiments in H522 cells will also give a more precise conclusion regarding whether or not the apoptotic cells appeared in the sub-G1 phase.

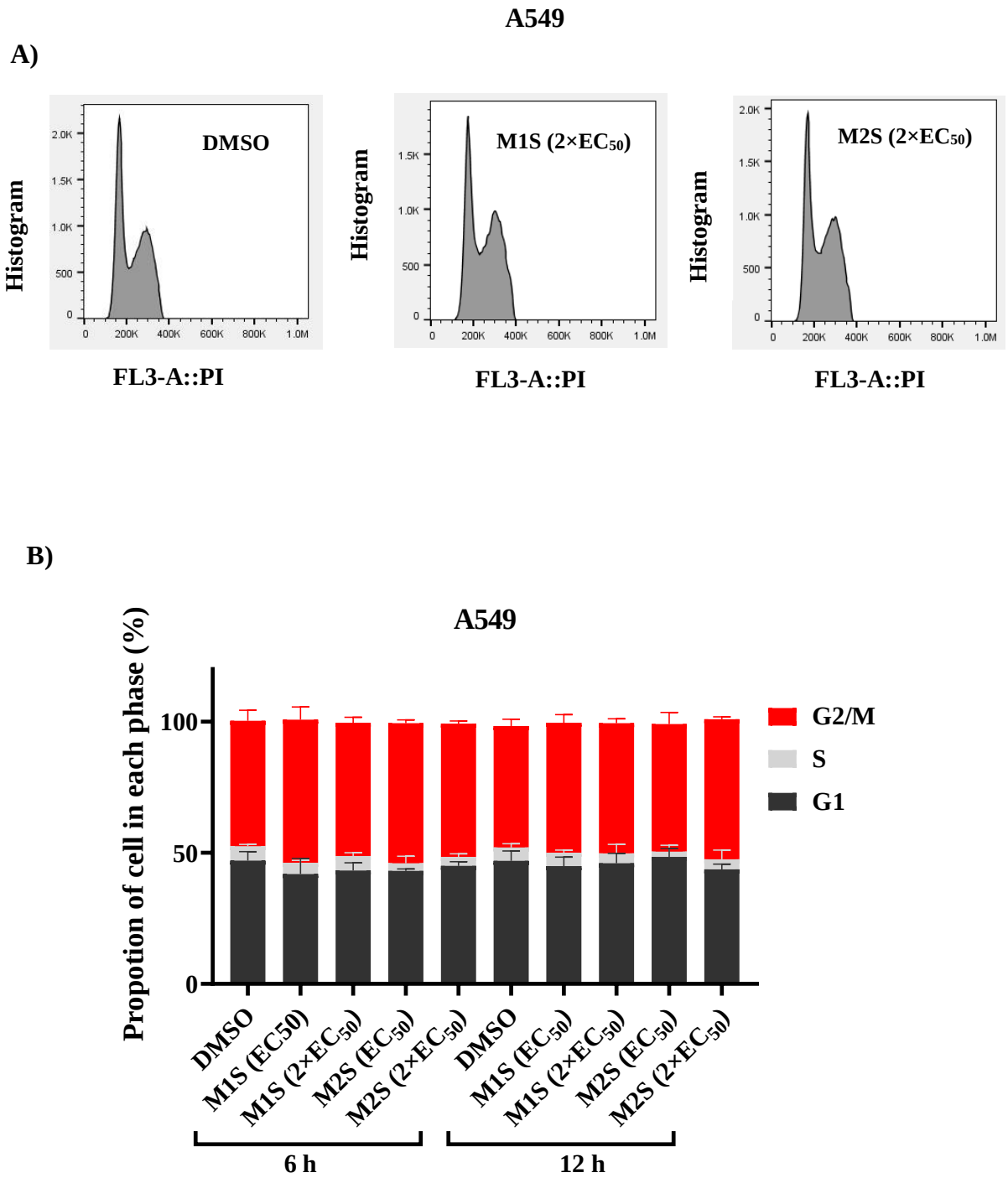

Figure 3.10: Cell cycle analysis in A549 cells exposed to M1S and M2S. A549 (1×10^6 cells per dish) cells were seeded in 10 cm cell culture dishes and left to attach for 24 h at 37ºC. Cells were then treated with 0.36, 0.72 µM of M1S, and 0.32, 0.64 µM of M2S for 6-12 h. Vehicle control cells were treated with DMSO 0.5%. A) Representative histograms of control and treatment. B) Bars indicate the mean proportion of cells in different cell cycle phases (% of total) ± SEM (n=3). Data were analysed with a two-way ANOVA coupled with a Bonferroni post-hoc test. None were significantly different.

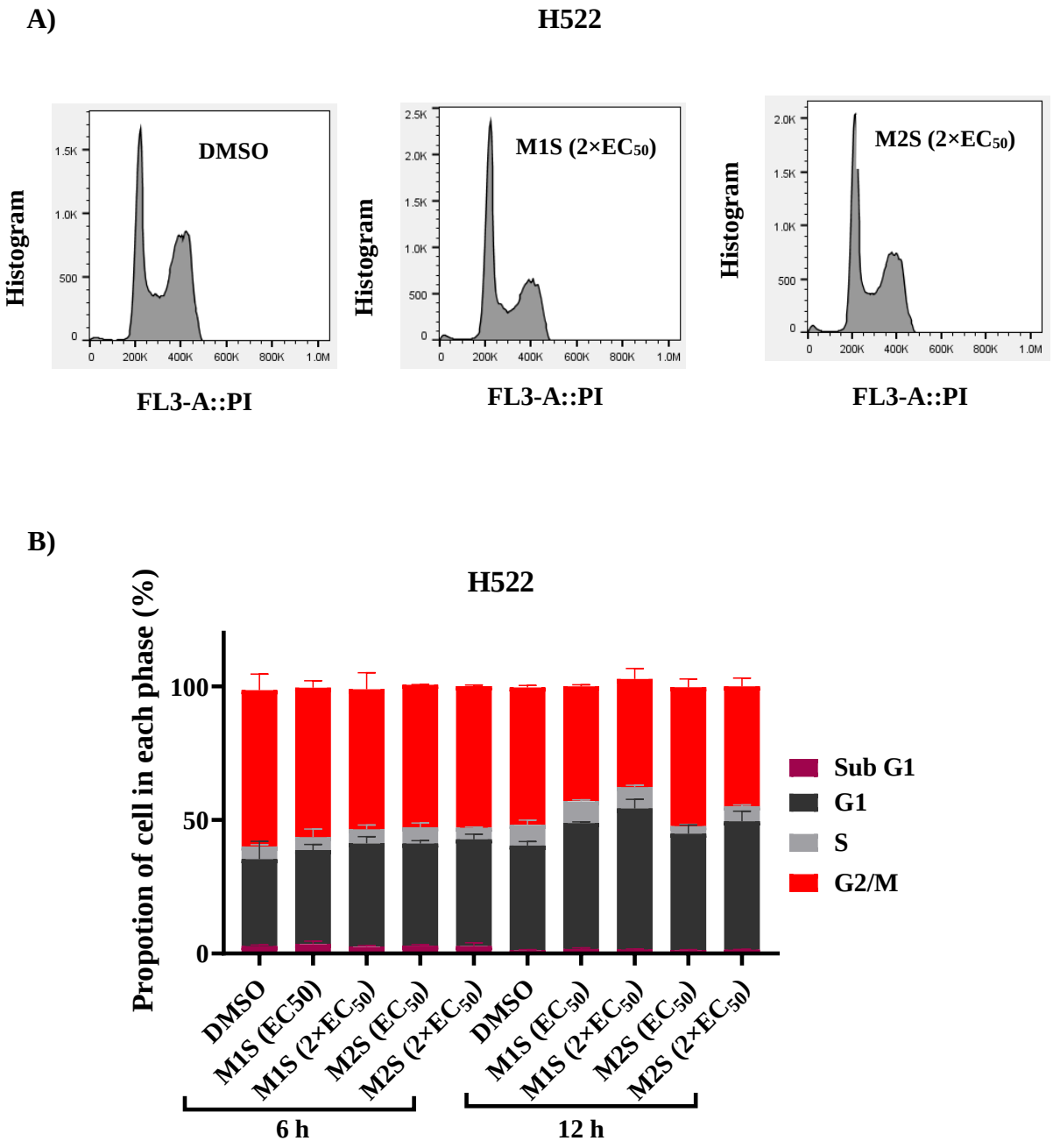

Figure 3.11: Cell cycle analysis in H522 cells exposed to M1S and M2S. H522 (3.0×10^5 cells per well) cells were seeded in 6-well plates and left to attach for 24 h at 37ºC. Cells were treated with 0.28, 0.56 µM of M1S and 0.23 0.46 µM for 6-12 h. Vehicle control cells were treated with DMSO 0.5%. A) Representative histograms of control and treatment. B) Bars indicate the mean proportion of cells in different cell cycle phases (% of total) ± SEM (n=2). Data could not be statistically analysed from n=2.

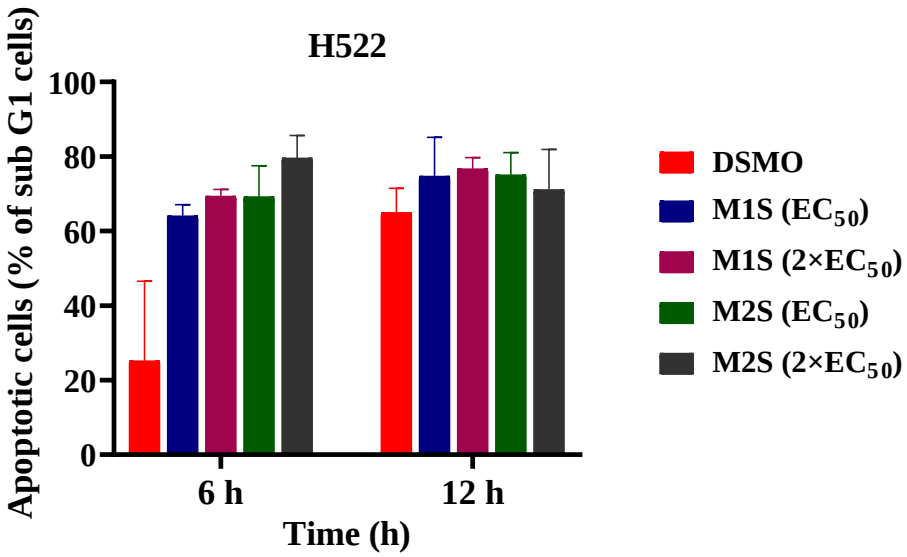

Figure 3.12: Apoptotic cells in sub-G1 phage in H522 cells after M1S and M2S treatment. H522 (3.0×10^5 cells per well) cells were seeded in 6-well plates and left to attach for 24 h at 37ºC. Cells were treated with 0.28, 0.56 µM of M1S and 0.23 0.46 µM for 6-12 h. Vehicle control cells were treated with DMSO 0.5%. Bars indicate the mean ± SEM (n=2). Data could not be statistically analysed from n=2.

3.5 Summary of results

Table 3.4: EC_{50} values of different classes of drug candidates in A549, H522, NIH3T3, and PNT1A cells

Class	Drug Candidate name	Mol. weight (g/mol)	EC_{50} (µM)			
			A549	H522	NIH3T3	PNT1A
Hydroxythiopyridone derivatives	M1S	231.31	0.36	0.28	0.44	1.29
	M2S	245.34	0.32	0.23	0.34	1.12
	M1S-Ru	501.05	1.73	6.66		
	M2S-Ru	515.07	1.66	7.42		
HDACis	SAHA	234.32	1.01	0.35		
	JAZZ-90	400.49	0.76	1.55		
	JAZZ-166	797.83	3.17			
	JAZZ-167	708.52	4.22			
Metal-based PCA ligands and complexes	JAZZ-121	541.31	Not determined			
	AASH-122	538.47	2.02			
Kinetically inert metal(arene) complexes of	ZR-012	894.37	1.64			
	ZR-014	1003.52	1.53			

Time course cytotoxicity of M1S and M2S

A549: M1S and M2S produced a similar cytostatic pattern in A549 cells, approximately initial seeding number (4000 cells) was maintained from 12-72 h.

H522: M1S and M2S decreased ~2 and 2.9-fold of initial cells (10,000 cells) respectively at 12 h, and this effect was maintained for 24-72 h.

Table 3.5: Effects of M1S and M2S on cell signalling proteins and cell cycle

Cell lines	Protein Expression (at 12 and 24 h)			Cell Cycle (at 6 and 12 h)
	Acetyl H3	Cyclin B1	Cyclin D1	G1, S and G2 Phases
A549	Non-significant at EC_{50} to $2\times EC_{50}$ concentration of M1S and M2S.			
H522	Non-significant at EC_{50} to $2\times EC_{50}$ concentration of M1S and M2S.		**M1S**: Significant changes at $2\times EC_{50}$ after 12 and 24 h. **M2S**: Significant changes at $2\times EC_{50}$ after 24 h.	M1S and M2S appeared to arrest at G1 phase at $2\times EC_{50}$. Statistical analysis could not performed from n=2.

CHAPTER IV

Discussions

4 Discussions

The current project was designed to study the cytotoxic effects and anticancer mechanisms of 11 novel metal-based and non-metal-based compounds against NSCLC cells *in vitro*. Previous investigations in the lung, cervical, and colorectal cancer cell lines have shown that these novel compounds have antiproliferative activity in the nanomolar to micromolar range. Therefore, it was hypothesised that potent cytotoxicity would also be observed in NSCLC cell lines. Based on the cytotoxicity screening, the two most potent compounds, M1S and M2S, were chosen to further investigate their effects on cell signalling proteins by Western blotting, and cell cycle progression by flow cytometry. To assure the reliability of the current results, it is important to understand the limitations of the protocols in order to interpret the experimental results.

4.1 Rationale for using different cell lines

4.1.1 A549 and H522 cell lines

KRAS mutations are heterogeneous and different genotypes could be linked with specific clinical outcomes [25]. Table 4.1 shows the diversities in KRAS mutation and KRAS-mutated NSCLC cancer cell lines. The A549 adenocarcinoma cell line has been widely studied since its discovery in 1976 [193] and has a higher expression phospho-AKT (protein kinase B) [194]. Additionally, A549 cells are resistant to MEK inhibitors [194]. Consecutive activation of KRAS promotes continuous stimulation of downstream signalling pathways that result in tumourigenesis, including activation of RAF-MEK-ERK and PI3K-AKT-mTOR signalling cascades [36]. Furthermore, co-occurring genetic alterations could alter other signalling pathways and thereby affect biological behaviours, clinical outcomes, and therapeutic responses in KRAS-mutant lung cancer [195]. Table 4.2 depicts co-mutation frequency of KRAS gene in NSCLC patients. In the KRAS-mutant NSCLC patients, p53 (guardian of the genome) is one of the most frequent co-mutations [196, 197]. H522, a solid tumour-derived, adenocarcinoma cell line, has a mutation at exon-6 of the p53 gene [198-200]. p53 protein functions as a central hub that receives and transmits multiple signals. It plays a vital role in tumour suppression notably by promoting apoptosis, autophagy process, growth arrest, and senescence, as well as by inhibiting angiogenesis [197, 201]. Furthermore, p53 enhances the sensitivity of cancer cells to chemoradiation and thereby, prolonging the survival. Thus, p53 becomes one of the most popular targets for mechanism-based anticancer drug discovery [197, 202]. Lastly, H522 and A549 cell lines have been commonly used to study the antimetastatic activity of drugs [203-205].

Table 4.1: Diversities in KRAS mutation in NSCLC patients and cell lines

	Mutated gene	Sample	Frequency	Source	Frequently mutated codon in KRAS	Mutation type	Representative cell Lines
Mutation of KRAS gene in NSCLC patients	KRAS	N=230 (ADC)	32.61%	CGMARN [6]	Codon 12	G12C	Calu-1, LU-65, LU-99, H1385, H1792, H2122, H23, H358, SW 1573, IA-LM, HOP-62, H2030, H2212 [206-210]
		N= 183 (ADC)	26.78%	Imielinksi et al. [6]		G12V	SW 900, LCLC-97TM1, H2444, H441, H727, RERF-LC-Ad2, COR-L23 [9, 207, 208, 211-213]
		N= 163 (ADC)	36.81%	Ding et al. [6]		G12A	H2009 [206]
		N= 532 (ADM & ADC)	27.26%	NCI GDC data portal [214]		G12D	SK-LU-1, T3M-10 [208]
		N= 129 (NSCLC)	20%	Dang et al. [215]		G2S	A549 [206]
		N= 129 (NSCLC)	30.2%	Svaton et al. [216]		G12R	H157 [206, 207]
		N= 179 (ADC)	48.57%	Nadal et al. [217]	Codon 13	G13D	H1944, H647 [208]
	KRAS-Amp.	N=230 (ADC)	9.33%	CGMARN [6]		G13C	H1355, H1734 [207]
		N= 183 (ADC)	6.12%	Imielinksi et al. [6]	Codon 61	Q61H	H460 [207]
		N= 385 (NSCLC)	~15%	Wagner et al. [218]		Q61K	Calu-6 [207]

NSCLC: Non-small cell lung cancer; Amp.: Amplification; ADC: Adenocarcinoma; ADM: Adenomas; CGMARN: Cancer Genome Atlas Research Network; NCI: National Cancer Institute; GDC: Genome Data Commons.

Table 4.2: Co-mutation frequency of KRAS gene in NSCLC patients

	Mutation Type	Mutated Genes	Frequency	Source	Ref.
Co-mutation of KRAS gene in NSCLC patients	Co-mutation of 2 genes	KRAS-TP53	30.67% N=230 (ADC)	CGMARN	[6]
			38.78% N= 183 (ADC)	Imielinksi et al.	
			35% N= 163 (ADC)	Ding et al.	
			31% N= 75 (NSCLC)	Lei et al.	[196]
		KRAS-STK1	26.67% N=230 (ADC)	CGMARN	[6]
			14.29% N= 183 (ADC)	Imielinksi et al.	
			16.67% N= 163 (ADC)	Ding et al.	
			8% N= 75 (NSCLC)	Lei et al.	[196]
		KRAS-EGFR	11% N= 75 (NSCLC)	Lei et al.	
			1.4% N= 350 (NSCLC)	Dang et al.	[215]
		KRAS-BRAF	0.3% N= 350 (NSCLC)	Dang et al.	
		KRAS-ALK	0.3% N= 350 (NSCLC)	Dang et al.	
		KRAS-ROS1	0.3% N= 350 (NSCLC)	Dang et al.	
	Co-mutation of 3 gene	KRAS-EGFR -BRAF	0.3% N= 350 (NSCLC)	Dang et al.	
		KRAS-TP53-STK1	1.33% N=230 (ADC)	CGMARN	[6]
			6.12% N= 183 (ADC)	Imielinksi et al.	
			5% N= 163 (ADC)	Ding et al.	

NSCLC: Non-small cell lung cancer; ADC: Adenocarcinoma, ADM: Adenomas; CGMARN: Cancer Genome Atlas Research; Ref.: References.

4.1.2 NIH3T3 cell line

NIH3T3 is an immortalised mouse embryonic fibroblast cell line used to promote survival and self-renewal of tissue progenitor cells [219, 220]. This cell line is also preferred for transfection experiments [220]. NIH3T3 is non-tumourigenic in athymic nude mice however, subcutaneous injection of NIH3T3 cells with basement membrane protein (matrigel) forms locally invasive and highly vascularised tumours. Additionally, intravenous administration of tumour-derived

NIH3T3 cells generates multiple colonies on the lung surface while the parental NIH3T3 cells are non-metastatic [221]. Thus, the NIH3T3 cell line is considered to be preneoplastic [222].

Fibroblasts are one of the key cellular components for tumours and reside in highly complex multicellular environments in the lung [223, 224] Fibroblast, endothelial and immune cells coexist along with transformed cells in the tumour microenvironment (TME) [225]. The TME is directly involved in tumour initiation, progression, drug resistance, and metastasis. Current therapeutic strategies focus only on the rapid-growing tumour "seeds" ignoring the tumour "soil" *i.e.* TEM [226]. A recent study showed that the NSCLC cell lines (A549 and H1299) co-cultured with two different fibroblast cells increased mitochondrial function in the tumour cells [225]. Mitochondria influence multiple cellular mechanisms that support tumour progression via the proliferation of transformed cells, adaptation under an unfavourable microenvironment, and finally the migration to distant anatomical sites [227]. Therefore, the antiproliferative activity of M1S and M2S was examined in NIH3T3 cells as a representation of fibroblast cells.

4.1.3 PNT1A cell line

PNT1A is a normal, immortalised non-transformed prostate epithelial cell line [228, 229]. PNT1A cells are positive for phosphatase and tensin (PTEN) homologue and cells harbour wild type p53 [230]. PNT1A is a reliable model for understanding the cellular processes, for instance, the proliferation of prostatic epithelium in response to androgen and growth factors [231]. It is noted that to immortalise the PNT1A cells, cells were transfected with a plasmid containing the SV40 genome with a defective replication origin and express large T protein [232]. Therefore, PNT1A cells are representative of a normal cell line having the aforementioned limitation.

Pulmonary epithelial cells play a crucial role in the maintenance of lung tissue homeostasis [233]. Specialised epithelial cells located in a different part of the lung tissue function in host defense, gas exchange, xenobiotic metabolism, chemoattractant, maintenance of structural integrity, expression of adhesion receptors, lipid mediators for communication with neighbouring cells and matrix attachment [233-235]. Interruption of the formation of special epithelial cells negatively impacts on lung morphology [235]. Therefore, the cytotoxic potential of M1S and M2S were tested on PNT1A cells as a representation of normal epithelial cells.

4.2 Critiques of experimental design and methods

4.2.1 SAHA as a control drug

SAHA is an FDA approved HDACi that showed antiproliferative activity toward NSCLC cells including A549 and H522 [236-239]. As the cytotoxic potency of SAHA against A549 cells

and H522 cells has been reported using the SRB assay [236-238], it was selected as an appropriate control drug with which to compare the various novel drugs.

4.2.2 Preclinical cytotoxicity study using the SRB assay

To develop a new therapeutic agent accurate and reliable data from *in vitro* cytotoxicity experiments is vitally important as these results are critical to choosing a lead drug candidate [240]. In cancer drug discovery studies, several *in vitro* assays are used to screen cell viability and these are based on a variety of parameters. These *in vitro* assays have their pros and cons, hence it is important to select the most reliable ones based on the literature [240, 241]. Additionally, the cost, experimental equipment, and method of detection should be taken into account before selecting an *in vitro* technique [241].

The 3-(4,5-dimethylthiazol-2yl)-2,5-diphenyltetrazolium bromide (MTT) assay has become a popular method for determination of drug cytotoxicity and cell viability [242]. Several tetrazolium-based assays, such as the sodium salt of 4-[3-(4-iodophenyl)-2-(4-nitrophenyl)-2H-5-tetrazolio]-1,3-benzene disulfonate (WST-1), [5-(3-carboxymethoxyphenyl)-2-(4,5,-dimethylthiazolyl)-3-(4-sulfophenyl)tetrazolium, inner salt] (MTS), and 2,3-bis(2-methoxy-4-nitro-5-sulfophenyl)-5-[(phenylamino)carbonyl]-2H-tetrazolium hydroxide (XTT) assays have yet to replace the well-established MTT assay [240, 243-245]. However, research has proven that the MTT assay is inconsistent and nonspecific due to dependency on cellular metabolic status including the number of viable mitochondria, mitochondrial activity, cellular metabolic and energy perturbations, variation in oxidoreductases activity, exo-/endocytosis and intracellular trafficking leading to both false-positive or false-negative results [242, 246-248]. Previously, resveratrol, verapamil, ursolic acid, rottlerin, imatinib, genistein nanoparticles, nano-TiO_2, some polypeptides and plant extracts (of *Hypericum adenotrichum*, *Salvia kronenburgii*, and *Pelargonium quercetorum*) were reported to interfere with MTT reduction and thereby also produce inconsistent data between the MTT assay and other assays [246-248]. Furthermore, resazurin reduction (RES), neutral red uptake (NRU), and SRB data gave a smaller variability across the linear range while larger variation was produced by the MTT assay. The results indicate that these assays would be more reliable in the detection of small changes in cell number than the MTT assay. Among these three techniques, results from the SRB assay have generated the most reproducible data as indicated by the coefficient of determination [240].

The SRB assay is a quick and sensitive colourimetric technique for the determination of drug-mediated cytotoxicity in both suspension and attached cells. This assay is described by Skehan and colleagues for the development of a large-scale *in vitro* anticancer discovery program at

the National Institute of Cancer (NCI) [249]. SRB is a bright pink aminoxanthene dye that binds to protein basic amino acid residues of TCA-fixed cells, which is related to the viable cell number. An advantage of this technique compared to others is that cell quantification is based on protein content that does not interfere with test compounds, thereby producing high reproducibility [249, 250]. Additionally, fewer steps are required to optimise the assay protocol compared with MTT [251]. Finally, this assay has higher sensitivity, better linearity, a stable endpoint, is independent of intermediary metabolism, and is less sensitivity to environmental fluctuations [249, 250]. The drawbacks of this assay include low sensitivity with nonadherent cells, as well as the need to add TCA to fix the cells [240]. In comparison with MTT, SRB stains recently lysed cells without staining the cell debris [251]. Overall, considering the test parameters, the cytotoxicity of our novel metal-based and non-metal-based synthetic compounds were screened by the SRB assay.

4.2.3 Western blotting

Western blotting, also called immunoblotting, is one of the most widely used and broadly useful techniques in cancer research to understand the cell signalling mechanism of proteins that are linked with cancer treatment [252, 253]. The techniques use SDS-PAGE to separate complex protein mixtures present in a sample. The separated proteins are then transferred onto PVDF or nitrocellulose membrane, where they bind to antibodies specific for target proteins [254]. The effectiveness of the protein transfer process is dependent on the type of gel (percentage of acrylamide, bisacrylamide: acrylamide ratio) and transfer membrane. Each membrane has a capacity limit for protein binding (*e.g.* PVDF ~ 170 µg/cm^2, 80-250 µg/cm^2), so it is wise to consider how much protein lysate to run per well on the gel [255]. The membrane must be blocked after the transfer process to avoid high background and non-specific binding of the antibody. A 1 h incubation with 3-5% non-fat dry milk, goat serum or BSA solution is usually recommended [256]. After that, the membrane is incubated with a primary antibody to the target protein. The primary antibody is detected by an enzyme tagged secondary antibody. The secondary antibody catalyses an enzymatic reaction with the substrate to produce light, which can be detected by X-ray film or digital imager [254, 256]. Enhanced chemiluminescence has become the most popular method for detection in Western blotting due to its high sensitivity [255]. It is important to note that the data generated with Western blotting is typically considered semi-quantitative. Western blotting measures a relative comparison of protein levels, but not an absolute measure of quantity. Though the protocol of Western blotting is simple, many experimental errors can arise, leading to undesirable results. The unexpected results can be grouped into five categories: (i) unusual or undesirable bands, (ii) faint bands or

weak signal, (iii) no band, (iv) uneven or patchy spots on the blot and (v) high background on the blot [257].

The advantage of immunoblotting is the ability to identify target proteins as low as 1 ng because of the high-resolution capacity of gel electrophoresis and specificity and strong sensitivity of the immunoassay [254]. The molecular mass of the identified protein can be determined by comparing with standards of known molecular weight. Additionally, the selective nature of the specific antibody promotes the determination of a target protein in a complex mixture having >100,000 different proteins [256]. Isoforms and post-translationally modified protein with the same molecular weight can be identified using 2D electrophoresis (2DE Western). Western blotting can also be used as an effective early diagnostic tool [256, 258].

Like all other experimental techniques, Western blotting has its limitations [256]. The major limitation of this method is dependent on the primary antibody against the target protein and many protein targets cannot be determined due to the unavailability of specific antibodies [259]. Another main drawback is that many antibodies are non-specific [256]. Approximately, 50% of commercially available antibodies are of low quality and should not be used for Western blotting [259]. Furthermore, each antibody requires independent optimisation and protocol modification. Larger proteins (>140 kDa) may not be transferred from the gel to the membrane and smaller proteins (<10 kDa) may not be retained by the membrane. Other limitations include the inability of the primary antibody to detect the denatured immobilised antigen, quick decay of the detection signal, and high background [256]. However, these limitations are mainly due to sub-standard antibodies and sub-standard protocols that can be overcome with quality antibodies and proper experimental techniques [256, 259].

4.2.4 Flow cytometry

Flow cytometry is a technique that offers rapid multi-parametric analysis of various properties of single cells in solution. A flow cytometer machine utilises lasers as light sources to generate both scattered and fluorescent light signals [260, 261]. The fluorescence can be used for qualitative and quantitative determination of various cellular properties including relative size, internal complexity, DNA, RNA, or protein content [261]. Flow cytometry is a powerful tool that has a wide range of applications in the biomedical field including cancer biology [260].

Flow cytometry can be used to examine cell cycle kinetics and progression based on the DNA content of individual cells. To quantify the DNA content cells are stained with a fluorescent die that interacts with the DNA [262]. PI is a widely used DNA binding die with red fluorescence. As PI stains double-stranded nucleic acids, to avoid RNA interference PI is used in combination

with RNAase for the accurate determination of cell cycle phases (*i.e.* G1, S, G2/M phases) [262, 263]. Ethanol preserves PI stained cells for up to 3 days without significant interference with the cell-cycle distribution [264]. Additionally, ethanol fixation leaks out the highly fragmented DNA of the apoptotic cells during their dehydration and staining, while fixation with other solvents, for instance, formaldehyde preserves the fragmented DNA inside the cells [265]. Ethanol fixation thereby provides an extra advantage in the detection of sub-G1 apoptotic cells. Furthermore, 70% ethanol fixed cells can be stored up to 4 weeks [262]. It should be noted that ethanol-based fixation often produces considerable aggregation of cells. Dropwise addition of ethanol along with vortexing is used to minimise the aggregation.

Advancement in analysis has improved flow cytometry as the total fluorescence of individual cells can be achieved via sophisticated gating from a cell population. The fluctuations in protein and gene expression could be due to variations in cell volume. To reduce cell variability, flow cytometry relies on "gating" (*i.e.* use of sequential gates in the FSC-A/SSC-A and FSC-H/FSC-W dot blots to discard undesired cells that located outside of the selected gates) thereby reducing variability in the cellular optical properties [266]. Cell volume and granularity are primary confounding characteristics that are linked with the forward scattered (FSC) light and side scattered (SSC) light measurements, respectively. For instance, larger cells may show an apparent increased fluorescence. To minimise the cell size and granularity effects on the fluorescence intensity, the phenotypic variability based regression model can be used [267]. A limitation of flow cytometry is that it can generate "false-positive" heterogeneity, most of the results are associated with cytotoxicity, apoptosis, and cellular differentiation [266, 268]. The false-positive results could be due to sample preparation artifacts and staining resulting from antibody cross-reactivity and lack of morphological information. Additionally, the flow cytometric study of adherent cells has the main disadvantage that cells have to be detached into a single cell suspension before analysis [266].

4.3 Interpretation of results

4.3.1 Dose-response cytotoxicity study

To determine the most potent drug for KRAS-mutant NSCLC eight metal-based and three non-metal-based compounds were screened in A549 cells. Potency is defined as the activity of a drug in terms of the amount or concentration of the drug required to produce the desired effect [269]. Potency has an influential role in *in vitro* drug testing and selection [270]. The lower the EC_{50} value, the lower the concentration required to kill 50% of cells, therefore, a higher potency [271]. Compounds with lower EC_{50} values are predicted to be more effective in *in vivo* with minimum side effects, as the effective dose will be small (assuming toxicity is proportional to

dose) [270]. The first large scale drug screen was performed in the NCI60 panel of cell lines using the SRB assay after 48 h of continuous incubation [272]. Another publicly available database (http://cancer.sanger.ac.uk/cosmic) reported that the anticancer potency of >100 drugs against ~1000 cells relied on 72 h continuous incubation with the drug [272]. Several other groups examined the potency of drugs after 72 h [273-275]. Furthermore, Gulden et al. reported that at least 72 h of incubation make the results more comparable to other *in vitro* assays and extrapolation to *in vivo* experiments more meaningful than shorter exposure times [276].

To achieve reliable and reproducible potency, all the metal-based and non-metal-based drug candidates were exposed to the experimental cell lines for 72 h. M2S, M1S, and JAZZ-90 showed the most potent cytotoxicity towards A549 cells with EC_{50} values <0.8 µM. On the other hand, the metal compound ZR-014, ZR-012, M2S-Ru, and M1S-Ru produced EC_{50} values of 1.5-1.8 µM. While the EC_{50} value of the control drug, SAHA, was 1 µM in A549 cells. Liu and colleagues determined the IC_{50} value of SAHA (2.6 µM) in A549 cells, using the SRB assay after 72 h [238]. Depending on the seeding cell number, cell viability assay, cell culture media, and experiment time, other groups have reported EC_{50} value of SAHA between 0.69 to 5.34 µM in A549 cells [277-279]. The antiproliferative activity of JAZZ-90, M1S, M2S, M1S-Ru, M2S-Ru, Z4-012, and ZR-014 was comparable to SAHA while the potency of AASH-121, JAZZ-166, and JAZZ-167 were significantly lower compared to SAHA. In terms of EC_{50} values, M2S, M1S, and JAZZ-90 were the most potent drug candidates and were selected for further experiments. Though M1S-Ru, M2S-Ru, ZR-012, and ZR-014 were equally potent, M1S-Ru and M2S-Ru were selected for the next experiments along with three most potent drugs considering that M1S-Ru and M2S-Ru contain the cytotoxic moieties of M1S and M2S.

SAR is crucial in understanding various aspects of drug discovery as it provides information regarding structural modifications to optimise drug physicochemical properties and biological activities that include potency improvement, toxicity reduction, and ensuring sufficient bioavailability [280]. Anticancer activity of non-metal and metal-based derivatives varied in A549 cells, the variation might be due to the structural differences. JAZZ-166 (EC_{50} value of 3.17 µM) and JAZZ-167 (EC_{50} value of 4.22 µM) are the Ir and Rh arene complex of JAZZ-90 (EC_{50} value of 0.76 µM), where the metal arene moiety is connected with the capping group. Hanif and colleagues also observed that JAZZ-90 was more potent compared to JAZZ-166 and JAZZ-167 in multiple cancer cell lines including HCT116, H460, SiHa, and SW480 [153]. Generally, the capping group is a hydrophobic structure that interacts with the rim amino acids [281]. The surface recognition cap group offers unique interaction with biological targets including overexpressed receptors that could influence the selective accumulation of HDACis

[282]. Modification of the cap group affects the *in vitro* HDAC inhibition and antiproliferative activity [283]. Based on previous studies and current results JAZZ-166 and JAZZ-167 were less potent than JAZZ-90 and this might be due to the steric hindrance of the bulky capping group. The compounds AASH-122 (EC_{50} value of 2.02 μM) and JAZZ-121 (EC_{50} not achieved) have a similar structure (PCA in the pharmacophore), except the metal and arene ligand, the p-cym (clogP value of 3.90) of AASH-122 (Ru based) was replaced with 1,2,3,4-tetramethyl-cyclopenta-1,3-diene (clogP value of 3.67) in JAZZ-121 (Rh based). Guichard and colleagues observed that [(η6-tetrahydroanthracene)Ru(ethylenediamine)Cl]PF_6 (HC11) exhibited promising anticancer activity against A549 and H520 NSCLC cell lines with IC_{50} values of 0.5 and 0.53 μM, respectively. The alteration of arene ligand (THA, clogP value of 3.43) of HC11 with bip (clog P value of 3.73) in RM175 remarkably decreased the antiproliferative activity towards A549 and H520 cells with IC_{50} values of 3 μM and 3.5 μM, repectively [96, 154]. Like AASH-122 and JAZZ-121, ZR-012 (Ru based) and ZR-014 (Os based) contain PCA in the structure with different metal coordination. ZR-012 and ZR-014 contained PPh_3 instead of chlorine atom with the metal in AASH-12, were equally potent with EC_{50} value of <1.64 μM, and showed slightly higher potency compared to AASH-121. Previous findings and our results indicated that metal complexes lacking the PPh_3 showed poor anticancer activity, suggesting the importance of PPh_3 to enhance the antiproliferative activity of metal complexes [118].

Cancer cells vary remarkably between individuals. Furthermore, some properties of *in situ* tumour cells are lost during the processing and immortalisation in culture. To overcome these limitations, scientists investigated the drug's effect in multiple cell lines with genetic and phenotypic variation; expecting that consistent results could be more generalisable and have a high predictive value [270]. A549 cells have a pebble-like shape and are connected with the neighbouring cells with close cell-cell adhesion [284, 285]. On the other hand, H522 cells grow as adherent, single cells, and loosely attached clusters [200, 286]. A549 cells are growing faster (approximate doubling time 22 h) [287] than H522 cells (doubling time 38.2 h) [288]. Slower growing cells respond differently to drugs than faster-growing cells and the variation may be driven by the cell cycle [289, 290]. Additionally, the seeding density and cultural conditions also contribute to the alteration in drug sensitivity [289]. The EC_{50} of JAZZ-90, M1S-Ru, and M2S-Ru in H522 cells were all higher compared to A549 cells. Additionally, the EC_{50} values of these drug candidates in H522 cells were significantly different from the control drug SAHA. While M1S and M2S showed consistent cytotoxicity toward H522 cells with EC_{50} values of ~0.2 μM; this value was comparable with SAHA. Based on SRB assay results, Penthala et al. reported that the thiobarbiturate acid analogue 4-((3-((4,6-dioxo-2-thioxotetrahydropyrimidine-5(2H)-ylidene)methyl)-2-methyl-1H-indol-1-yl)methyl)benzoate) (7k) displayed similar

cytotoxic activity in H522 cells with an IC_{50} value of 0.25 µM after 48 h. However, the IC_{50} value of the same compound rose to 1.36 µM in A549 cells [291]. The N-hyroxypyridone derivative militarinones E also exhibited 7k like antiproliferative activity in A549 cells with an IC_{50} value of 1.59 µM [292]. Similar to M1S and M2S, the control drug of the present study (SAHA) displayed more cytotoxicity in H522 cells compared to A549 cells with EC_{50} values of 0.35 and 1µM, respectively. SAHA induced more cytotoxic effect in mutant, rather than p53 null or wild-type human cancer cells [293]. However, Karelia and coworkers reported similar IC_{50} values (0.87 and 0.83 µM) for SAHA in A549 and H522 cells using the SRB assay after 24 h [236]. However, using the CellTiter 96 AQueous assay, it was reported that A549 cells were more sensitive to SAHA compared with H522 cells with IC_{50} values of 1.5 and 2.1 µM, respectively [279]. The variation in the IC_{50} of SAHA in the A549 and H522 might be due to different assay types, growth media, and seeding density [236, 279, 294].

The main targets of anticancer drugs are intracellular and, therefore, the drugs must pass the cell membrane and, finally, the nuclear membrane to drive pharmacological activity [295]. Lipinski's "Rule of 5" is considered as the most prominent framework in predicting bioavailability and cell membrane permeability in the field of small-molecule drug development. One of the five rules is that compounds that have a molecular weight over 500 are less permeable to the lipid membrane, however, all the compounds do not follow this rule [296]. It has been previously reported that lung cells are naturally permeable to all the small-molecule drugs, therapeutic peptides, and proteins [297]. It was hypothesised that the size of M1S and M2S might be a factor that determines their potency. M1S and M2S were smaller (in terms of molecular weight) and more potent among the tested compounds in both the NSCLC cell lines (A549 and H522). M1S-Ru and M2S-Ru are the Ru complex of M1S and M2S, respectively. While JAZZ-166 and JAZZ-167 are the Ir and Rh complex of JAZZ-90, respectively. The molecular weight of JAZZ-90, M1S, and M2S is lower than the metal-based counterparts of the compounds. As mentioned earlier, JAZZ-90 was more potent than JAZZ-166 and JAZZ-167 in A549 cells while M1S and M2S were more potent than their corresponding metal-based compounds in both A549 and H522 cell lines. Additionally, the presence of a free sulfur group in the drug candidate structure might be another factor that modulates a drug's activity as this group influences cellular uptake. It has been reported that the presence of thiol groups in the drug structure may facilitate the interaction with the cell surface via disulfide exchange reaction at the plasma membrane and reactive cell surface thiol groups may promote absorptive endocytosis [160]. The breakdown of the disulfide bonds in a macromolecule having disulfide bridge (-S-S-) occurs at the cell membrane after endocytosis, thus exofacial thiols can act as a natural system for the entry of extracellular compounds inside

the cells [160]. JAZZ-90, M1S, and M2S have an available sulfur group while the metal-based complexes of these compounds the sulfur group interacts with metal. In A549 cells, all the drug candidates (JAZZ-90, M1S, and M2S) with the free sulfur group were more potent than their metal-based counterparts, which might be due to higher cellular uptake. El-Sayed and colleagues reported that [4-(3-(4- fluorophenyl)-1-phenyl-1H-pyrazol-4-yl)-2-(2-mercaptophenylamino)-6-(naphthalen-1-yl)-nicotinonitrile] displayed promising antiproliferative activity towards HepG2 and HeLa cells with IC_{50} values of 12.2 and 19.4 µM, respectively. This compound contains an NH group and a free SH group, which may interact with DNA bases either via thia/aza Michael addition or through the formation of hydrogen bonds, thereby causing DNA damage [298]. Furthermore, experimental drug candidates were dissolved in DMSO, this might be unfavourable for the metal compounds. Hall and colleagues reported that DMSO interacts with platinum drugs (*e.g.* cisplatin) containing monodentate ligands, thereby causing ligand displacement and structural changes. These changes were found to reduce the antiproliferative activity of monodentate ligand-based platinum drugs. However, bidentate ligand-containing platinum drugs (*e.g.* oxaliplatin) were found to be more active in DMSO compared to aqueous solvents [299]. In the current study, all the experimental drugs contained one mono and one bidentate ligand. Hall and colleagues showed the activity of the carboplatin and [$PtCl_2$(en)] (having both mono and bidentate ligand) decreased remarkably against DLD-1 colorectal cancer and KB-3-1 cervical carcinoma cell lines when DMSO was used as a solvent compared to saline [299]. However, the opposite effect of the solvents was observed towards cisplatin-resistant KB-CP.5 cells (cisplatin-resistant sub-line of KB-3-1). Therefore, testing the cytotoxic activity of the experimental novel metal compounds in other solvents could confirm the potential effect of DMSO.

Fibroblast cells are one of the key components of the TME [225] and both the drug candidates (M1S and M2S) displayed cytotoxic potential against the NIH3T3 cell line, a fibroblast cell line with intact p53 function [300]. Based on the cytotoxicity screening of 1,408 compounds in multiple cell lines, it was summarised that NIH3T3 was one of the most sensitive cell lines to compound induced cytotoxicity [301]. M2S showed a similar cytotoxic effect in A549 cells, while the potency of M1S decreased by 1.2-fold compared to A549 cells. Using the MTT assay it was reported that 48 h post-treatment of Au(2-thiopyridine) 2-(diphenylphosphino)ethylamine-2-carbonylthiophene (a gold (I) complex) caused higher antiproliferative activity against NIH3T3 compared to A549 cells as evident from the IC_{50} values, 2.1 and 24.5 µM, respectively. Under the same experimental condition, cisplatin showed more cytotoxic activity towards A549 cells compared to NIH3T3 cells with IC_{50} values

of 64 and 145 µM [302].

Conventional chemotherapeutic agents are non-selective and can damage normal tissues, which results in undesirable and severe side effects [303, 304]. Higher cytotoxicity of antiproliferative agents towards normal cell line is one of the preliminary concerns in drug screening [305]. The development of a new therapeutic agent that actively or passively targets cancerous cells, can not only improve therapeutic outcomes but also minimise drug-induced toxicity [303, 304]. A SI greater than one indicated that the drugs were less toxic to normal tissue cells compared with cancer cells, therefore, compounds with high SI value were assumed to be safer for therapy [306]. In the current study, M1S and M2S showed a similar SI, as both the drugs exhibited the highest selectivity against H522 cells (SI value of 4.46 to 4.87), intermediate selectivity in A549 cells (SI value of 3.50 to 3.55) and lowest selectivity towards NIH3T3 cells (SI value of 2.91 to 3.29). It has been reported that (E)-resveratrol 3-O-rutinoside (SI value of 11.3) displayed better selectivity towards A549 cells compared to vinblastine (a drug used in NSCLC treatment) (SI value of 1); SI in A549 cells was calculated using PNT2 (normal human prostate cell line) as the normal cell [306, 307]. Novel coumarin-based benzopyranone derivatives exhibited selective anticancer activity (SI value of 1.01 to 4.08) in A549 cells; the SI was calculated using LL49 lung cell line as normal cells [305]. The SI value of artemisinin in A549 cells was 2.40 which is comparable with the selectivity of M1S and M2S in A549 cells. However, the artemisinin SI value was calculated using HBE (normal human bronchial epithelial cell line normal cell line) as the normal cell line [308]. Interestingly, M1S and M2S displayed more toxicity and selectivity towards p53 mutated H522 cells compared with p53 intact cells (A549 and NIH3T3 cells). The clinically used agent, taxol, was reported to be more effective against p53 mutated cells, but toxic towards normal cells as well [309].

The hydroxythiopyridone derivatives, M1S and M2S contain a pyridine and benzene ring in their chemical structure. Novel 2 pyridone derivatives displayed anticancer activity against six human cancer cell lines including A549 lung cancer cells. 5-methoxy-2-(6-oxo-1-*o*-tolyl-1,6-dihydropyridine-3-carbonyl)phenyl propyl carbonate (8i), a 2 pyridine derivative showed cytotoxicity in A549 cells with an IC_{50} value of 6.13 µM. The addition of benzyl and ethyl group to 8i, increased its cytotoxicity by 5-fold [310]. Both M1S and M2S have a benzyl group in their structure. Additionally, M1S and M2S have a structural moiety similar to 3-HPT. 3-HPT displayed no cytotoxic potential in DU-145 (androgen-independent prostate cancer), LNCaP (androgen-dependent prostate cancer), and Jurkat (T-cell leukaemia) cells. Interestingly, 3-HPT derivatives 1-(4-dimethylamino-(1,1'-biphenylmethyl))-3-hydroxyoxypyridin-2-thione, 1-(2-cyano-(1,1'-biphenylmethyl))-3-hydroxyoxypyridin-2-

thione and 1-(2-methyl-(1,1'-biphenylmethyl))-3-hydroxyoxypyridin-2-thione showed cytotoxicity against all three cell lines, but these compounds were less potent compared to SAHA [163].

M2S showed slightly higher cytotoxic potential than M1S in neoplastic, pre-neoplastic, and normal prostate epithelial cells. M2S has an identical chemical structure as M1S except one additional carbon attached to the benzyl group. Lipophilicity and cytotoxicity tends to increase with the increase of carbon chain (up to a certain number). This might due to a favourable balance between lipophilicity and hydrophobicity [311, 312]. Lipophilicity is one of the crucial parameters that determine the cellular uptake of small molecules including drugs [160], it also aligned with drug potency and pharmacokinetics [313]. The octanol/water partition coefficient, logP, predicts the lipophilicity of compounds, where a high logP value corresponds to higher lipophilicity [314]. logP is also a determining factor in the anticancer activity of some compounds, for instance, crown ether compounds showed anticancer activity with an optimum logP value of 5.5 [312]. The logP value for M1S and M2S were calculated using Molinspiration online software tool [154] and the values obtained were 2.02 and 2.23 for M1S and M2S, respectively. The slightly higher logP value of M2S compared to M1S might facilitate its cellular uptake, and thereby, enhance its cytotoxic potential.

4.3.2 Time course of cytotoxicity

Most of the cell-based assays are performed at a standard time point of 48 h to 72 h post-treatment to investigate the potential effect of the drug. Due to this extended time point, the effect of the drug at the early treatment period could not be determined. However, a time-course is necessary to examine whether the drug is cytostatic, cytotoxic or it simply arrests cell division [242]. Additionally, it has been reported that cytotoxicity shifts with time [253, 315, 316].

The time course study observed the anticancer potential of M1S and M2S towards A549 and H522 cells after 0, 12, 24, 36, 48, 60, and 72 h of treatment at $2\times EC_{50}$ concentrations. Both drug candidates showed an almost identical cytostatic pattern in A549 cells. A statistically significant difference in cell number was observed from 12 h and 24 h of M2S and M1S treatment, respectively. No significant difference in cell number was seen between each time point of M1S and M2S treatment. Time-dependent activity of M1S and M2S towards A549 cells indicated that these compounds could have blocked cell division, without inducing cell death [317, 318]. Therefore, M1S and M2S appeared to be cytostatic at the concentrations examined in A549 cells [319]. Interestingly, the two drug candidates displayed cytotoxicity at 12 h in H522 cells. Compared with control, the initial cell population showed an approximately 2 and 2.9-fold decrease after M1S and M2S treatment, followed by a static cell number up until

72 h.

4.3.3 Drug-mediated changes in protein levels

Diverse cell signalling proteins are involved in the cytostatic and cytotoxic activity of a drug [320]. Furthermore, cytostatic and cytotoxic activity of a drug relies on the applied drug concentration, frequency of drug treatment, the action of a drug on cell cycle phases, and cellular context [319]. To investigate the potential mechanism underlying the cytostatic and cytotoxic activity towards different cell lines, acetyl H3, cyclin D1, and cyclin B1 expression was tested.

4.3.3.1 Acetyl H3

HDACis attenuate acetylation events and block several cancer-related signalling pathways [321]. HDACis either alone or in combination with other cytotoxic agents showed promising activity in the treatment of NSCLC [321, 322]. While the structure of M1S and M2S do not support the idea that they would be potent HDACis, this was confirmed by Western blotting analysis of acetyl H3 expression. No significant differences in acetyl H3 expression were produced when A549 and H522 cells were treated with EC_{50} and $2\times EC_{50}$ of either M1S or M2S. These results indicate that the pharmacophore of M1S and M2S was not able to interact with the active site of HDACs. Therefore, no changes in the acetylation of H3 were observed in response to drug candidates. A previous study reported that the channel to the HDAC 1 active site is small as compared to HDAC 6 whose hydrophobic channel entrance seems large enough to interact with 3-HPT [323], a compound that possesses a similar pharmacophore to the M1S and M2S zinc-binding domain. Sodji et al. observed that five $–CH_2$ methylene groups were optimal between the hyroxythiopyridone (act as Zn^{2+} chelator) and triazole (act as capping group) for inhibition of HDAC 6 and HDAC 8. 1-phenyltriazolylethyl-3-hydroxypyridine-2-thione (10a) (two $–CH_2$ methylene linker) was reported to have IC_{50} value of >10 μM for HDAC 6 and HDAC 10, which decreased to 911 nM and 917 nM in 1-phenyltriazolylpentyl-3-hydroxypyridine-2-thione (10d) (five $–CH_2$ methylene linker) [323]. Increased potency towards HDAC 6 inhibition was reported to occur due to a stable π-stacking interaction between the phenyl ring of 10d and Phe680 at the entrance to the active site of HDAC 6, resulting in improved HDACi binding and activity. On the other hand, enhanced potency against HDAC 8 was reported to occur as a result of the capping group incorporation into an inaccessible hydrophobic pocket close to the active site, which was inaccessible for 10a due to the shorter methylene spacers [323]. M1S and M2S contains one $–CH_2$ and two $–CH_2$ methylene groups between the capping group and the zinc-binding domain, respectively. Previously, M1S and M2S like compounds with shorter methylene groups were reported to have HDACi activity.

For example, 3-HPT based compounds with one aryl group connected via single $–CH_2$ methylene linker, 1-benzyl-3-hydroxypyridin-2-thione, showed HDAC 6 and HDAC 8 inhibitory activity with IC_{50} values of 457 and 1272 nM, respectively. While 1-(1,1'-biphenylmethyl)-3-hydroxypyridin-2-thione, synthesised by the addition of two phenyl groups with 3-HPT, produced decreased HDACi activity towards HDAC 6 and HDAC 8, where the IC_{50} value increased to 847 and 4283 nM, respectively [163]. These results indicated that the pharmacophore of M1S and M2S lacks HDAC selectivity. Furthermore, drug docking modelling studies in our lab showed that M1S did not fit the active site of HDACs (Z. Rana, personal communication).

4.3.3.2 Cyclin D1

D- type cyclins (cyclin D1, D2, D3) activated via mitogenic growth factors (notably RAS signalling pathways), stimulate the quiescent cells (G0 phase) to enter into the G1 phase of the cell cycle [324]. Cyclin D1 is a regulatory subunit of the CDKs including CDK4/6, which controls cell proliferation and development via its transcriptional regulatory activity [325]. Overexpression of cyclin D1 results in dysregulation of CDK activity, uncontrolled cell division under restricted mitogen signalling, bypass of cell cycle checkpoints, and ultimately oncogenic consequences [326]. These consequences include angiogenesis, through the regulation of VEGF expression, DNA damage response, and centrosome depletion [53]. Furthermore, an alternation of cyclin D1 expression could significantly affect the cellular responses to drug treatment [59].

Cyclin D1 overexpression is common in NSCLC (~5% - 76%) which leads to a loss of the G0/G1 to S checkpoint [53, 326]. Stage I and II NSCLC patients (n=98) with cyclin D1 positive tumours had shorter survival than those with cyclin D1 negative tumours (5-year survival of 48% vs 74%, respectively; p=0.006 determined through the log-rank test). A higher percentage of NSCLC patients with poor differentiation of the tumour, visceral pleural invasion, chronic pulmonary obstructive disease have positive cyclin D1 expression than other lung tumours [327]. KRAS-driven NSCLC is particularly dependent on the CKD4 and is sensitive to the cyclin D1-degrading combination bexarotene (repress cyclin D1 through proteasomal degradation) and erlotinib (selectively and reversibly inhibits the tyrosine kinase activity of EGFR), although the response of KRAS-mutated cancer to the erlotinib is poor [53, 328, 329].

Pyrimidine and pyridine based derivatives have diverse selectivity and inhibitory potential for CDK/cyclin [330, 331]. Benzyl group containing purine based compounds, olomoucine (6-(benzylamino)-2-[(2-hydroxyethyl)amino]-9-methylpurine), roscovitine (6-(benzylamino)-

2(R)-[[1-(hydroxymethyl)propyl]amino]-9-isopropylpurine) and R-roscovitine (2-(R)-(1-ethyl-2-hydroxyethylamino)-6-benzylamino-9-isopropylpurine) were more potent against CDK1 and CDK2 than CDK4 [330, 332-334]. Interestingly, the R- roscovitine (IC_{50} value of 14.2 μM) displayed more specificity towards CKD4/cyclin D1 compared to olomoucine and roscovitine with IC_{50} values >1000 and >100 μM, respectively [332, 333]. Furthermore, R-roscovitine exhibited cytotoxic activity against A549 and H460 cell lines with IC_{50} values of 15.9 and 13.1 μM, respectively [333]. Similar to purine based compounds, pyrimidine ring containing compounds also displayed variation in terms of selectivity towards CDKs [330, 331]. Recently, the pyrido[2,3-d]pyrimidin-7-one has become an effective pharmacophore in inhibiting CDKs. An *in vitro* study showed that modification of C-2 position of pyrido[2,3-d]pyrimidin-7-ones with a 2-aminopyridine side-chain enhanced the selectivity for CDK4/6. 8-cyclopentyl-2-(pyridin-2-ylamino)-8H-pyrido[2,3-d]-pyrimidine-7-one, synthesised through modification of pyrido[2,3-d]pyrimidin-7-ones with a 2-aminopyridine side chain at C-2, showed more selectively towards CDK4/D than CDK2/A with IC_{50} values of 0.14 and 5.01 μM, respectively [331]. The C-2 modification with aniline exhibited more selectivity in the inhibition of CDK2/A than CDK4/D, where the IC_{50} decreased to 0.01 and 0.21 μM, respectively. However, aniline modification with aminopyridine-containing side chains enhanced the efficacy and selectivity towards CDK4/D compared to the CDK2/A with IC_{50} values of 0.002 and 0.04 μM, respectively [331]. It should be noted that both M1S and M2S contain the benzyl group and the pyridine core. Previously it was reported that 3-hydroxy-4-pyridone ring containing non-protein amino acid mimosine (β-[N-(3-hydroxy-4-oxypyridyl)]-α-aminopropionic acid), decreased the cyclin D1 activity, inhibited cyclin D1-associated kinase activity, increased p21 mRNA and protein level and upregulated p27 expression [335, 336].

Western blotting analysis of cyclin D1 protein expression demonstrated that when A549 and H522 were treated with either M1S or M2S at their respective EC_{50} and $2\times EC_{50}$ concentration, a trend of concentration-dependent decrease of cyclin D1 expression was observed at 12 h and 24 h. In A549 cells, no statistically significant difference in any of the treatment groups was observed. It should be noted that data variation in biological replicates was too large to detect a difference. On the other hand, in H522 cells, the EC_{50} concentration of both the compounds failed to produce a significant effect in the reduction of cyclin D1 level. The $2\times EC_{50}$ concentration of M1S significantly downregulated cyclin D1 expression level by 68.1% of control at 24 h. While the $2\times EC_{50}$ concentration of M2S significantly reduced the cyclin D1/β-tubulin ratio by 69.7% and 84.9% of control at 12 and 24 h, respectively. A decrease of cyclin D1 activity could block the G1 phase of the cell cycle [337]. These results demonstrate that

M1S and M2S may provide a therapeutic advantage to the NSCLC patients by inhibiting cyclin D1 expression. However, further experiments are required to determine the cell line-specific effects.

4.3.3.3 Cyclin B1

Cyclin B1 in combination with CDK1 plays a vital role in the regulation of the G2/M phase transition in the cell cycle. The expression of cyclin B1 starts to increase in the G2 phase and peaks in the M phase [312, 338]. Cyclin B1/CDK1 complexes assist chromosome condensation, nuclear envelope breakdown, and mitotic spindle assembly [338]. Besides its role in the cell cycle, the regulatory function of cyclin B1 is also involved in stem cell self-renewal, DNA damage repair, epigenetic regulation, and mediation of pro-apoptotic signalling in response to mitotic arrest [324, 339]. Cyclin B1 is overexpressed in a considerable number of NSCLC patients, whose survival time is shorter than patients with low levels of cyclin B1 [61]. Additionally, CCNB1, a gene that encodes cyclin B1, plays a vital role in the development and progression of NSCLC [340]. As the deregulation of cyclin B1 expression leads to neoplastic transformation, suppression of cyclin B1 activity could be a potential target for antiproliferative therapy [341]. Cells with an elevated cyclin B1/CDK1 activity could favour mitosis while cells with a suppressed cyclin B1/ CDK1 activity could be arrested in the G2 phase [342].

In the current study, no significant changes in cyclin B1 level between any of the treatment groups and control were observed in A549 and H522 cells after 12 h and 24 h of M1S or M2S treatment. Previously, it was reported that 12 h post-treatment of A549 cells with 2-(4-hexyloxyphenyl)-5-(4-hydroxyphenyl)pyrimidine (C1) cyclin B1 increased while the phosphorylation of cdc2 was decreased. These results indicated that C1 activated cdc2/cyclin B1 kinase and induced mitotic arrest rather than G2 arrest [312]. On the other hand, in H522 cells both M1S and M2S exhibited a concentration-dependent decrease of cyclin B1/β-actin ratio at 24 h. Based on the *in vitro* NSCLC model using H522 and H460 cells it was reported that a decrease of cyclin B1 encoding CCNB1gene expression suppressed the proliferation, migration, and invasion of NSCLC cells [340].

4.3.4 Effects of M1S and M2S in cell cycle

Cell cycle arrest is a halting point in the cell cycle, where cells are no longer involved in the processes of duplication and division [343]. Anticancer agents may act at multiple steps during the cell cycle progression, however, G1/S or G2/M arrest occurs most frequently [344]. Cell proliferation can be effectively restricted if the G1/S checkpoint is arrested, as this is the limiting phase of the cell cycle [345].

In the current study, no significant changes in the cell cycle distribution was observed in A549 cells after 6 and 12 h post-treatment of M1S and M2S at either EC_{50} or $2\times EC_{50}$ concentration, while the statistical significance was not calculated for H522 cells as only two biological repeats were conducted. Interestingly, A549 cells were distributed more at the G2/M phase following treatment, however, a concentration-dependent effect was not seen. At 12 h, the $2\times EC_{50}$ concentration of M1S and M2S increased 3.3 and 7.1% of cells in the G2/M phase compared to control. Wakasaya and colleagues reported that 12 μM ($2\times IC_{50}$) of 2-(4-butoxyphenyl)-5-(4-hydroxyphenyl)pyrimidine significantly arrested A549 cells at the G2/M phase after 12 h, however, the effect disappeared at 24 h [346]. Cell cycle arrest is linked with the activity of the different cyclin/CDK complexes that control the successive phases of the cell cycle [347]. The Western blotting results of the current study showed a concentration-dependent trend of decreasing cyclin D1 level at 12 h in A549 cells. It has been reported that KRAS mediated proliferation converges on the CDK4/6 cyclin-D complex, which regulates G1 and S phase transition [348]. Huang et al. showed that cyclin D1-suppressing siRNA caused G1 arrest in rapidly proliferating A549 cells [349]. Furthermore, Ras-induced cyclin D1 expression at the G2 phase in rapidly proliferating cells and the levels of cyclin D1 in the G2 phase were sufficient to switch post-mitotic cells into their next S phase [350]. The results of the current study indicate that M1S and M2S could have a G2/M phase arresting activity and a higher concentration of the drug candidates might produce significant changes in the cell cycle.

p53 mutation in cancer cells caused defective G1 checkpoint activity [351]. In H522 cells, it appeared that M1S and M2S produced a weak effect in arresting cells at the G1 phase at 12 h, where the $2\times EC_{50}$ concentration of M1S and M2S increased 9.9 and 8.9% cell proportion at the G1 phase, respectively. However, the experiments were not performed in triplicate and should be considered preliminary. It has been reported that the Mdm2 inhibitor (MI) disrupts the interaction between Mdm2 and p53 and 10 to 30 μM of MI-43 induced G2 arrest (from 5% to 20%) in A549 cells, which was 5.9 to 17.6-fold higher than the IC_{50} concentration. Furthermore, the calculated IC_{50} value was 21 μM in H522 cells. On the other hand, 10 μM (approximately $0.5\times IC_{50}$) of MI-43 failed to induce G1 arrest in H522 cells, but increasing the concentration to 30 μM caused 18.6% of arrest at the G1 phase [352].

In the present study, a minor sub-G1 peak that was to the far left of the G1 peak was observed both in the treatment and control groups of H522 cells. This minor peak is an indicator of apoptosis [353, 354]. While the results were considered preliminary, it appeared as though M1S and M2S treatment raised the percentage of apoptotic cells. This effect may be related to the cytotoxic response of the drug candidates towards H522 cells. In the A549 cells, no sub-G1

peak was observed. Therefore, the apoptotic populations could not be determined from the cell cycle analysis. A previous study showed that untreated A549 cells have a small sub-G1 population compared to untreated H522 cells after 72 h [355]. Zhu et al. observed that glycyrrhetinic acid, a natural compound, induced G0/G1 phase arrest in a time and concentration-dependent manner, without causing apoptosis [49].

4.4 Conclusions and future directions

Among the 11 screened novel compounds of four different drug classes, the two smallest hydroxythiopyridone derivatives, M1S and M2S, exhibited the most potent anticancer activity in both A549 and H522 cells. The drug candidates were also cytotoxic towards pre-neoplastic NIH3T3 cells. The SI value indicated that the compounds were more selective towards cancer cells than pre-neoplastic cells. In the time course cytotoxicity studies M1S and M2S (at $2\times EC_{50}$ concentration) exhibited almost identical cytostatic and cytotoxic activity in A549 and H522 cells, respectively. Western blotting results showed that the pharmacophore of M1S and M2S was not active or potent in inhibiting HDACs. The $2\times EC_{50}$ concentration of M1S or M2S significantly downregulated cyclin D1 expression only in H522 cells, suggesting that the drug candidates induced either G1/S or G2/M phase arrest. However, the same concentration was unable to produce a significant effect in changing the expression of cyclin B1 and cell cycle progression in both A549 and H522 cells. Therefore, clear conclusions could not be drawn. To better understand the effects of the compounds on cell cycle progression, a triplicate experiment is needed in H522 cells. Additionally, to confirm the anticancer activity and selectivity of M1S and M2S in KRAS-mutated NSCLC cells further investigations using multiple KRAS-mutated NSCLC and wild type non-cancerous lung cell lines are recommended. Since treatment with M1S and M2S resulted in changes in A549 and H522 cell viability, the potential mechanism underlying this activity should be confirmed. Time-course and concentration-response experiments may give a clear picture of the effects of the drug candidates on cell cycle progression and other cell signalling proteins. Expression of KRAS and KRAS associated upstream and downstream signalling proteins in both KRAS-mutated and wild type cell lines should be tested to investigate the effects of M1S and M2S on KRAS mutations. Flow cytometry analysis after annexin V/PI staining would confirm the early apoptotic and late apoptotic or necrotic effect of M1S or M2S. Finally, investigation of cleaved caspase-3, cleaved caspase 8, and cyclophilin A expression using Western blotting or biochemical kit can provide a conclusive result regarding cell death via intrinsic apoptotic, extrinsic apoptotic, or necrotic mechanism, respectively.

CHAPTER V

References

5 References

[1] Wang, S., Y. Yan, Z. Cheng, Y. Hu, and T. Liu. (2018). Sotetsuflavone suppresses invasion and metastasis in non-small-cell lung cancer A549 cells by reversing EMT via the TNF-α/NF-κB and PI3K/AKT signaling pathway. *Cell Death Discov, **4**,* 26. doi:10.1038/s41420-018-0026-9

[2] Bray, F., J. Ferlay, I. Soerjomataram, R.L. Siegel, L.A. Torre, et al. (2018). Global cancer statistics 2018: GLOBOCAN estimates of incidence and mortality worldwide for 36 cancers in 185 countries. *CA Cancer J Clin, **68***(6), 394-424. doi:10.3322/caac.21492

[3] Didkowska, J., U. Wojciechowska, M. Manczuk, and J. Lobaszewski. (2016). Lung cancer epidemiology: contemporary and future challenges worldwide. *Ann Transl Med, **4***(8), 150. doi:10.21037/atm.2016.03.11

[4] de Groot, P. and R.F. Munden. (2012). Lung cancer epidemiology, risk factors, and prevention. *Radiol Clin North Am, **50***(5), 863-876. doi:10.1016/j.rcl.2012.06.006

[5] Schwartz, A.G. and M.L. Cote. (2016). Epidemiology of Lung Cancer. In A. Ahmad and S. Gadgeel (Eds.), *Lung Cancer and Personalized Medicine: Current Knowledge and Therapies* (pp. 21-41). Cham: Springer International Publishing. doi:10.1007/978-3-319-24223-1_2

[6] Garrido, P., M.E. Olmedo, A. Gómez, L. Paz Ares, F. López-Ríos, et al. (2017). Treating KRAS-mutant NSCLC: latest evidence and clinical consequences. *Ther Adv Med Oncol, **9***(9), 589-597. doi:10.1177/1758834017719829

[7] Dogan, S., R. Shen, D.C. Ang, M.L. Johnson, S.P. D'Angelo, et al. (2012). Molecular epidemiology of EGFR and KRAS mutations in 3,026 lung adenocarcinomas: higher susceptibility of women to smoking-related KRAS-mutant cancers. *Clin Cancer Res, **18***(22), 6169-6177. doi:10.1158/1078-0432.CCR-11-3265

[8] de Sousa, V.M.L. and L. Carvalho. (2018). Heterogeneity in Lung Cancer. *Pathobiology, **85***(1-2), 96-107. doi:10.1159/000487440

[9] Korrodi-Gregório, L., V. Soto-Cerrato, R. Vitorino, M. Fardilha, and R. Pérez-Tomás. (2016). From Proteomic Analysis to Potential Therapeutic Targets: Functional Profile of Two Lung Cancer Cell Lines, A549 and SW900, Widely Studied in Pre-Clinical Research. *PLoS One, **11***(11), e0165973. doi:10.1371/journal.pone.0165973

[10] Travis, W.D. (2012). Update on small cell carcinoma and its differentiation from squamous cell carcinoma and other non-small cell carcinomas. *Mod Pathol, **25 Suppl 1***, S18-30. doi:10.1038/modpathol.2011.150

[11] Yang, S., Z. Zhang, and Q. Wang. (2019). Emerging therapies for small cell lung cancer. *J Hematol Oncol, **12***(1), 47. doi:10.1186/s13045-019-0736-3

[12] Cerami, E., J. Gao, U. Dogrusoz, B.E. Gross, S.O. Sumer, et al. (2012). The cBio cancer genomics portal: an open platform for exploring multidimensional cancer genomics data. *Cancer Discov*, ***2***(5), 401-404. doi:10.1158/2159-8290.Cd-12-0095

[13] Gao, J., B.A. Aksoy, U. Dogrusoz, G. Dresdner, B. Gross, et al. (2013). Integrative analysis of complex cancer genomics and clinical profiles using the cBioPortal. *Sci Signal*, ***6***(269), pl1. doi:10.1126/scisignal.2004088

[14] Hellmann, M.D., T. Nathanson, H. Rizvi, B.C. Creelan, F. Sanchez-Vega, et al. (2018). Genomic Features of Response to Combination Immunotherapy in Patients with Advanced Non-Small-Cell Lung Cancer. *Cancer Cell*, ***33***(5), 843-852.e4. doi:10.1016/j.ccell.2018.03.018

[15] Rizvi, H., F. Sanchez-Vega, K. La, W. Chatila, P. Jonsson, et al. (2018). Molecular Determinants of Response to Anti-Programmed Cell Death (PD)-1 and Anti-Programmed Death-Ligand 1 (PD-L1) Blockade in Patients With Non-Small-Cell Lung Cancer Profiled With Targeted Next-Generation Sequencing. *J Clin Oncol*, ***36***(7), 633-641. doi:10.1200/jco.2017.75.3384

[16] Jamal-Hanjani, M., G.A. Wilson, N. McGranahan, N.J. Birkbak, T.B.K. Watkins, et al. (2017). Tracking the Evolution of Non-Small-Cell Lung Cancer. *N Engl J Med*, ***376***(22), 2109-2121. doi:10.1056/NEJMoa1616288

[17] Vavalà, T., V. Monica, M. Lo Iacono, T. Mele, S. Busso, et al. (2017). Precision medicine in age-specific non-small-cell-lung-cancer patients: Integrating biomolecular results into clinical practice-A new approach to improve personalized translational research. *Lung Cancer*, ***107***, 84-90. doi:10.1016/j.lungcan.2016.05.021

[18] Ding, L., G. Getz, D.A. Wheeler, E.R. Mardis, M.D. McLellan, et al. (2008). Somatic mutations affect key pathways in lung adenocarcinoma. *Nature*, ***455***(7216), 1069-1075. doi:10.1038/nature07423

[19] Campbell, J.D., A. Alexandrov, J. Kim, J. Wala, A.H. Berger, et al. (2016). Distinct patterns of somatic genome alterations in lung adenocarcinomas and squamous cell carcinomas. *Nat Genet*, ***48***(6), 607-616. doi:10.1038/ng.3564

[20] Rizvi, N.A., M.D. Hellmann, A. Snyder, P. Kvistborg, V. Makarov, et al. (2015). Cancer immunology. Mutational landscape determines sensitivity to PD-1 blockade in non-small cell lung cancer. *Science*, ***348***(6230), 124-128. doi:10.1126/science.aaa1348

[21] Román, M., I. Baraibar, I. López, E. Nadal, C. Rolfo, et al. (2018). KRAS oncogene in non-small cell lung cancer: clinical perspectives on the treatment of an old target. *Mol Cancer*, ***17***(1), 33. doi:10.1186/s12943-018-0789-x

[22] Yang, S., X. Yu, Y. Fan, X. Shi, and Y. Jin. (2018). Clinicopathologic characteristics and survival outcome in patients with advanced lung adenocarcinoma and KRAS mutation. *J Cancer*, ***9***(16), 2930-2937. doi:10.7150/jca.24425

[23] Kempf, E., B. Rousseau, B. Besse, and L. Paz-Ares. (2016). KRAS oncogene in lung cancer: focus on molecularly driven clinical trials. *Eur Respir Rev,* ***25***(139), 71-76. doi:10.1183/16000617.0071-2015

[24] Scheffler, M., M.A. Ihle, R. Hein, S. Merkelbach-Bruse, A.H. Scheel, et al. (2019). K-ras Mutation Subtypes in NSCLC and Associated Co-occuring Mutations in Other Oncogenic Pathways. *J Thorac Oncol,* ***14***(4), 606-616. doi:10.1016/j.jtho.2018.12.013

[25] Ferrer, I., J. Zugazagoitia, S. Herbertz, W. John, L. Paz-Ares, et al. (2018). KRAS-Mutant non-small cell lung cancer: From biology to therapy. *Lung Cancer,* ***124***, 53-64. doi:10.1016/j.lungcan.2018.07.013

[26] cBioPortal. Non-small Cell Lung Cancer. [cited 15 June, 2020]; Available from: https://bit.ly/2AEx3WC.

[27] D'arcangelo, M. and F. Cappuzzo. (2012). K-Ras mutations in non-small-cell lung cancer: prognostic and predictive value. *ISRN Mol Biol,* ***2012***, 8. doi:10.5402/2012/837306

[28] Xu, K., D. Park, A.T. Magis, J. Zhang, W. Zhou, et al. (2019). Small Molecule KRAS Agonist for Mutant KRAS Cancer Therapy. *Mol Cancer,* ***18***(1), 85. doi:10.1186/s12943-019-1012-4

[29] Moran, D.M., P.B. Trusk, K. Pry, K. Paz, D. Sidransky, et al. (2014). KRAS mutation status is associated with enhanced dependency on folate metabolism pathways in non-small cell lung cancer cells. *Mol Cancer Ther,* ***13***(6), 1611-1624. doi:10.1158/1535-7163.Mct-13-0649

[30] Porru, M., L. Pompili, C. Caruso, A. Biroccio, and C. Leonetti. (2018). Targeting KRAS in metastatic colorectal cancer: current strategies and emerging opportunities. *J Exp Clin Cancer Res,* ***37***(1), 57. doi:10.1186/s13046-018-0719-1

[31] Cox, A.D., S.W. Fesik, A.C. Kimmelman, J. Luo, and C.J. Der. (2014). Drugging the undruggable RAS: Mission possible? *Nat Rev Drug Discov,* ***13***(11), 828-851. doi:10.1038/nrd4389

[32] Ye, N. and J. Zhou. (2014). KRAS - An Evolving Cancer Target. *Austin J Cancer Clin Res,* ***1***(1), 1004.

[33] Adderley, H., F.H. Blackhall, and C.R. Lindsay. (2019). KRAS-mutant non-small cell lung cancer: Converging small molecules and immune checkpoint inhibition. *EBioMedicine,* ***41***, 711-716. doi:10.1016/j.ebiom.2019.02.049

[34] Cooper, W.A., D.C. Lam, S.A. O'Toole, and J.D. Minna. (2013). Molecular biology of lung cancer. *J Thorac Dis,* ***5***(Suppl 5), S479. doi:10.3978/j.issn.2072-1439.2013.08.03

[35] Westcott, P.M. and M.D. To. (2013). The genetics and biology of KRAS in lung cancer. *Chin J Cancer,* ***32***(2), 63. doi:10.5732/cjc.012.10098

[36] Leung, E.L.H., L.X. Luo, Z.Q. Liu, V.K.W. Wong, L.L. Lu, et al. (2018). Inhibition of KRAS-dependent lung cancer cell growth by deltarasin: blockage of autophagy increases its cytotoxicity. *Cell Death Dis,* ***9***(2), 216. doi:10.1038/s41419-017-0065-9

[37] Park, J., Y.H. Cho, W.J. Shin, S.K. Lee, J. Lee, et al. (2019). A Ras destabilizer KYA1797K overcomes the resistance of EGFR tyrosine kinase inhibitor in KRAS-mutated non-small cell lung cancer. *Sci Rep,* ***9***(1), 648. doi:10.1038/s41598-018-37059-8

[38] Quevedo, C.E., A. Cruz-Migoni, N. Bery, A. Miller, T. Tanaka, et al. (2018). Small molecule inhibitors of RAS-effector protein interactions derived using an intracellular antibody fragment. *Nat Commun,* ***9***(1), 3169. doi:10.1038/s41467-018-05707-2

[39] Abdel-Rahman, O. (2016). Targeting the MEK signaling pathway in non-small cell lung cancer (NSCLC) patients with RAS aberrations. *Ther Adv Respir Dis,* ***10***(3), 265-274. doi:10.1177/1753465816632111

[40] Kelly, K., J. Mazieres, N.B. Leighl, F. Barlesi, G. Zalcman, et al. (2013). Oral MEK1/MEK2 inhibitor trametinib (GSK1120212) in combination with pemetrexed for KRAS-mutant and wild-type (WT) advanced non-small cell lung cancer (NSCLC): A phase I/Ib trial. *J Clin Oncol* ***31***(15), 8027-8027. doi:10.1200/jco.2013.31.15_suppl.8027

[41] Sunaga, N., Y. Miura, Y. Tsukagoshi, N. Kasahara, T. Masuda, et al. (2019). Dual inhibition of MEK and p38 impairs tumor growth in KRAS-mutated non-small cell lung cancer. *Oncol Lett,* ***17***(3), 3569-3575. doi:10.3892/ol.2019.10009

[42] Li, S., S. Liu, J. Deng, E.A. Akbay, J. Hai, et al. (2018). Assessing Therapeutic Efficacy of MEK Inhibition in a KRAS(G12C)-Driven Mouse Model of Lung Cancer. *Clin Cancer Res,* ***24***(19), 4854-4864. doi:10.1158/1078-0432.Ccr-17-3438

[43] Hai, J., S. Liu, L. Bufe, K. Do, T. Chen, et al. (2017). Synergy of WEE1 and mTOR Inhibition in Mutant KRAS-Driven Lung Cancers. *Clin Cancer Res,* ***23***(22), 6993-7005. doi:10.1158/1078-0432.Ccr-17-1098

[44] Kalinichenko, V.V. and T.V. Kalin. (2015). Is there potential to target FOXM1 for 'undruggable' lung cancers? *Expert Opin Ther Targets,* ***19***(7), 865-867. doi:10.1517/14728222.2015.1042366

[45] Balaji, S., M.K. Mohamed Subarkhan, R. Ramesh, H. Wang, and D. Semeril. (2020). Synthesis and Structure of Arene Ru (II) N∧ O-Chelating Complexes: In Vitro Cytotoxicity and Cancer Cell Death Mechanism. *Organometallics,* ***39***(8), 1366-1375. doi:10.1021/acs.organomet.0c00092

[46] Bállega, E., R. Carballar, B. Samper, N. Ricco, M.P. Ribeiro, et al. (2019). Comprehensive and quantitative analysis of G1 cyclins. A tool for studying the cell cycle. *PLoS One,* ***14***(6), e0218531. doi:10.1371/journal.pone.0218531

[47] Tarn, W.-Y. and M.-C. Lai. (2011). Translational control of cyclins. *Cell Div,* ***6***(1), 5. doi:10.1186/1747-1028-6-5

[48] Casem, M.L. (2016). Cell Cycle. In M.L. Casem (Ed.), *Case Studies in Cell Biology* (pp. 299-326): Academic Press. doi:10.1016/B978-0-12-801394-6.00013-0

[49] Zhu, J., M. Chen, N. Chen, A. Ma, C. Zhu, et al. (2015). Glycyrrhetinic acid induces G1-phase cell cycle arrest in human non-small cell lung cancer cells through endoplasmic reticulum stress pathway. *Int J Oncol,* ***46***(3), 981-988. doi:10.3892/ijo.2015.2819

[50] Lavoie, J.N., G. L'Allemain, A. Brunet, R. Müller, and J. Pouysségur. (1996). Cyclin D1 expression is regulated positively by the p42/p44MAPK and negatively by the p38/HOGMAPK pathway. *J Biol Chem,* ***271***(34), 20608-20616. doi:10.1074/jbc.271.34.20608

[51] Yang, V.W. (2018). The Cell Cycle. In H.M. Said (Ed.), *Physiology of the Gastrointestinal Tract* (Sixth ed., pp. 197-219): Academic Press. doi:10.1016/B978-0-12-809954-4.00008-6

[52] Diehl, J.A. (2002). Cycling to cancer with cyclin D1. *Cancer Biol Ther,* ***1***(3), 226-231. doi:10.4161/cbt.72

[53] Musgrove, E.A., C.E. Caldon, J. Barraclough, A. Stone, and R.L. Sutherland. (2011). Cyclin D as a therapeutic target in cancer. *Nat Rev Cancer,* ***11***(8), 558-572. doi:10.1038/nrc3090

[54] Klein, E.A. and R.K. Assoian. (2008). Transcriptional regulation of the cyclin D1 gene at a glance. *J Cell Sci,* ***121***(Pt 23), 3853-3857. doi:10.1242/jcs.039131

[55] Al-Aynati, M.M., N. Radulovich, J. Ho, and M.S. Tsao. (2004). Overexpression of G1-S cyclins and cyclin-dependent kinases during multistage human pancreatic duct cell carcinogenesis. *Clin Cancer Res,* ***10***(19), 6598-6605. doi:10.1158/1078-0432.Ccr-04-0524

[56] Fu, M., C. Wang, Z. Li, T. Sakamaki, and R.G. Pestell. (2004). Minireview: Cyclin D1: normal and abnormal functions. *Endocrinology,* ***145***(12), 5439-5447. doi:10.1210/en.2004-0959

[57] Arinaga, M., T. Noguchi, S. Takeno, M. Chujo, T. Miura, et al. (2003). Clinical implication of cyclin B1 in non-small cell lung cancer. *Oncol Rep,* ***10***(5), 1381-1386. doi:10.3892/or.10.5.1381

[58] Yokokoji, T. and A.S. Narayanan. (2001). Role of D1 and E cyclins in cell cycle progression of human fibroblasts adhering to cementum attachment protein. *J Bone Miner Res,* ***16***(6), 1062-1067. doi:10.1359/jbmr.2001.16.6.1062

[59] Żuryń, A., A. Krajewski, A. Klimaszewska-Wiśniewska, A. Grzanka, and D. Grzanka. (2019). Expression of cyclin B1, D1 and K in non-small cell lung cancer H1299 cells following treatment with sulforaphane. *Oncol Rep,* ***41***(2), 1313-1323. doi:10.3892/or.2018.6919

[60] Zhu, Z., H.G. Golay, and D.A. Barbie. (2014). Targeting pathways downstream of KRAS in lung adenocarcinoma. *Pharmacogenomics*, ***15***(11), 1507-1518. doi:10.2217/pgs.14.108

[61] Soria, J.C., S.J. Jang, F.R. Khuri, K. Hassan, D. Liu, et al. (2000). Overexpression of cyclin B1 in early-stage non-small cell lung cancer and its clinical implication. *Cancer Res*, ***60***(15), 4000-4004.

[62] Puyol, M., A. Martín, P. Dubus, F. Mulero, P. Pizcueta, et al. (2010). A synthetic lethal interaction between K-Ras oncogenes and Cdk4 unveils a therapeutic strategy for non-small cell lung carcinoma. *Cancer Cell*, ***18***(1), 63-73. doi:10.1016/j.ccr.2010.05.025

[63] Bouclier, C., M. Simon, G. Laconde, M. Pellerano, S. Diot, et al. (2020). Stapled peptide targeting the CDK4/Cyclin D interface combined with Abemaciclib inhibits KRAS mutant lung cancer growth. *Theranostics*, ***10***(5), 2008-2028. doi:10.7150/thno.40971

[64] Mishina, T., H. Dosaka-Akita, I. Kinoshita, F. Hommura, T. Morikawa, et al. (1999). Cyclin D1 expression in non-small-cell lung cancers: its association with altered p53 expression, cell proliferation and clinical outcome. *Br J Cancer*, ***80***(8), 1289-1295. doi:10.1038/sj.bjc.6990500

[65] Luangdilok, S., P. Wanchaijiraboon, P. Chantranuwatana, C. Teerapakpinyo, S. Shuangshoti, et al. (2019). Cyclin D1 expression as a potential prognostic factor in advanced KRAS-mutant non-small cell lung cancer. *Transl Lung Cancer Res*, ***8***(6), 959-966. doi:10.21037/tlcr.2019.12.01

[66] Muñoz-Maldonado, C., Y. Zimmer, and M. Medová. (2019). A Comparative Analysis of Individual RAS Mutations in Cancer Biology. *Front Oncol*, ***9***, 1088. doi:10.3389/fonc.2019.01088

[67] Fang, Y., X. Liang, W. Jiang, J. Li, J. Xu, et al. (2015). Cyclin b1 suppresses colorectal cancer invasion and metastasis by regulating e-cadherin. *PLoS One*, ***10***(5), e0126875. doi:10.1371/journal.pone.0126875

[68] Caputi, M., G. Russo, V. Esposito, A. Mancini, and A. Giordano. (2005). Role of cell-cycle regulators in lung cancer. *J Cell Physiol*, ***205***(3), 319-327. doi:10.1002/jcp.20424

[69] Niu, C., C. Liang, J. Guo, L. Cheng, H. Zhang, et al. (2012). Downregulation and growth inhibitory role of FHL1 in lung cancer. *Int J Cancer*, ***130***(11), 2549-2556. doi:10.1002/ijc.26259

[70] Chen, X., Y. Liao, D. Long, T. Yu, F. Shen, et al. (2017). The Cdc2/Cdk1 inhibitor, purvalanol A, enhances the cytotoxic effects of taxol through Op18/stathmin in non-small cell lung cancer cells in vitro. *Int J Mol Med*, ***40***(1), 235-242. doi:10.3892/ijmm.2017.2989

[71] Subarkhan, M.K.M. and R. Ramesh. (2016). Ruthenium (II) arene complexes containing benzhydrazone ligands: synthesis, structure and antiproliferative activity. *Inorg Chem Front,* ***3***(10), 1245-1255. doi:10.1039/C6QI00197A

[72] Savić, A., T. Marzo, F. Scaletti, L. Massai, G. Bartoli, et al. (2019). New platinum(II) and palladium(II) complexes with substituted terpyridine ligands: synthesis and characterization, cytotoxicity and reactivity towards biomolecules. *Biometals,* ***32***(1), 33-47. doi:10.1007/s10534-018-0155-x

[73] Frezza, M., S. Hindo, D. Chen, A. Davenport, S. Schmitt, et al. (2010). Novel metals and metal complexes as platforms for cancer therapy. *Curr Pharm Des,* ***16***(16), 1813-1825. doi:10.2174/138161210791209009

[74] Ndagi, U., N. Mhlongo, and M.E. Soliman. (2017). Metal complexes in cancer therapy - an update from drug design perspective. *Drug Des Devel Ther,* ***11***, 599-616. doi:10.2147/dddt.S119488

[75] Graf, N. and S.J. Lippard. (2012). Redox activation of metal-based prodrugs as a strategy for drug delivery. *Adv Drug Deliv Rev,* ***64***(11), 993-1004. doi:10.1016/j.addr.2012.01.007

[76] Egorova, K.S. and V.P. Ananikov. (2017). Toxicity of metal compounds: knowledge and myths. *Organometallics,* ***36***(21), 4071-4090. doi:10.1021/acs.organomet.7b00605

[77] Jungwirth, U., C.R. Kowol, B.K. Keppler, C.G. Hartinger, W. Berger, et al. (2011). Anticancer activity of metal complexes: involvement of redox processes. *Antioxid Redox Signal,* ***15***(4), 1085-1127. doi:10.1089/ars.2010.3663

[78] Zhang, P. and P.J. Sadler. (2017). Advances in the design of organometallic anticancer complexes. *J Organomet Chem,* ***839***, 5-14. doi:10.1016/j.jorganchem.2017.03.038

[79] Ferreira-Silva, G.A., M.M. Ortega, M.A. Banionis, G.Y. Garavelli, F.T. Martins, et al. (2017). [Ru(pipe)(dppb)(bipy)]PF(6): A novel ruthenium complex that effectively inhibits ERK activation and cyclin D1 expression in A549 cells. *Toxicol In Vitro,* ***44***, 382-391. doi:10.1016/j.tiv.2017.07.019

[80] Romero-Canelón, I., M. Mos, and P.J. Sadler. (2015). Enhancement of Selectivity of an Organometallic Anticancer Agent by Redox Modulation. *J Med Chem,* ***58***(19), 7874-7880. doi:10.1021/acs.jmedchem.5b00655

[81] Leung, C.-H., H.-J. Zhong, D.S.-H. Chan, and D.-L. Ma. (2013). Bioactive iridium and rhodium complexes as therapeutic agents. *Coord Chem Rev,* ***257***(11-12), 1764-1776. doi:doi.org/10.1016/j.ccr.2013.01.034

[82] Haldar, S.K. (2017). Introduction. In S.K. Haldar (Ed.), *Platinum-Nicel-Chromium Deposits* (pp. 1-35): Elsevier. doi:10.1016/B978-0-12-802041-8.00001-8

[83] McConnell, J.R., D.P. Rananaware, D.M. Ramsey, K.N. Buys, M.L. Cole, et al. (2013). A potential rhodium cancer therapy: studies of a cytotoxic organorhodium(I) complex that binds DNA. *Bioorg Med Chem Lett,* ***23***(9), 2527-2531. doi:10.1016/j.bmcl.2013.03.016

[84] Rao, A.B.P., K. Gulati, N. Joshi, D.K. Deb, D. Rambabu, et al. (2017). Synthesis and biological studies of ruthenium, rhodium and iridium metal complexes with pyrazole-based ligands displaying unpredicted bonding modes. *Inorganica Chim Acta,* ***462***, 223-235. doi:10.1016/j.ica.2017.03.037

[85] Katsaros, N. and A. Anagnostopoulou. (2002). Rhodium and its compounds as potential agents in cancer treatment. *Crit Rev Oncol Hematol,* ***42***(3), 297-308. doi:10.1016/s1040-8428(01)00222-0

[86] Desoize, B. (2004). Metals and metal compounds in cancer treatment. *Anticancer Res,* ***24***(3a), 1529-1544.

[87] Komor, A.C., C.J. Schneider, A.G. Weidmann, and J.K. Barton. (2012). Cell-selective biological activity of rhodium metalloinsertors correlates with subcellular localization. *J Am Chem Soc,* ***134***(46), 19223-1933. doi:10.1021/ja3090687

[88] Markham, J., J. Liang, A. Levina, R. Mak, B. Johannessen, et al. (2017). (Pentamethylcyclopentadienato) rhodium Complexes for Delivery of the Curcumin Anticancer Drug. *Eur J Inorg Chem,* ***2017***(12), 1812-1823. doi:10.1002/ejic.201601331

[89] Markowska, A., B. Kasprzak, K. Jaszczyńska-Nowinka, J. Lubin, and J. Markowska. (2015). Noble metals in oncology. *Contemp Oncol (Pozn),* ***19***(4), 271-275. doi:10.5114/wo.2015.54386

[90] Li, J., Z. Tian, Z. Xu, S. Zhang, Y. Feng, et al. (2018). Highly potent half-sandwich iridium and ruthenium complexes as lysosome-targeted imaging and anticancer agents. *Dalton Trans,* ***47***(44), 15772-15782. doi:10.1039/c8dt02963f

[91] Ma, W., X. Ge, Z. Xu, S. Zhang, X. He, et al. (2019). Theranostic Lysosomal Targeting Anticancer and Antimetastatic Agents: Half-Sandwich Iridium(III) Rhodamine Complexes. *ACS Omega,* ***4***(12), 15240-15248. doi:10.1021/acsomega.9b01863

[92] Liu, Z., I. Romero-Canelón, A. Habtemariam, G.J. Clarkson, and P.J. Sadler. (2014). Potent Half-Sandwich Iridium(III) Anticancer Complexes Containing C(∧)N-Chelated and Pyridine Ligands. *Organometallics,* ***33***(19), 5324-5333. doi:10.1021/om500644f

[93] Qasim Warraich, M., A. Ghion, L. Perdisatt, L. O'Neill, A. Casey, et al. (2019). In vitro cytotoxicity, cellular uptake, reactive oxygen species and cell cycle arrest studies of novel ruthenium(II) polypyridyl complexes towards A549 lung cancer cell line. *Drug Chem Toxicol,* 1-11. doi:10.1080/01480545.2019.1589492

[94] Malik, M.A., M.K. Raza, O.A. Dar, Amadudin, M. Abid, et al. (2019). Probing the antibacterial and anticancer potential of tryptamine based mixed ligand Schiff base Ruthenium(III) complexes. *Bioorg Chem, **87***, 773-782. doi:10.1016/j.bioorg.2019.03.080

[95] Mohamed Subarkhan, M.K., L. Ren, B. Xie, C. Chen, Y. Wang, et al. (2019). Novel tetranuclear ruthenium(II) arene complexes showing potent cytotoxic and antimetastatic activity as well as low toxicity in vivo. *Eur J Med Chem, **179***, 246-256. doi:10.1016/j.ejmech.2019.06.061

[96] Guichard, S.M., R. Else, E. Reid, B. Zeitlin, R. Aird, et al. (2006). Anti-tumour activity in non-small cell lung cancer models and toxicity profiles for novel ruthenium(II) based organo-metallic compounds. *Biochem Pharmacol, **71***(4), 408-415. doi:10.1016/j.bcp.2005.10.053

[97] Flocke, L.S., R. Trondl, M.A. Jakupec, and B.K. Keppler. (2016). Molecular mode of action of NKP-1339 - a clinically investigated ruthenium-based drug - involves ER- and ROS-related effects in colon carcinoma cell lines. *Invest New Drugs, **34***(3), 261-268. doi:10.1007/s10637-016-0337-8

[98] Manegold, C. (2004). Gemcitabine (Gemzar) in non-small cell lung cancer. *Expert Rev Anticancer Ther, **4***(3), 345-360. doi:10.1586/14737140.4.3.345

[99] Ropp, R.C. (2013). Group 8 (Fe, Ru and Os) Alkaline Earth Compounds. In R.C. Ropp (Ed.), *Encyclopedia of the alkaline earth compounds* (pp. 911-960): Elsevier. doi:10.1016/B978-0-444-59550-8.00012-0

[100] Zhang, P. and H. Huang. (2018). Future potential of osmium complexes as anticancer drug candidates, photosensitizers and organelle-targeted probes. *Dalton Trans, **47***(42), 14841-14854. doi:10.1039/c8dt03432j

[101] Hearn, J.M., I. Romero-Canelón, A.F. Munro, Y. Fu, A.M. Pizarro, et al. (2015). Potent organo-osmium compound shifts metabolism in epithelial ovarian cancer cells. *Proc Natl Acad Sci U S A, **112***(29), E3800-5. doi:10.1073/pnas.1500925112

[102] Stepanenko, I.N., A.A. Krokhin, R.O. John, A. Roller, V.B. Arion, et al. (2008). Synthesis, structure, spectroscopic properties, and antiproliferative activity in vitro of novel osmium(III) complexes with azole heterocycles. *Inorg Chem, **47***(16), 7338-7347. doi:10.1021/ic8006958

[103] Büchel, G.E., I.N. Stepanenko, M. Hejl, M.A. Jakupec, B.K. Keppler, et al. (2011). En route to osmium analogues of KP1019: synthesis, structure, spectroscopic properties and antiproliferative activity of trans-[Os(IV)Cl4(Hazole)2]. *Inorg Chem, **50***(16), 7690-7697. doi:10.1021/ic200728b

[104] Zaki, M., S. Hairat, and E.S. Aazam. (2019). Scope of organometallic compounds based on transition metal-arene systems as anticancer agents: starting from the classical paradigm to targeting multiple strategies. *RSC Adv, **9***(6), 3239-3278.

[105] Coverdale, J.P., T. Laroiya-McCarron, and I. Romero-Canelón. (2019). Designing Ruthenium Anticancer Drugs: What Have We Learnt from the Key Drug Candidates? *Inorganics, **7***(3), 31. doi:10.3390/inorganics7030031

[106] Singh, S.K. and D.S. Pandey. (2014). Multifaceted half-sandwich arene–ruthenium complexes: interactions with biomolecules, photoactivation, and multinuclearity approach. *RSC Adv, **4***(4), 1819-1840. doi:10.1039/C3RA44131H

[107] Gatti, A., A. Habtemariam, I. Romero-Canelón, J.-I. Song, B. Heer, et al. (2018). Half-sandwich arene ruthenium (II) and osmium (II) thiosemicarbazone complexes: solution behavior and antiproliferative activity. *Organometallics, **37***(6), 891-899. doi:10.1021/acs.organomet.7b00875

[108] van Rijt, S.H., I. Romero-Canelón, Y. Fu, S.D. Shnyder, and P.J. Sadler. (2014). Potent organometallic osmium compounds induce mitochondria-mediated apoptosis and S-phase cell cycle arrest in A549 non-small cell lung cancer cells. *Metallomics, **6***(5), 1014-1022. doi:10.1039/c4mt00034j

[109] Dempsey, J.L., J.R. Winkler, and H.B. Gray. (2011). Redox reactivity of photogenerated osmium(II) complexes. *Dalton Trans, **40***(40), 10633-10636. doi:10.1039/c1dt11138h

[110] Fu, Y., A. Habtemariam, A.M. Pizarro, S.H. van Rijt, D.J. Healey, et al. (2010). Organometallic osmium arene complexes with potent cancer cell cytotoxicity. *J Med Chem, **53***(22), 8192-8196. doi:10.1021/jm100560f

[111] Shnyder, S.D., Y. Fu, A. Habtemariam, S.H. van Rijt, P.A. Cooper, et al. (2011). Anti-colorectal cancer activity of an organometallic osmium arene azopyridine complex. *MedChemComm, **2***(7), 666-668. doi:10.1039/C1MD00075F

[112] Peacock, A.F., S. Parsons, and P.J. Sadler. (2007). Tuning the hydrolytic aqueous chemistry of osmium arene complexes with N,O-chelating ligands to achieve cancer cell cytotoxicity. *J Am Chem Soc, **129***(11), 3348-3357. doi:10.1021/ja068335p

[113] Vekariya, P.A., P.S. Karia, B.S. Bhatt, and M.N. Patel. (2018). Effect of Substituents on the Biological Activities of Piano Stool η5-Cyclopentadienyl Rh(III) and Ir(III) Complexes. *J Inorg Organomet Polym Mater*, ***28***(6), 2749-2758. doi:10.1007/s10904-018-0957-x

[114] Bruijnincx, P.C. and P.J. Sadler. (2009). Controlling platinum, ruthenium, and osmium reactivity for anticancer drug design. *Adv Inorg Chem*, ***61***, 1-62. doi:10.1016/S0898-8838(09)00201-3

[115] Phillips, A.D., O. Zava, R. Scopelitti, A.A. Nazarov, and P.J. Dyson. (2010). Rational Design of Highly Cytotoxic η6-Arene β-Diketiminato− Ruthenium Complexes. *Organometallics*, ***29***(2), 417-427. doi:10.1021/om900991b

[116] Peacock, A.F. and P.J. Sadler. (2008). Medicinal organometallic chemistry: designing metal arene complexes as anticancer agents. *Chem Asian J*, ***3***(11), 1890-1899. doi:10.1002/asia.200800149

[117] Wang, H.Y., Y. Qian, F.X. Wang, A. Habtemariam, Z.W. Mao, et al. (2017). Ruthenium (II)–Arene Metallacycles: Crystal Structures, Interaction with DNA, and Cytotoxicity. *Eur J Inorg Chem*, ***2017***(12), 1792-1799. doi:10.1002/ejic.201601226

[118] Sáez, R., J. Lorenzo, M.J. Prieto, M. Font-Bardia, T. Calvet, et al. (2014). Influence of PPh_3 moiety in the anticancer activity of new organometallic ruthenium complexes. *J Inorg Biochem*, ***136***, 1-12. doi:10.1016/j.jinorgbio.2014.03.002

[119] Lawlor, L. and X.B. Yang. (2019). Harnessing the HDAC–histone deacetylase enzymes, inhibitors and how these can be utilised in tissue engineering. *Int J Oral Sci*, ***11***(2), 20. doi:10.1038/s41368-019-0053-2

[120] Lakshmaiah, K.C., L.A. Jacob, S. Aparna, D. Lokanatha, and S.C. Saldanha. (2014). Epigenetic therapy of cancer with histone deacetylase inhibitors. *J Cancer Res Ther*, ***10***(3), 469-478. doi:10.4103/0973-1482.137937

[121] Suraweera, A., K.J. O'Byrne, and D.J. Richard. (2018). Combination Therapy With Histone Deacetylase Inhibitors (HDACi) for the Treatment of Cancer: Achieving the Full Therapeutic Potential of HDACi. *Front Oncol*, ***8***, 92. doi:10.3389/fonc.2018.00092

[122] Eckschlager, T., J. Plch, M. Stiborova, and J. Hrabeta. (2017). Histone Deacetylase Inhibitors as Anticancer Drugs. *Int J Mol Sci*, ***18***(7), 1414. doi:10.3390/ijms18071414

[123] Ma, Z., D. Liu, S. Di, Z. Zhang, W. Li, et al. (2019). Histone deacetylase 9 downregulation decreases tumor growth and promotes apoptosis in non-small cell lung cancer after melatonin treatment. *J Pineal Res*, ***67***(2), e12587. doi:10.1111/jpi.12587

[124] Damaskos, C., I. Tomos, N. Garmpis, A. Karakatsani, D. Dimitroulis, et al. (2018). Histone Deacetylase Inhibitors as a Novel Targeted Therapy Against Non-small Cell Lung Cancer: Where Are We Now and What Should We Expect? *Anticancer Res*, ***38***(1), 37-43. doi:10.21873/anticanres.12189

[125] Kim, H.J. and S.C. Bae. (2011). Histone deacetylase inhibitors: molecular mechanisms of action and clinical trials as anti-cancer drugs. *Am J Transl Res*, ***3***(2), 166-179.

[126] Mottamal, M., S. Zheng, T.L. Huang, and G. Wang. (2015). Histone deacetylase inhibitors in clinical studies as templates for new anticancer agents. *Molecules*, ***20***(3), 3898-3941. doi:10.3390/molecules20033898

[127] Wang, L., H. Li, Y. Ren, S. Zou, W. Fang, et al. (2016). Targeting HDAC with a novel inhibitor effectively reverses paclitaxel resistance in non-small cell lung cancer via multiple mechanisms. *Cell Death Dis*, ***7***(1), e2063-e2063. doi:10.1038/cddis.2015.328

[128] Yamada, T., J.M. Amann, A. Tanimoto, H. Taniguchi, T. Shukuya, et al. (2018). Histone Deacetylase Inhibition Enhances the Antitumor Activity of a MEK Inhibitor in Lung Cancer Cells Harboring RAS Mutations. *Mol Cancer Ther,* ***17***(1), 17-25. doi:10.1158/1535-7163.Mct-17-0146

[129] Yang, H., S.Q. Liang, R.A. Schmid, and R.W. Peng. (2019). New Horizons in KRAS-Mutant Lung Cancer: Dawn After Darkness. *Front Oncol,* ***9***, 953. doi:10.3389/fonc.2019.00953

[130] Owonikoko, T.K., S.S. Ramalingam, B. Kanterewicz, T.E. Balius, C.P. Belani, et al. (2010). Vorinostat increases carboplatin and paclitaxel activity in non-small-cell lung cancer cells. *Int J Cancer,* ***126***(3), 743-755. doi:10.1002/ijc.24759

[131] Dokmanovic, M., C. Clarke, and P.A. Marks. (2007). Histone deacetylase inhibitors: overview and perspectives. *Mol Cancer Res,* ***5***(10), 981-989. doi:10.1158/1541-7786.Mcr-07-0324

[132] Schemies, J., U. Uciechowska, W. Sippl, and M. Jung. (2010). NAD(+) -dependent histone deacetylases (sirtuins) as novel therapeutic targets. *Med Res Rev,* ***30***(6), 861-889. doi:10.1002/med.20178

[133] Park, S.Y. and J.S. Kim. (2020). A short guide to histone deacetylases including recent progress on class II enzymes. *Exp Mol Med,* ***52***(2), 204-212. doi:10.1038/s12276-020-0382-4

[134] Ramakrishnan, S. and R. Pili. (2013). Histone deacetylase inhibitors and epigenetic modifications as a novel strategy in renal cell carcinoma. *Cancer J,* ***19***(4), 333-340. doi:10.1097/PPO.0b013e3182a09e07

[135] Zong, H., D. Shah, K. Selwa, R.E. Tsuchida, R. Rattan, et al. (2015). Design and Evaluation of Tumor-Specific Dendrimer Epigenetic Therapeutics. *ChemistryOpen,* ***4***(3), 335-341. doi:10.1002/open.201402141

[136] Pal, D. and S. Saha. (2012). Hydroxamic acid–A novel molecule for anticancer therapy. *J Adv Pharm Technol Res,* ***3***(2), 92–99. doi:10.4103/2231-4040.97281

[137] Xu, W.S., R.B. Parmigiani, and P.A. Marks. (2007). Histone deacetylase inhibitors: molecular mechanisms of action. *Oncogene,* ***26***(37), 5541-5552. doi:10.1038/sj.onc.1210620

[138] Bubna, A.K. (2015). Vorinostat—an overview. *Indian J Dermatol,* ***60***(4), 419. doi:10.4103/0019-5154.160511

[139] Duvic, M., R. Talpur, X. Ni, C. Zhang, P. Hazarika, et al. (2007). Phase 2 trial of oral vorinostat (suberoylanilide hydroxamic acid, SAHA) for refractory cutaneous T-cell lymphoma (CTCL). *Blood,* ***109***(1), 31-39. doi:10.1182/blood-2006-06-025999

[140] Gerson, S.L., P.F. Caimi, B.M. William, and R.J. Creger. (2018). Pharmacology and molecular mechanisms of antineoplastic agents for hematologic malignancies. In E.J.B. Ronald

Hoffman, Leslie E. Silberstein, Helen E. Heslop, Jeffrey I. Weitz, John Anastasi, Mohamed E. Salama, Syed Ali Abutalib (Ed.), *Hematology* (Seventh ed., pp. 849-912): Elsevier. doi:10.1016/B978-0-323-35762-3.00057-3

[141] Yang, F., N. Zhao, Y. Hu, C.-S. Jiang, and H. Zhang. (2020). The Development Process: from SAHA to Hydroxamate HDAC Inhibitors with Branched CAP Region and Linear Linker. *Chem Biodivers*, ***17***(1), e1900427. doi:10.1002/cbdv.201900427

[142] Choi, S.E. and M.K. Pflum. (2012). The structural requirements of histone deacetylase inhibitors: suberoylanilide hydroxamic acid analogs modified at the C6 position. *Bioorg Med Chem Lett*, ***22***(23), 7084-7086. doi:10.1016/j.bmcl.2012.09.093

[143] Bieliauskas, A.V., S.V. Weerasinghe, and M.K.H. Pflum. (2007). Structural requirements of HDAC inhibitors: SAHA analogs functionalized adjacent to the hydroxamic acid. *Bioorg Med Chem Lett*, ***17***(8), 2216-2219. doi:10.1016/j.bmcl.2007.01.117

[144] Choi, S.E., S.V. Weerasinghe, and M.K. Pflum. (2011). The structural requirements of histone deacetylase inhibitors: Suberoylanilide hydroxamic acid analogs modified at the C3 position display isoform selectivity. *Bioorg Med Chem Lett*, ***21***(20), 6139-6142. doi:10.1016/j.bmcl.2011.08.027

[145] Ghosh, B., W.N. Zhao, S.A. Reis, D. Patnaik, D.M. Fass, et al. (2016). Dissecting structure-activity-relationships of crebinostat: Brain penetrant HDAC inhibitors for neuroepigenetic regulation. *Bioorg Med Chem Lett*, ***26***(4), 1265-1271. doi:10.1016/j.bmcl.2016.01.022

[146] Spencer, J., J. Amin, M. Wang, G. Packham, S.S. Alwi, et al. (2011). Synthesis and Biological Evaluation of JAHAs: Ferrocene-Based Histone Deacetylase Inhibitors. *ACS Med Chem Lett*, ***2***(5), 358-362. doi:10.1021/ml100295v

[147] Kang, T.S., C.N. Ko, J.T. Zhang, C. Wu, C.Y. Wong, et al. (2018). Rhodium(III)-Based Inhibitor of the JMJD3-H3K27me3 Interaction and Modulator of the Inflammatory Response. *Inorg Chem*, ***57***(22), 14023-14026. doi:10.1021/acs.inorgchem.8b02256

[148] Liu, L.J., L. Lu, H.J. Zhong, B. He, D.W. Kwong, et al. (2015). An Iridium(III) Complex Inhibits JMJD2 Activities and Acts as a Potential Epigenetic Modulator. *J Med Chem*, ***58***(16), 6697-6703. doi:10.1021/acs.jmedchem.5b00375

[149] Ali, A., D. Bansal, N.K. Kaushik, N. Kaushik, E.H. Choi, et al. (2014). Syntheses, characterization, and anti-cancer activities of pyridine-amide based compounds containing appended phenol or catechol groups. *J Chem Sci*, ***126***(4), 1091-1105. doi:10.1007/s12039-014-0671-3

[150] Smith, F. and K.L. Ee. (1980). Organotin complexes of pyridine-2-carbothioamide. *Experientia*, ***36***(4), 391-392. doi:10.1007/BF01975104

[151] Zhang, J., X. Ke, C. Tu, J. Lin, J. Ding, et al. (2003). Novel Cu(II)-quinoline carboxamide complexes: structural characterization, cytotoxicity and reactivity towards 5'-GMP. *Biometals,* ***16***(3), 485-496. doi:10.1023/a:1022577420708

[152] Dharman, P., V. Babu, and K.A. Basha. (2019). A facile synthesis of novel 5-substituted pyridine 2 carboxamide derivatives and their biological evaluation and 3D QSAR studies. *J Chin Chem Soc,* ***66***(4), 415-426. doi:10.1002/jccs.201800035

[153] Hanif, M., J. Arshad, J. Astin, Z. Rana, A. Zafar, et al. (2020). A Multitargeted Approach in the Discovery of an Organorhodium Anticancer Agent Based On Vorinostat as a Potent Histone Deacetylase Inhibitor. *Angew Chem Int Ed Engl*. doi:10.1002/anie.202005758

[154] Molinspiration. Calculation of molecular physicochemical properties. [cited 20 May, 2020]; Available from: https://bit.ly/3i4k41n.

[155] Baumann, M. and I.R. Baxendale. (2013). An overview of the synthetic routes to the best selling drugs containing 6-membered heterocycles. *Beilstein J Org Chem,* ***9***(1), 2265-2319. doi:10.3762/bjoc.9.265

[156] Hamada, Y. (2018). Role of Pyridines in Medicinal Chemistry and Design of BACE1 Inhibitors Possessing a Pyridine Scaffold. In *Pyridine* (pp. 9). doi:10.5772/intechopen.74719

[157] El-Sayed, H., A. Moustafa, A. El-Torky, and E.A. El-Salam. (2017). A series of pyridines and pyridine based sulfa-drugs as antimicrobial agents: Design, synthesis and antimicrobial activity. *Russ J Gen Chem,* ***87***(10), 2401-2408. doi: 10.1134/S107036321710022X

[158] Altaf, A.A., A. Shahzad, Z. Gul, N. Rasool, A. Badshah, et al. (2015). A review on the medicinal importance of pyridine derivatives. *J Med Chem Drug Des,* ***1***(1), 1. doi:10.11648/j.jddmc.20150101.11

[159] Grguric-Sipka, S., C.R. Kowol, S.M. Valiahdi, R. Eichinger, M.A. Jakupec, et al. (2007). Ruthenium (II) Complexes of Thiosemicarbazones: The First Water-Soluble Complex with pH-Dependent Antiproliferative Activity. *Eur J Inorg Chem,* ***2007***(18), 2870-2878. doi:10.1002/ejic.200601196

[160] Zhang, R., X. Qin, F. Kong, P. Chen, and G. Pan. (2019). Improving cellular uptake of therapeutic entities through interaction with components of cell membrane. *Drug Deliv,* ***26***(1), 328-342. doi:10.1080/10717544.2019.1582730

[161] Darwish, S., N. Sadeghiani, S. Fong, S. Mozaffari, P. Hamidi, et al. (2019). Synthesis and antiproliferative activities of doxorubicin thiol conjugates and doxorubicin-SS-cyclic peptide. *Eur J Med Chem,* ***161***, 594-606. doi:10.1016/j.ejmech.2018.10.042

[162] Muthyala, R., W.S. Shin, J. Xie, and Y.Y. Sham. (2015). Discovery of 1-hydroxypyridine-2-thiones as selective histone deacetylase inhibitors and their potential

application for treating leukemia. *Bioorg Med Chem Lett*, ***25***(19), 4320-4324. doi:10.1016/j.bmcl.2015.07.065

[163] Patil, V., Q.H. Sodji, J.R. Kornacki, M. Mrksich, and A.K. Oyelere. (2013). 3-Hydroxypyridin-2-thione as novel zinc binding group for selective histone deacetylase inhibition. *J Med Chem*, ***56***(9), 3492-3506. doi:10.1021/jm301769u

[164] Kandioller, W., A. Kurzwernhart, M. Hanif, S.M. Meier, H. Henke, et al. (2011). Pyrone derivatives and metals: From natural products to metal-based drugs. *J Organomet Chem*, ***696***(5), 999-1010. doi:10.1016/j.jorganchem.2010.11.010

[165] Prachayasittikul, S., Treeratanapiboon, L., and S. Ruchirawat, Prachayasittikul, V. (2009). Novel activities of 1-adamantylthiopyridines as antibacterials, antimalarials and anticancers. *EXCLI Journal*, ***8***, 121-129. doi:10.17877/DE290R-641

[166] Salina, E.G., O. Ryabova, A. Vocat, B. Nikonenko, S.T. Cole, et al. (2017). New 1-hydroxy-2-thiopyridine derivatives active against both replicating and dormant Mycobacterium tuberculosis. *J Infect Chemother*, ***23***(11), 794-797. doi:10.1016/j.jiac.2017.04.012

[167] Süss-Fink, G. (2010). Arene ruthenium complexes as anticancer agents. *Dalton Trans*, ***39***(7), 1673-1688. doi:10.1039/b916860p

[168] Kandioller, W., C.G. Hartinger, A.A. Nazarov, C. Bartel, M. Skocic, et al. (2009). Maltol-derived ruthenium-cymene complexes with tumor inhibiting properties: the impact of ligand-metal bond stability on anticancer activity in vitro. *Chemistry*, ***15***(45), 12283-12291. doi:10.1002/chem.200901939

[169] Hanif, M., S. Meier, A. Nazarov, J. Risse, A. Legin, et al. (2013). Influence of the π-coordinated arene on the anticancer activity of ruthenium (II) carbohydrate organometallic complexes. *Front Chem*, ***1***, 27. doi:10.3389/fchem.2013.00027

[170] Noffke, A.L., A. Habtemariam, A.M. Pizarro, and P.J. Sadler. (2012). Designing organometallic compounds for catalysis and therapy. *Chem Commun*, ***48***(43), 5219-5246. doi:10.1039/C2CC30678F

[171] Kato, Y., H. Nakamura, H. Tojo, M. Nomura, T. Nagao, et al. (2015). A proteomic profiling of laser-microdissected lung adenocarcinoma cells of early lepidic-types. *Clin Transl Med*, ***4***(1), 64. doi:10.1186/s40169-015-0064-3

[172] Raymond, A.C., B. Gao, L. Girard, J.D. Minna, and D. Gomika Udugamasooriya. (2019). Unbiased peptoid combinatorial cell screen identifies plectin protein as a potential biomarker for lung cancer stem cells. *Sci Rep*, ***9***(1), 14954. doi:10.1038/s41598-019-51004-3

[173] Meier, S.M., D. Kreutz, L. Winter, M.H.M. Klose, K. Cseh, et al. (2017). An Organoruthenium Anticancer Agent Shows Unexpected Target Selectivity For Plectin. *Angew Chem Int Ed Engl*, ***56***(28), 8267-8271. doi:10.1002/anie.201702242

[174] Meier-Menches, S.M., K. Zappe, A. Bileck, D. Kreutz, A. Tahir, et al. (2019). Time-dependent shotgun proteomics revealed distinct effects of an organoruthenium prodrug and its activation product on colon carcinoma cells. *Metallomics*, ***11***(1), 118-127. doi:10.1039/c8mt00152a

[175] Klose, M.H.M., S. Theiner, C. Kornauth, S.M. Meier-Menches, P. Heffeter, et al. (2018). Bioimaging of isosteric osmium and ruthenium anticancer agents by LA-ICP-MS. *Metallomics*, ***10***(3), 388-396. doi:10.1039/c8mt00012c

[176] Cheng, H.-C., R.Z. Qi, H. Paudel, and H.-J. Zhu. (2011). Regulation and function of protein kinases and phosphatases. *Enzyme Res*, ***2011***, 3. doi:10.4061/2011/329098

[177] Duronio, R.J. and Y.J.C.S.H.p.i.b. Xiong. (2013). Signaling pathways that control cell proliferation. *Cold Spring Harb Perspect Biol*, ***5***(3), a008904. doi:10.1101/cshperspect.a008904

[178] Knapp, S. (2018). New opportunities for kinase drug repurposing and target discovery. *Br J Cancer*, ***118***(7), 936-937. doi:10.1038/s41416-018-0045-6

[179] Bhullar, K.S., N.O. Lagarón, E.M. McGowan, I. Parmar, A. Jha, et al. (2018). Kinase-targeted cancer therapies: progress, challenges and future directions. *Mol Cancer*, ***17***(1), 48. doi:10.1186/s12943-018-0804-2

[180] Gilewska, A., B. Barszcz, J. Masternak, K. Kazimierczuk, J. Sitkowski, et al. (2019). Similarities and differences in d6 low-spin ruthenium, rhodium and iridium half-sandwich complexes: synthesis, structure, cytotoxicity and interaction with biological targets. *J Biol Inorg Chem*, ***24***(4), 591-606. doi:10.1007/s00775-019-01665-2

[181] Meier-Menches, S.M., C. Gerner, W. Berger, C.G. Hartinger, and B.K. Keppler. (2018). Structure-activity relationships for ruthenium and osmium anticancer agents - towards clinical development. *Chem Soc Rev*, ***47***(3), 909-928. doi:10.1039/c7cs00332c

[182] Koltai, T. (2016). Cancer: fundamentals behind pH targeting and the double-edged approach. *Onco Targets Ther*, ***9***, 6343. doi:10.2147/OTT.S115438

[183] Purkait, K., Anticancer Activity of Palladium & Ruthenium Complexes: Effect of Steric Hindrance on Cytotoxicity and GSH Resistance. 2019, Indian Institute of Science Education and Research Kolkata.

[184] Meier, S.M., M. Hanif, Z. Adhireksan, V. Pichler, M. Novak, et al. (2013). Novel metal (II) arene 2-pyridinecarbothioamides: a rationale to orally active organometallic anticancer agents. *Chem Sci*, ***4***(4), 1837-1846. doi:10.1039/c3sc22294b

[185] Bergamo, A., A. Masi, A.F. Peacock, A. Habtemariam, P.J. Sadler, et al. (2010). In vivo tumour and metastasis reduction and in vitro effects on invasion assays of the ruthenium RM175 and osmium AFAP51 organometallics in the mammary cancer model. *J Inorg Biochem*, ***104***(1), 79-86. doi:10.1016/j.jinorgbio.2009.10.005

[186] Dhakal, B., L. Bohé, and D. Crich. (2017). Trifluoromethanesulfonate Anion as Nucleophile in Organic Chemistry. *J Org Chem*, ***82***(18), 9263-9269. doi:10.1021/acs.joc.7b01850

[187] Hayashida, T., H. Kondo, J.-i. Terasawa, K. Kirchner, Y. Sunada, et al. (2007). Trifluoromethanesulfonate (triflate) as a moderately coordinating anion: Studies from chemistry of the cationic coordinatively unsaturated mono-and diruthenium amidinates. *J Organomet Chem*, ***692***(1-3), 382-394. doi:10.1016/j.jorganchem.2006.08.069

[188] Yadav, B., S. Taurin, R.J. Rosengren, M. Schumacher, M. Diederich, et al. (2010). Synthesis and cytotoxic potential of heterocyclic cyclohexanone analogues of curcumin. *Bioorg Med Chem*, ***18***(18), 6701-6707. doi:10.1016/j.bmc.2010.07.063

[189] Postnikova, E., Y. Cong, L.E. DeWald, J. Dyall, S. Yu, et al. (2018). Testing therapeutics in cell-based assays: Factors that influence the apparent potency of drugs. *PLoS One*, ***13***(3), e0194880. doi:10.1371/journal.pone.0194880

[190] GraphPad. Equation: log(inhibitor) vs. response -- Variable slope. [cited 26 July, 2019]; Available from: https://bit.ly/3i2YE4G.

[191] Swinney, D.C. (2011). Molecular mechanism of action (MMoA) in drug discovery. In J.E. Macor (Ed.), *Annual Reports in Medicinal Chemistry* (Vol. 46, pp. 301-317): Academic Press. doi:10.1016/B978-0-12-386009-5.00009-6

[192] Badisa, R.B., S.F. Darling-Reed, P. Joseph, J.S. Cooperwood, L.M. Latinwo, et al. (2009). Selective cytotoxic activities of two novel synthetic drugs on human breast carcinoma MCF-7 cells. *Anticancer Res*, ***29***(8), 2993-2996.

[193] Gazdar, A.F., L. Girard, W.W. Lockwood, W.L. Lam, and J.D. Minna. (2010). Lung cancer cell lines as tools for biomedical discovery and research. *J Natl Cancer Inst*, ***102***(17), 1310-1321. doi:10.1093/jnci/djq279

[194] Chiba, M., Y. Togashi, S. Tomida, H. Mizuuchi, Y. Nakamura, et al. (2016). MEK inhibitors against MET-amplified non-small cell lung cancer. *Int J Oncol*, ***49***(6), 2236-2244. doi:10.3892/ijo.2016.3736

[195] Yang, H., S.-Q. Liang, R.A. Schmid, and R.-W. Peng. (2019). New Horizons in KRAS-Mutant Lung Cancer: Dawn After Darkness. *Front Oncol*, ***9***, 953. doi:10.3389/fonc.2019.00953

[196] Lei, L., W.X. Wang, Z.Y. Yu, X.B. Liang, W.W. Pan, et al. (2020). A Real-World Study in Advanced Non-Small Cell Lung Cancer with KRAS Mutations. *Transl Oncol*, ***13***(2), 329-335. doi:10.1016/j.tranon.2019.12.004

[197] Wang, Z. and Y. Sun. (2010). Targeting p53 for novel anticancer therapy. *Transl Oncol*, ***3***(1), 1-12. doi:10.1593/tlo.09250

[198] Fer, N.D., R.H. Shoemaker, and A. Monks. (2010). Adaphostin toxicity in a sensitive non-small cell lung cancer model is mediated through Nrf2 signaling and heme oxygenase 1. *J Exp Clin Cancer Res, **29***, 91. doi:10.1186/1756-9966-29-91

[199] Grzegrzolka, J., A. Gomulkiewicz, M. Olbromski, N. Glatzel-Plucinska, A. Piotrowska, et al. (2019). Expression of tesmin (MTL5) in nonsmall cell lung cancer: A preliminary study. *Oncol Rep, **42***(1), 253-262. doi:10.3892/or.2019.7145

[200] Tsai, C.M., K.T. Chang, L.H. Wu, J.Y. Chen, A.F. Gazdar, et al. (1996). Correlations between intrinsic chemoresistance and HER-2/neu gene expression, p53 gene mutations, and cell proliferation characteristics in non-small cell lung cancer cell lines. *Cancer Res, **56***(1), 206-209.

[201] Leroy, B., M. Anderson, and T. Soussi. (2014). TP53 mutations in human cancer: database reassessment and prospects for the next decade. *Hum Mutat, **35***(6), 672-688. doi:10.1002/humu.22552

[202] Xie, L., C. Gazin, S.M. Park, L.J. Zhu, M.A. Debily, et al. (2012). A synthetic interaction screen identifies factors selectively required for proliferation and TERT transcription in p53-deficient human cancer cells. *PLoS Genet, **8***(12), e1003151. doi:10.1371/journal.pgen.1003151

[203] Jang, Y.S., J.H. Kang, J.K. Woo, H.M. Kim, J.I. Hwang, et al. (2016). Ninjurin1 suppresses metastatic property of lung cancer cells through inhibition of interleukin 6 signaling pathway. *Int J Cancer, **139***(2), 383-395. doi:10.1002/ijc.30021

[204] Lee, S.H., I.B. Jaganath, S.M. Wang, and S.D. Sekaran. (2011). Antimetastatic effects of Phyllanthus on human lung (A549) and breast (MCF-7) cancer cell lines. *PLoS One, **6***(6), e20994. doi:10.1371/journal.pone.0020994

[205] Zhou, Z., Y. Su, and X. Fa. (2015). Restoration of BRG1 inhibits proliferation and metastasis of lung cancer by regulating tumor suppressor miR-148b. *Onco Targets Ther, **8***, 3603-3612. doi:10.2147/ott.S95500

[206] Guin, S., Y. Ru, M.W. Wynes, R. Mishra, X. Lu, et al. (2013). Contributions of KRAS and RAL in non-small-cell lung cancer growth and progression. *J Thorac Oncol, **8***(12), 1492-1501. doi:10.1097/jto.0000000000000007

[207] Acquaviva, J., D.L. Smith, J. Sang, J.C. Friedland, S. He, et al. (2012). Targeting KRAS-mutant non-small cell lung cancer with the Hsp90 inhibitor ganetespib. *Mol Cancer Ther, **11***(12), 2633-2643. doi:10.1158/1535-7163.Mct-12-0615

[208] NIH. National Cancer Institute. *RAS Cell Lines* [cited 10 April, 2020]; Available from: https://bit.ly/2B5pGro.

[209] Biamonte, F., A.M. Battaglia, F. Zolea, D.M. Oliveira, I. Aversa, et al. (2018). Ferritin heavy subunit enhances apoptosis of non-small cell lung cancer cells through modulation of miR-125b/p53 axis. *Cell Death Dis, **9***(12), 1174. doi:10.1038/s41419-018-1216-3

[210] Ikediobi, O.N., H. Davies, G. Bignell, S. Edkins, C. Stevens, et al. (2006). Mutation analysis of 24 known cancer genes in the NCI-60 cell line set. *Mol Cancer Ther, **5***(11), 2606-2612. doi:10.1158/1535-7163.Mct-06-0433

[211] Bepler, G., A. Koehler, P. Kiefer, K. Havemann, K. Beisenherz, et al. (1988). Characterization of the state of differentiation of six newly established human non-small-cell lung cancer cell lines. *Differentiation, **37***(2), 158-171. doi:10.1111/j.1432-0436.1988.tb00806.x

[212] Grundner-Culemann, K., J.N. Dybowski, M. Klammer, A. Tebbe, C. Schaab, et al. (2016). Comparative proteome analysis across non-small cell lung cancer cell lines. *J Proteomics, **130***, 1-10. doi:10.1016/j.jprot.2015.09.003

[213] Nagai, Y., H. Miyazawa, Huqun, T. Tanaka, K. Udagawa, et al. (2005). Genetic heterogeneity of the epidermal growth factor receptor in non-small cell lung cancer cell lines revealed by a rapid and sensitive detection system, the peptide nucleic acid-locked nucleic acid PCR clamp. *Cancer Res, **65***(16), 7276-7282. doi:10.1158/0008-5472.Can-05-0331

[214] NIH. NCI GDC Data Portal. *Primary site bronchus and lung, disease type adenomas and ademocarcinomas* [cited June 15, 2020]; Available from: https://bit.ly/2Y2NGEl

[215] Dang, A.H., V.U. Tran, T.T. Tran, H.A. Thi Pham, D.T. Le, et al. (2020). Actionable Mutation Profiles of Non-Small Cell Lung Cancer patients from Vietnamese population. *Sci Rep, **10***(1), 2707. doi:10.1038/s41598-020-59744-3

[216] Svaton, M., O. Fiala, M. Pesek, Z. Bortlicek, M. Minarik, et al. (2016). The Prognostic Role of KRAS Mutation in Patients with Advanced NSCLC Treated with Second- or Third-line Chemotherapy. *Anticancer Res, **36***(3), 1077-1082.

[217] Nadal, E., G. Chen, J.R. Prensner, H. Shiratsuchi, C. Sam, et al. (2014). KRAS-G12C mutation is associated with poor outcome in surgically resected lung adenocarcinoma. *J Thorac Oncol, **9***(10), 1513-1522. doi:10.1097/jto.0000000000000305

[218] Wagner, P.L., A.C. Stiedl, T. Wilbertz, K. Petersen, V. Scheble, et al. (2011). Frequency and clinicopathologic correlates of KRAS amplification in non-small cell lung carcinoma. *Lung Cancer, **74***(1), 118-123. doi:10.1016/j.lungcan.2011.01.029

[219] Park, S.H. and Y. Qin. (2019). NIH3T3 directs memory-fated CTL programming and represses high expression of PD-1 on antitumor CTLs. *Front Immunol, **10***, 761. doi:10.3389/fimmu.2019.00761

[220] Xu, K. and H.J.C.R. Rubin. (1990). Cell transformation as aberrant differentiation: environmentslly dependent spontaneous transformation of NIH 3t3 cells. *Cell Res, **1***(2), 197-206. doi:10.1038/cr.1990.20

[221] Fridman, R., T.M. Sweeney, M. Zain, G.R. Martin, and H.K. Kleinman. (1992). Malignant transformation of NIH-3T3 cells after subcutaneous co-injection with a reconstituted basement membrane (matrigel). *Int J Cancer, **51***(5), 740-744. doi:10.1002/ijc.2910510513

[222] Hollingsworth, M.A., L.M. Rebellato, J.W. Moore, O.J. Finn, and R.S. Metzgar. (1986). Antigens expressed on NIH 3T3 cells following transformation with DNA from human pancreatic tumor. *Cancer Res, **46***(5), 2482-2487.

[223] Kalluri, R. and M. Zeisberg. (2006). Fibroblasts in cancer. *Nat Rev Cancer, **6***(5), 392-401. doi:10.1038/nrc1877

[224] Murray, L.A., D.A. Knight, and G.J. Laurent. (2009). Fibroblasts. In J.M.D. Peter J. Barnes, Stephen I. Rennard, Neil C. Thomson (Ed.), *Asthma and COPD* (Second ed., pp. 193-200): Academic Press. doi:10.1016/B978-0-12-374001-4.00015-8

[225] Cruz-Bermudez, A., R. Laza-Briviesca, R.J. Vicente-Blanco, A. Garcia-Grande, M.J. Coronado, et al. (2019). Cancer-associated fibroblasts modify lung cancer metabolism involving ROS and TGF-beta signaling. *Free Radic Biol Med, **130***, 163-173. doi:10.1016/j.freeradbiomed.2018.10.450

[226] Liu, T., L. Zhou, D. Li, T. Andl, and Y. Zhang. (2019). Cancer-Associated Fibroblasts Build and Secure the Tumor Microenvironment. *Front Cell Dev Biol, **7***, 60. doi:10.3389/fcell.2019.00060

[227] Porporato, P.E., N. Filigheddu, J.M.B. Pedro, G. Kroemer, and L. Galluzzi. (2018). Mitochondrial metabolism and cancer. *Cell Res, **28***(3), 265-280. doi:10.1038/cr.2017.155

[228] Lang, S.H., M. Stower, and N.J. Maitland. (2000). In vitro modelling of epithelial and stromal interactions in non-malignant and malignant prostates. *Br J Cancer, **82***(4), 990-997. doi:10.1054/bjoc.1999.1029

[229] Valero, M.L., F. Mello de Queiroz, W. Stuhmer, F. Viana, and L.A. Pardo. (2012). TRPM8 ion channels differentially modulate proliferation and cell cycle distribution of normal and cancer prostate cells. *PLoS One, **7***(12), e51825. doi:10.1371/journal.pone.0051825

[230] Raudenska, M., M. Kratochvilova, T. Vicar, J. Gumulec, J. Balvan, et al. (2019). Cisplatin enhances cell stiffness and decreases invasiveness rate in prostate cancer cells by actin accumulation. *Sci Rep, **9***(1), 1660. doi:10.1038/s41598-018-38199-7

[231] Avances, C., V. Georget, B. Terouanne, F. Orio, O. Cussenot, et al. (2001). Human prostatic cell line PNT1A, a useful tool for studying androgen receptor transcriptional activity and its differential subnuclear localization in the presence of androgens and antiandrogens. *Mol Cell Endocrinol, **184***(1-2), 13-24. doi:10.1016/s0303-7207(01)00669-4

[232] Berthon, P., O. Cussenot, L. Hopwood, A. Leduc, and N. Maitland. (1995). Functional expression of sv40 in normal human prostatic epithelial and fibroblastic cells - differentiation pattern of nontumorigenic cell-lines. *Int J Oncol, **6***(2), 333-343. doi:10.3892/ijo.6.2.333

[233] Rackley, C.R. and B.R. Stripp. (2012). Building and maintaining the epithelium of the lung. *J Clin Invest, **122***(8), 2724-2730. doi:10.1172/jci60519

[234] Castell, J.V., M.T. Donato, and M.J. Gomez-Lechon. (2005). Metabolism and bioactivation of toxicants in the lung. The in vitro cellular approach. *Exp Toxicol Pathol, **57 Suppl 1***, 189-204. doi:10.1016/j.etp.2005.05.008

[235] Mercer, B.A., V. Lemaître, C.A. Powell, and J. D'Armiento. (2006). The Epithelial Cell in Lung Health and Emphysema Pathogenesis. *Curr Respir Med Rev**2***(2), 101-142. doi:10.2174/157339806776843085

[236] Karelia, N., D. Desai, J.A. Hengst, S. Amin, S.V. Rudrabhatla, et al. (2010). Selenium-containing analogs of SAHA induce cytotoxicity in lung cancer cells. *Bioorg Med Chem Lett, **20***(22), 6816-6819. doi:10.1016/j.bmcl.2010.08.113

[237] Reddy, N.D., M.H. Shoja, S. Biswas, P.G. Nayak, N. Kumar, et al. (2016). An appraisal of cinnamyl sulfonamide hydroxamate derivatives (HDAC inhibitors) for anti-cancer, anti-angiogenic and anti-metastatic activities in human cancer cells. *Chem Biol Interact, **253***, 112-124. doi:10.1016/j.cbi.2016.05.008

[238] Liu, S., Z. Hu, Q. Zhang, Q. Zhu, Y. Chen, et al. (2020). Co-Prodrugs of 7-Ethyl-10-hydroxycamptothecin and Vorinostat with in Vitro Hydrolysis and Anticancer Effects. *ACS Omega, **5***(1), 350-357. doi:10.1021/acsomega.9b02786

[239] Komatsu, N., N. Kawamata, S. Takeuchi, D. Yin, W. Chien, et al. (2006). SAHA, a HDAC inhibitor, has profound anti-growth activity against non-small cell lung cancer cells. *Oncol Rep, **15***(1), 187-191. doi:10.3892/or.15.1.187

[240] van Tonder, A., A.M. Joubert, and A.D. Cromarty. (2015). Limitations of the 3-(4,5-dimethylthiazol-2-yl)-2,5-diphenyl-2H-tetrazolium bromide (MTT) assay when compared to three commonly used cell enumeration assays. *BMC Res Notes, **8***, 47. doi:10.1186/s13104-015-1000-8

[241] Ediriweera, M.K., K.H. Tennekoon, and S.R. Samarakoon. (2019). In vitro assays and techniques utilized in anticancer drug discovery. *J Appl Toxicol, **39***(1), 38-71. doi:10.1002/jat.3658

[242] Kumar, N., R. Afjei, T.F. Massoud, and R. Paulmurugan. (2018). Comparison of cell-based assays to quantify treatment effects of anticancer drugs identifies a new application for Bodipy-L-cystine to measure apoptosis. *Sci Rep, **8***(1), 16363. doi:10.1038/s41598-018-34696-x

[243] Scudiero, D.A., R.H. Shoemaker, K.D. Paull, A. Monks, S. Tierney, et al. (1988). Evaluation of a soluble tetrazolium/formazan assay for cell growth and drug sensitivity in culture using human and other tumor cell lines. *Cancer Res*, ***48***(17), 4827-4833.

[244] Sutherland, M.W. and B.A. Learmonth. (1997). The tetrazolium dyes MTS and XTT provide new quantitative assays for superoxide and superoxide dismutase. *Free Radic Res*, ***27***(3), 283-289. doi:10.3109/10715769709065766

[245] Peskin, A.V. and C.C. Winterbourn. (2000). A microtiter plate assay for superoxide dismutase using a water-soluble tetrazolium salt (WST-1). *Clin Chim Acta*, ***293***(1-2), 157-166. doi:10.1016/s0009-8981(99)00246-6

[246] Karakas, D., F. Ari, and E. Ulukaya. (2017). The MTT viability assay yields strikingly false-positive viabilities although the cells are killed by some plant extracts. *Turk J Biol*, ***41***(6), 919-925. doi:10.3906/biy-1703-104

[247] Stepanenko, A.A. and V.V. Dmitrenko. (2015). Pitfalls of the MTT assay: Direct and off-target effects of inhibitors can result in over/underestimation of cell viability. *Gene*, ***574***(2), 193-203. doi:10.1016/j.gene.2015.08.009

[248] Wang, S., H. Yu, and J.K. Wickliffe. (2011). Limitation of the MTT and XTT assays for measuring cell viability due to superoxide formation induced by nano-scale TiO2. *Toxicol In Vitro*, ***25***(8), 2147-2151. doi:10.1016/j.tiv.2011.07.007

[249] Skehan, P., R. Storeng, D. Scudiero, A. Monks, J. McMahon, et al. (1990). New colorimetric cytotoxicity assay for anticancer-drug screening. *J Natl Cancer Inst*, ***82***(13), 1107-1112. doi:10.1093/jnci/82.13.1107

[250] Kuete, V., O. Karaosmanoğlu, and H. Sivas. (2017). Anticancer activities of African medicinal spices and vegetables. In V. Kuete (Ed.), *Medicinal Spices and Vegetables from Africa* (pp. 271-297): Academic Press. doi:10.1016/B978-0-12-809286-6.00010-8

[251] Keepers, Y.P., P.E. Pizao, G.J. Peters, J. van Ark-Otte, B. Winograd, et al. (1991). Comparison of the sulforhodamine B protein and tetrazolium (MTT) assays for in vitro chemosensitivity testing. *Eur J Cancer*, ***27***(7), 897-900. doi:10.1016/0277-5379(91)90142-z

[252] Osborne, C. and S.A. Brooks. (2006). SDS-PAGE and Western blotting to detect proteins and glycoproteins of interest in breast cancer research. *Methods Mol Med*, ***120***, 217-229. doi:10.1385/1-59259-969-9:217

[253] Chen, S., M. Nimick, A.G. Cridge, B.C. Hawkins, and R.J. Rosengren. (2018). Anticancer potential of novel curcumin analogs towards castrate-resistant prostate cancer. *Int J Oncol*, ***52***(2), 579-588. doi:10.3892/ijo.2017.4207

[254] Roy, J., N. Jain, G. Singh, B. Das, and B. Mallick. (2019). Small RNA proteome as disease biomarker: An incognito treasure of clinical utility. In B. Mallick (Ed.), *AGO-Driven Non-Coding RNAs* (pp. 101-136): Academic Press. doi:10.1016/B978-0-12-815669-8.00005-1

[255] MacPhee, D.J. (2010). Methodological considerations for improving Western blot analysis. *J Pharmacol Toxicol Methods, **61***(2), 171-177. doi:10.1016/j.vascn.2009.12.001

[256] Ghosh, R., J.E. Gilda, and A.V. Gomes. (2014). The necessity of and strategies for improving confidence in the accuracy of western blots. *Expert Rev Proteomics, **11***(5), 549-560. doi:10.1586/14789450.2014.939635

[257] Mahmood, T. and P.C. Yang. (2012). Western blot: technique, theory, and trouble shooting. *N Am J Med Sci, **4***(9), 429-434. doi:10.4103/1947-2714.100998

[258] Stack, M., R. Focosi-Snyman, S. Cawthraw, L. Davis, R. Jenkins, et al. (2009). Two unusual bovine spongiform encephalopathy cases detected in Great Britain. *Zoonoses Public Health, **56***(6-7), 376-383. doi:10.1111/j.1863-2378.2008.01202.x

[259] Gilda, J.E., R. Ghosh, J.X. Cheah, T.M. West, S.C. Bodine, et al. (2015). Western Blotting Inaccuracies with Unverified Antibodies: Need for a Western Blotting Minimal Reporting Standard (WBMRS). *PLoS One, **10***(8), e0135392. doi:10.1371/journal.pone.0135392

[260] McKinnon, K.M. (2018). Flow Cytometry: An Overview. *Curr Protoc Immunol, **120***, 5.1.1-5.1.11. doi:10.1002/cpim.40

[261] Brown, M. and C. Wittwer. (2000). Flow cytometry: principles and clinical applications in hematology. *Clin Chem, **46***(8 Pt 2), 1221-1229. doi:10.1093/clinchem/46.8.1221

[262] Pozarowski, P. and Z. Darzynkiewicz. (2004). Analysis of cell cycle by flow cytometry. *Methods Mol Biol, **281***, 301-311. doi:10.1385/1-59259-811-0:301

[263] Kim, K.H. and J.M. Sederstrom. (2015). Assaying Cell Cycle Status Using Flow Cytometry. *Curr Protoc Mol Biol, **111***, 28.6.1-28.6.11. doi:10.1002/0471142727.mb2806s111

[264] Ciancio, G., A. Pollack, M.A. Taupier, N.L. Block, and G.L. Irvin, 3rd. (1988). Measurement of cell-cycle phase-specific cell death using Hoechst 33342 and propidium iodide: preservation by ethanol fixation. *J Histochem Cytochem, **36***(9), 1147-1152. doi:10.1177/36.9.2457047

[265] Darzynkiewicz, Z., H.D. Halicka, and H. Zhao. (2010). Analysis of cellular DNA content by flow and laser scanning cytometry. *Adv Exp Med Biol, **676***, 137-147. doi:10.1007/978-1-4419-6199-0_9

[266] Barteneva, N.S., E. Fasler-Kan, and I.A. Vorobjev. (2012). Imaging flow cytometry: coping with heterogeneity in biological systems. *J Histochem Cytochem, **60***(10), 723-733. doi:10.1369/0022155412453052

[267] Knijnenburg, T.A., O. Roda, Y. Wan, G.P. Nolan, J.D. Aitchison, et al. (2011). A regression model approach to enable cell morphology correction in high-throughput flow cytometry. *Mol Syst Biol, **7**,* 531. doi:10.1038/msb.2011.64

[268] Crisman, T.J., C.N. Parker, J.L. Jenkins, J. Scheiber, M. Thoma, et al. (2007). Understanding false positives in reporter gene assays: in silico chemogenomics approaches to prioritize cell-based HTS data. *J Chem Inf Model, **47***(4), 1319-1327. doi:10.1021/ci6005504

[269] Waldman, S.A. (2002). Does potency predict clinical efficacy? Illustration through an antihistamine model. *Ann Allergy Asthma Immunol, **89***(1), 7-12. doi:10.1016/s1081-1206(10)61904-7

[270] Wong, C.C., K.W. Cheng, and B. Rigas. (2012). Preclinical predictors of anticancer drug efficacy: critical assessment with emphasis on whether nanomolar potency should be required of candidate agents. *J Pharmacol Exp Ther, **341***(3), 572-578. doi:10.1124/jpet.112.191957

[271] MacEwan, D.J., G.D. Kim, and G. Milligan. (1995). Analysis of the role of receptor number in defining the intrinsic activity and potency of partial agonists in neuroblastoma x glioma hybrid NG108-15 cells transfected to express differing levels of the human beta 2-adrenoceptor. *Mol Pharmacol, **48***(2), 316-325.

[272] Eastman, A. (2017). Improving anticancer drug development begins with cell culture: misinformation perpetrated by the misuse of cytotoxicity assays. *Oncotarget, **8***(5), 8854-8866. doi:10.18632/oncotarget.12673

[273] Yadav, B., T. Pemovska, A. Szwajda, E. Kulesskiy, M. Kontro, et al. (2014). Quantitative scoring of differential drug sensitivity for individually optimized anticancer therapies. *Sci Rep, **4**,* 5193. doi:10.1038/srep05193

[274] Pemovska, T., M. Kontro, B. Yadav, H. Edgren, S. Eldfors, et al. (2013). Individualized systems medicine strategy to tailor treatments for patients with chemorefractory acute myeloid leukemia. *Cancer Discov, **3***(12), 1416-1429. doi:10.1158/2159-8290.Cd-13-0350

[275] Lepikhova, T., P.R. Karhemo, R. Louhimo, B. Yadav, A. Murumagi, et al. (2018). Drug-Sensitivity Screening and Genomic Characterization of 45 HPV-Negative Head and Neck Carcinoma Cell Lines for Novel Biomarkers of Drug Efficacy. *Mol Cancer Ther, **17***(9), 2060-2071. doi:10.1158/1535-7163.Mct-17-0733

[276] Gulden, M., D. Kahler, and H. Seibert. (2015). Incipient cytotoxicity: A time-independent measure of cytotoxic potency in vitro. *Toxicology, **335**,* 35-45. doi:10.1016/j.tox.2015.07.002

[277] Zhao, N., F. Yang, L. Han, Y. Qu, D. Ge, et al. (2020). Development of Coumarin-Based Hydroxamates as Histone Deacetylase Inhibitors with Antitumor Activities. *Molecules, **25***(3), 717. doi:10.3390/molecules25030717

[278] Feng, J., H. Fang, X. Wang, Y. Jia, L. Zhang, et al. (2011). Discovery of N-hydroxy-4-(3-phenylpropanamido)benzamide derivative 5j, a novel histone deacetylase inhibitor, as a potential therapeutic agent for human breast cancer. *Cancer Biol Ther,* ***11***(5), 477-489. doi:10.4161/cbt.11.5.14529

[279] Chun, S.M., J.Y. Lee, J. Choi, J.H. Lee, J.J. Hwang, et al. (2015). Epigenetic modulation with HDAC inhibitor CG200745 induces anti-proliferation in non-small cell lung cancer cells. *PLoS One,* ***10***(3), e0119379. doi:10.1371/journal.pone.0119379

[280] Guha, R. (2013). On exploring structure-activity relationships. *Methods Mol Biol,* ***993***, 81-94. doi:10.1007/978-1-62703-342-8_6

[281] Marks, P.A. (2010). The clinical development of histone deacetylase inhibitors as targeted anticancer drugs. *Expert Opin Investig Drugs,* ***19***(9), 1049-1066. doi:10.1517/13543784.2010.510514

[282] Gryder, B.E., Q.H. Sodji, and A.K. Oyelere. (2012). Targeted cancer therapy: giving histone deacetylase inhibitors all they need to succeed. *Future Med Chem,* ***4***(4), 505-524. doi:10.4155/fmc.12.3

[283] Chen, P.C., V. Patil, W. Guerrant, P. Green, and A.K. Oyelere. (2008). Synthesis and structure-activity relationship of histone deacetylase (HDAC) inhibitors with triazole-linked cap group. *Bioorg Med Chem,* ***16***(9), 4839-4853. doi:10.1016/j.bmc.2008.03.050

[284] Minchom, A., P. Thavasu, Z. Ahmad, A. Stewart, A. Georgiou, et al. (2017). A study of PD-L1 expression in KRAS mutant non-small cell lung cancer cell lines exposed to relevant targeted treatments. *PLoS One,* ***12***(10), e0186106. doi:10.1371/journal.pone.0186106

[285] Ren, Z.X., H.B. Yu, J.S. Li, J.L. Shen, and W.S. Du. (2015). Suitable parameter choice on quantitative morphology of A549 cell in epithelial-mesenchymal transition. *Biosci Rep,* ***35***(3), e00202. doi:10.1042/bsr20150070

[286] ATCC. NCI-H522 [H522] (ATCC® CRL-5810™). [cited 4 April, 2020]; Available from: https://bit.ly/2B4R5tn

[287] ATCC. A549 (ATCC® CCL-185™). [cited 4 April, 2020]; Available from: https://bit.ly/30J2g5D

[288] ExPASy. NCI-H522 (CVCL_1567). [cited 4 April, 2020]; Available from: https://bit.ly/2MW4vKS

[289] Gupta, A., P. Gautam, K. Wennerberg, and T. Aittokallio. (2020). A normalized drug response metric improves accuracy and consistency of anticancer drug sensitivity quantification in cell-based screening. *Commun Biol,* ***3***(1), 42. doi:10.1038/s42003-020-0765-z

[290] Brauer, M.J., C. Huttenhower, E.M. Airoldi, R. Rosenstein, J.C. Matese, et al. (2008). Coordination of growth rate, cell cycle, stress response, and metabolic activity in yeast. *Mol Biol Cell*, ***19***(1), 352-367. doi:10.1091/mbc.e07-08-0779

[291] Penthala, N.R., A. Ketkar, K.R. Sekhar, M.L. Freeman, R.L. Eoff, et al. (2015). 1-Benzyl-2-methyl-3-indolylmethylene barbituric acid derivatives: Anti-cancer agents that target nucleophosmin 1 (NPM1). *Bioorg Med Chem*, ***23***(22), 7226-7233. doi:10.1016/j.bmc.2015.10.019

[292] Ma, C., Y. Li, S. Niu, H. Zhang, X. Liu, et al. (2011). N-hydroxypyridones, phenylhydrazones, and a quinazolinone from Isaria farinosa. *J Nat Prod*, ***74***(1), 32-37. doi:10.1021/np100568w

[293] Li, D., N.D. Marchenko, and U.M. Moll. (2011). SAHA shows preferential cytotoxicity in mutant p53 cancer cells by destabilizing mutant p53 through inhibition of the HDAC6-Hsp90 chaperone axis. *Cell Death Differ*, ***18***(12), 1904-1913. doi:10.1038/cdd.2011.71

[294] Haverty, P.M., E. Lin, J. Tan, Y. Yu, B. Lam, et al. (2016). Reproducible pharmacogenomic profiling of cancer cell line panels. *Nature*, ***533***(7603), 333-337. doi:10.1038/nature17987

[295] Alves, A.C., D. Ribeiro, C. Nunes, and S. Reis. (2016). Biophysics in cancer: The relevance of drug-membrane interaction studies. *Biochim Biophys Acta*, ***1858***(9), 2231-2244. doi:10.1016/j.bbamem.2016.06.025

[296] Yang, N.J. and M.J. Hinner. (2015). Getting across the cell membrane: an overview for small molecules, peptides, and proteins. *Methods Mol Biol*, ***1266***, 29-53. doi:10.1007/978-1-4939-2272-7_3

[297] Patton, J.S., C.S. Fishburn, and J.G. Weers. (2004). The lungs as a portal of entry for systemic drug delivery. *Proc Am Thorac Soc*, ***1***(4), 338-344. doi:10.1513/pats.200409-049TA

[298] A, A.E.-S., E.A. AE, K.E.-Z. A, and A.E. E. (2019). Cytotoxic Effects of Newly Synthesized Heterocyclic Candidates Containing Nicotinonitrile and Pyrazole Moieties on Hepatocellular and Cervical Carcinomas. *Molecules*, ***24***(10), 1965. doi:10.3390/molecules24101965

[299] Hall, M.D., K.A. Telma, K.E. Chang, T.D. Lee, J.P. Madigan, et al. (2014). Say no to DMSO: dimethylsulfoxide inactivates cisplatin, carboplatin, and other platinum complexes. *Cancer Res*, ***74***(14), 3913-3922. doi:10.1158/0008-5472.Can-14-0247

[300] Steinmeyer, K., H. Maacke, and W. Deppert. (1990). Cell cycle control by p53 in normal (3T3) and chemically transformed (Meth A) mouse cells. I. Regulation of p53 expression. *Oncogene*, ***5***(11), 1691-1699.

[301] Xia, M., R. Huang, K.L. Witt, N. Southall, J. Fostel, et al. (2008). Compound cytotoxicity profiling using quantitative high-throughput screening. *Environ Health Perspect,* ***116***(3), 284-291. doi:10.1289/ehp.10727

[302] Goitia, H., M.D. Villacampa, A. Laguna, and M.C. Gimeno. (2019). Cytotoxic gold (I) complexes with amidophosphine ligands containing thiophene moieties. *Inorganics,* ***7***(2), 13. doi:10.3390/inorganics7020013

[303] Senapati, S., A.K. Mahanta, S. Kumar, and P. Maiti. (2018). Controlled drug delivery vehicles for cancer treatment and their performance. *Signal Transduct Target Ther,* ***3***, 7. doi:10.1038/s41392-017-0004-3

[304] Falzone, L., S. Salomone, and M. Libra. (2018). Evolution of Cancer Pharmacological Treatments at the Turn of the Third Millennium. *Front Pharmacol,* ***9***, 1300. doi:10.3389/fphar.2018.01300

[305] Musa, M.A., V.L. Badisa, L.M. Latinwo, C. Waryoba, and N. Ugochukwu. (2010). In vitro cytotoxicity of benzopyranone derivatives with basic side chain against human lung cell lines. *Anticancer Res,* ***30***(11), 4613-4617.

[306] Segun, P.A., O.O. Ogbole, F.M.D. Ismail, L. Nahar, A.R. Evans, et al. (2019). Resveratrol derivatives from Commiphora africana (A. Rich.) Endl. display cytotoxicity and selectivity against several human cancer cell lines. *Phytother Res,* ***33***(1), 159-166. doi:10.1002/ptr.6209

[307] Grunberg, S.M., J.J. Crowley, R.B. Livingston, F.M. Muggia, J.S. MacDonald, et al. (1991). Treatment of non-small-cell lung cancer with vinblastine and very high-dose cisplatin. A Southwest Oncology Group study. *Cancer Chemother Pharmacol,* ***28***(3), 211-213. doi:10.1007/bf00685511

[308] Li, X., S. Gu, D. Sun, H. Dai, H. Chen, et al. (2018). The selectivity of artemisinin-based drugs on human lung normal and cancer cells. *Environ Toxicol Pharmacol,* ***57***, 86-94. doi:10.1016/j.etap.2017.12.004

[309] El-Deiry, W.S. (2003). The role of p53 in chemosensitivity and radiosensitivity. *Oncogene,* ***22***(47), 7486-7495. doi:10.1038/sj.onc.1206949

[310] Lv, Z., Y. Zhang, M. Zhang, H. Chen, Z. Sun, et al. (2013). Design and synthesis of novel 2'-hydroxy group substituted 2-pyridone derivatives as anticancer agents. *Eur J Med Chem,* ***67***, 447-453. doi:10.1016/j.ejmech.2013.06.046

[311] Gao, E., M. Zhu, L. Liu, Y. Huang, L. Wang, et al. (2010). Impact of the carbon chain length of novel palladium(II) complexes on interaction with DNA and cytotoxic activity. *Inorg Chem,* ***49***(7), 3261-3270. doi:10.1021/ic902176e

[312] Fukushi, S., H. Yoshino, A. Yoshizawa, and I. Kashiwakura. (2016). p53-independent structure-activity relationships of 3-ring mesogenic compounds' activity as cytotoxic effects

against human non-small cell lung cancer lines. *BMC Cancer*, ***16***, 521. doi:10.1186/s12885-016-2585-6

[313] Winiwarter, S., M. Ridderström, A.-L. Ungell, T. Andersson, and I. Zamora. (2007). 5.22 - Use of Molecular Descriptors for Absorption, Distribution, Metabolism, and Excretion Predictions. In D.J.T. John B. Taylor (Ed.), *Comprehensive Medicinal Chemistry II* (Vol. 5, pp. 531-554): Elsevier. doi:10.1016/B0-08-045044-X/00140-1

[314] Shekar, K., J.A. Roberts, A.G. Barnett, S. Diab, S.C. Wallis, et al. (2015). Can physicochemical properties of antimicrobials be used to predict their pharmacokinetics during extracorporeal membrane oxygenation? Illustrative data from ovine models. *Crit Care*, ***19***, 437. doi:10.1186/s13054-015-1151-y

[315] Paknejadi, M., M. Bayat, M. Salimi, and V. Razavilar. (2018). Concentration-and time-dependent cytotoxicity of silver nanoparticles on normal human skin fibroblast cell line. *Iran Red Crescent*, ***20***(10), e79183. doi:10.5812/ircmj.79183

[316] Yadav, B., S. Taurin, L. Larsen, and R.J. Rosengren. (2012). RL71, a second-generation curcumin analog, induces apoptosis and downregulates Akt in ER-negative breast cancer cells. *Int J Oncol*, ***41***(3), 1119-1127. doi:10.3892/ijo.2012.1521

[317] Anttila, J.V., M. Shubin, J. Cairns, F. Borse, Q. Guo, et al. (2019). Contrasting the impact of cytotoxic and cytostatic drug therapies on tumour progression. *PLoS Comput Biol*, ***15***(11), e1007493. doi:10.1371/journal.pcbi.1007493

[318] O'Donovan, M. (2012). A critique of methods to measure cytotoxicity in mammalian cell genotoxicity assays. *Mutagenesis*, ***27***(6), 615-621. doi:10.1093/mutage/ges045

[319] Rixe, O. and T. Fojo. (2007). Is cell death a critical end point for anticancer therapies or is cytostasis sufficient? *Clin Cancer Res*, ***13***(24), 7280-7287. doi:10.1158/1078-0432.Ccr-07-2141

[320] Shafer, S.H. and C.L. Williams. (2003). Non-small and small cell lung carcinoma cell lines exhibit cell type-specific sensitivity to edelfosine-induced cell death and different cell line-specific responses to edelfosine treatment. *Int J Oncol*, ***23***(2), 389-400. doi:10.3892/ijo.23.2.389

[321] Lee, W.Y., P.C. Chen, W.S. Wu, H.C. Wu, C.H. Lan, et al. (2017). Panobinostat sensitizes KRAS-mutant non-small-cell lung cancer to gefitinib by targeting TAZ. *Int J Cancer*, ***141***(9), 1921-1931. doi:10.1002/ijc.30888

[322] Witta, S. (2012). Histone Deacetylase Inhibitors in Non–Small-Cell Lung Cancer. *J Thorac Oncol*, ***7***(12), S404-S406. doi:10.1097/JTO.0b013e31826df29c

[323] Sodji, Q.H., V. Patil, J.R. Kornacki, M. Mrksich, and A.K. Oyelere. (2013). Synthesis and structure-activity relationship of 3-hydroxypyridine-2-thione-based histone deacetylase inhibitors. *J Med Chem, **56***(24), 9969-9981. doi:10.1021/jm401225q

[324] Peyressatre, M., C. Prével, M. Pellerano, and M.C. Morris. (2015). Targeting cyclin-dependent kinases in human cancers: from small molecules to Peptide inhibitors. *Cancers (Basel), **7***(1), 179-237. doi:10.3390/cancers7010179

[325] Fusté, N.P., R. Fernández-Hernández, T. Cemeli, C. Mirantes, N. Pedraza, et al. (2016). Cytoplasmic cyclin D1 regulates cell invasion and metastasis through the phosphorylation of paxillin. *Nat Commun, **7***, 11581. doi:10.1038/ncomms11581

[326] Qie, S. and J.A. Diehl. (2016). Cyclin D1, cancer progression, and opportunities in cancer treatment. *J Mol Med (Berl), **94***(12), 1313-1326. doi:10.1007/s00109-016-1475-3

[327] A, K.A. and A. Adesina. (2006). Prognostic significance of cyclin D1 expression in resected stage I, II non-small cell lung cancer in Arabs. *Interact Cardiovasc Thorac Surg, **5***(1), 47-51. doi:10.1510/icvts.2005.120030

[328] Schettino, C., M.A. Bareschino, V. Ricci, and F. Ciardiello. (2008). Erlotinib: an EGF receptor tyrosine kinase inhibitor in non-small-cell lung cancer treatment. *Expert Rev Respir Med, **2***(2), 167-178. doi:10.1586/17476348.2.2.167

[329] Dragnev, K.H., T. Ma, J. Cyrus, F. Galimberti, V. Memoli, et al. (2011). Bexarotene plus erlotinib suppress lung carcinogenesis independent of KRAS mutations in two clinical trials and transgenic models. *Cancer Prev Res (Phila), **4***(6), 818-828. doi:10.1158/1940-6207.Capr-10-0376

[330] VanderWel, S.N., P.J. Harvey, D.J. McNamara, J.T. Repine, P.R. Keller, et al. (2005). Pyrido[2,3-d]pyrimidin-7-ones as specific inhibitors of cyclin-dependent kinase 4. *J Med Chem, **48***(7), 2371-2387. doi:10.1021/jm049355+

[331] Toogood, P.L., P.J. Harvey, J.T. Repine, D.J. Sheehan, S.N. VanderWel, et al. (2005). Discovery of a potent and selective inhibitor of cyclin-dependent kinase 4/6. *J Med Chem, **48***(7), 2388-2406. doi:10.1021/jm049354h

[332] Meijer, L., A. Borgne, O. Mulner, J.P. Chong, J.J. Blow, et al. (1997). Biochemical and cellular effects of roscovitine, a potent and selective inhibitor of the cyclin-dependent kinases cdc2, cdk2 and cdk5. *Eur J Biochem, **243***(1-2), 527-536. doi:10.1111/j.1432-1033.1997.t01-2-00527.x

[333] McClue, S.J., D. Blake, R. Clarke, A. Cowan, L. Cummings, et al. (2002). In vitro and in vivo antitumor properties of the cyclin dependent kinase inhibitor CYC202 (R-roscovitine). *Int J Cancer, **102***(5), 463-468. doi:10.1002/ijc.10738

[334] Havlícek, L., J. Hanus, J. Veselý, S. Leclerc, L. Meijer, et al. (1997). Cytokinin-derived cyclin-dependent kinase inhibitors: synthesis and cdc2 inhibitory activity of olomoucine and related compounds. *J Med Chem, **40***(4), 408-412. doi:10.1021/jm960666x

[335] Xuan, T.D., S. Tawata, and T.D. Khanh. (2013). Herbicidal activity of mimosine and its derivatives. In *Herbicides-advances in research* (pp. 299-312). doi:10.5772/55845

[336] Samuni, Y., W. DeGraff, M. Chevion, J.B. Mitchell, and J.A. Cook. (2001). Radiation sensitization of mammalian cells by metal chelators. *Radiat Res, **155***(2), 304-310. doi:10.1667/0033-7587(2001)155[0304:RSOMCB]2.0.CO;2

[337] Zhou, J., L.U. Li, L.I. Fang, H. Xie, W. Yao, et al. (2016). Quercetin reduces cyclin D1 activity and induces G1 phase arrest in HepG2 cells. *Oncol Lett, **12***(1), 516-522. doi:10.3892/ol.2016.4639

[338] Satyanarayana, A. and P. Kaldis. (2009). Mammalian cell-cycle regulation: several Cdks, numerous cyclins and diverse compensatory mechanisms. *Oncogene, **28***(33), 2925-2939. doi:10.1038/onc.2009.170

[339] Eichhorn, J.M., A. Kothari, and T.C. Chambers. (2014). Cyclin B1 overexpression induces cell death independent of mitotic arrest. *PLoS One, **9***(11), e113283. doi:10.1371/journal.pone.0113283

[340] Wang, S., H. Sun, X. Zhan, and Q. Wang. (2020). MicroRNA-718 serves a tumor-suppressive role in non-small cell lung cancer by directly targeting CCNB1. *Int J Mol Med, **45***(1), 33-44. doi:10.3892/ijmm.2019.4396

[341] Yuan, J., R. Yan, A. Krämer, F. Eckerdt, M. Roller, et al. (2004). Cyclin B1 depletion inhibits proliferation and induces apoptosis in human tumor cells. *Oncogene, **23***(34), 5843-5852. doi:10.1038/sj.onc.1207757

[342] Choi, H.J., M. Fukui, and B.T. Zhu. (2011). Role of cyclin B1/Cdc2 up-regulation in the development of mitotic prometaphase arrest in human breast cancer cells treated with nocodazole. *PLoS One, **6***(8), e24312. doi:10.1371/journal.pone.0024312

[343] Li, Y., J. Fan, and D. Ju. (2019). Neurotoxicity concern about the brain targeting delivery systems. In X.G. Huile Gao (Ed.), *Brain Targeted Drug Delivery System* (pp. 377-408): Academic Press. doi:10.1016/B978-0-12-814001-7.00015-9

[344] Shapiro, G.I. and J.W. Harper. (1999). Anticancer drug targets: cell cycle and checkpoint control. *J Clin Invest, **104***(12), 1645-1653. doi:10.1172/jci9054

[345] Yang, X., L. Zhao, T. Zhang, J. Xi, S. Liu, et al. (2019). Protosappanin B promotes apoptosis and causes G(1) cell cycle arrest in human bladder cancer cells. *Sci Rep, **9***(1), 1048. doi:10.1038/s41598-018-37553-z

[346] Wakasaya, T., H. Yoshino, Y. Fukushi, A. Yoshizawa, and I. Kashiwakura. (2013). A liquid crystal-related compound induces cell cycle arrest at the G2/M phase and apoptosis in the A549 human non-small cell lung cancer cell line. *Int J Oncol,* ***42***(4), 1205-1211. doi:10.3892/ijo.2013.1804

[347] Gérard, C. and A. Goldbeter. (2014). The balance between cell cycle arrest and cell proliferation: control by the extracellular matrix and by contact inhibition. *Interface Focus,* ***4***(3), 20130075. doi:10.1098/rsfs.2013.0075

[348] Del Re, M., E. Rofi, G. Restante, S. Crucitta, E. Arrigoni, et al. (2018). Implications of KRAS mutations in acquired resistance to treatment in NSCLC. *Oncotarget,* ***9***(5), 6630-6643. doi:10.18632/oncotarget.23553

[349] Huang, H., Y.D. Hu, N. Li, and Y. Zhu. (2009). Inhibition of tumor growth and metastasis by non-small cell lung cancer cells transfected with cyclin D1-targeted siRNA. *Oligonucleotides,* ***19***(2), 151-162. doi:10.1089/oli.2008.0174

[350] Sherr, C.J. (2002). D1 in G2. *Cell Cycle,* ***1***(1), 32-34. doi:10.4161/cc.1.1.106

[351] Zhou, X., Q. Hao, and H. Lu. (2019). Mutant p53 in cancer therapy-the barrier or the path. *J Mol Cell Biol,* ***11***(4), 293-305. doi:10.1093/jmcb/mjy072

[352] Sun, S.H., M. Zheng, K. Ding, S. Wang, and Y. Sun. (2008). A small molecule that disrupts Mdm2-p53 binding activates p53, induces apoptosis and sensitizes lung cancer cells to chemotherapy. *Cancer Biol Ther,* ***7***(6), 845-852. doi:10.4161/cbt.7.6.5841

[353] Kajstura, M., H.D. Halicka, J. Pryjma, and Z. Darzynkiewicz. (2007). Discontinuous fragmentation of nuclear DNA during apoptosis revealed by discrete "sub-G1" peaks on DNA content histograms. *Cytometry A,* ***71***(3), 125-131. doi:10.1002/cyto.a.20357

[354] Ormerod, M.G., X.M. Sun, D. Brown, R.T. Snowden, and G.M. Cohen. (1993). Quantification of apoptosis and necrosis by flow cytometry. *Acta Oncol,* ***32***(4), 417-424. doi:10.3109/02841869309093620

[355] Almeida, G.M., T.L. Duarte, P.B. Farmer, W.P. Steward, and G.D. Jones. (2008). Multiple end-point analysis reveals cisplatin damage tolerance to be a chemoresistance mechanism in a NSCLC model: implications for predictive testing. *Int J Cancer,* ***122***(8), 1810-1819. doi:10.1002/ijc.23188